A VIRTUAL STUDY OF SURFACE ACTIVITY OF CHITOSAN AND DERIVATIVES

Thesis submitted to
the University of Calicut in partial fulfilment of
the requirements for the degree of

DOCTOR OF PHILOSOPHY IN CHEMISTRY

Under the Faculty of Science

by

BASILA HASSAN O. K.

Supervising Teacher

Dr.V.M Abdul Mujeeb
Professor

DEPARTMENT OF CHEMISTRY
UNIVERSITY OF CALICUT
KERALA 673635
INDIA
2016

DECLARATION

I declare that the work presented in the thesis **A virtual study of surface activity of chitosan and derivatives** is an authentic record of the original work done by me under the direct supervision and guidance of **Dr.V.M Abdul Mujeeb**, Professor, Department of Chemistry, University of Calicut in the partial fulfilment of the requirements for the award of Doctor of Philosophy in Chemistry of the University of Calicut, and further that no part thereof has been included in any other thesis submitted previously for the award of any other degree of this university or any other university or institution.

Basila Hassan. O. K.

Dr.V.M.Abdul Mujeeb
Professor
Department of Chemistry
University of Calicut

CERTIFICATE

This is to certify that the dissertation entitled "**A virtual study of surface activity of chitosan and derivatives"** bound herewith is a bonafide work done by **Basila Hassan. O. K.** under my supervision in the Department of Chemistry in partial fulfilment of the requirements for the award of degree of Doctor of Philosophy in Chemistry of the University of Calicut, and that the work has not been included in any other thesis submitted previously for the award of any other degree.

Dr.V.M Abdul Mujeeb

Dr.V.M.Abdul Mujeeb
Professor
Department of Chemistry
University of Calicut

CERTIFICATE

This is to certify that the dissertation entitled "**A virtual study of surface activity of chitosan and derivatives"** bound herewith is a bonafide work done by **Basila Hassan. O. K.** under my supervision in the Department of Chemistry in partial fulfilment of the requirements for the award of degree of Doctor of Philosophy in Chemistry of the University of Calicut, and that the work has not been included in any other thesis submitted previously for the award of any other degree.

Modifications and suggestions made by the examiners are incorporated in the new volume. Other typographical errors are also rectified.

Dr.V.M Abdul Mujeeb

ACKNOWLEDGEMENT

I would like to express my sincere thanks and indebtedness to ***Dr.V.M Abdul Mujeeb****, Professor, Department of Chemistry, University of Calicut, for his guidance and constant encouragement. He not only provides valuable suggestions but is the source of inspiration for me to complete the course of investigation. I am grateful to him for all the ways he was directed me to move forward.*

I would express my deep sense of thanks and gratitude to ***Dr.K.Muraleedharan****, Head of the department, Department of Chemistry, University of Calicut for providing necessary facilities to complete the course. I am grateful to him for his valuable suggestions, help and encouragement.*

I acknowledge all the faculty members of the department, Department of Chemistry, University of Calicut for their kindness and generosity. I would like to express my gratitude to technical and ministerial staff in the department of Chemistry for their help throughout the course period.

I express my thanks and gratefulness to ***Mr.Noushad, Ms.Jisha, Ms.Kavitha ,Mr.Alikutty, Ms.Ajmala, Ms.Jaseela, Ms.Vijisha, Mr.Mujeeb Rahman and Ms. Shameera****, the research scholars of our group for providing me all sorts of help, kindness, love and encouragement whenever needed.*

I would also like to acknowledge each of my family members who sacrificed their precious time to provide kind support and encouragement throughout the course period. All of my gratitude and indebtedness comes from the God almighty who blessed me by showering his kindness.

Basila Hassan. O. K.

PREFACE

Computational chemistry methods are widely used for solving chemical problems. It is a fast growing research field. Computational methods are sufficient not only to support experimentally proved facts but also useful to predict success of experimental attempts. The present work is an application of computational methods to understand the surface activity of chitosan and some of its derivatives. Chitosan is a natural biopolymer having unique properties like biodegradability, non toxicity etc. The major applications of chitosan are based on its surface activity or the metal binding capacity. The present study is focused on metal chelation, corrosion inhibition and druggability of chitosan and it's certain derivatives.

Schiff bases of chitosan are well known because of their wide applications in various fields especially in catalysis. In this work six carbonyls compounds were chosen for the Schiff base formation with chitosan. The carbonyl compounds chosen were citral, glyoxillic acid/oxoacetic acid, pyruvic acid, pyridine carboxaldehyde, pyridoxal hydrochloride and salicylaldehyde. All of them were previously reported experimentally. Schiff bases were modeled computationally. Their N-reduced derivatives also modeled for the studies.

The dissertation contains ten chapters. Chapter 1 gives an introduction to computational chemistry. Second chapter is the literature survey and third contains the materials and methods section. In chapters 4 to 9 results and discussion were given. Modeling of derivatives and their optimization were described in fourth chapter.

The important bond parameters also discussed in this. Natural bond orbital (NBO) analysis of the chitosan and the derivatives were given in the next chapter. Chapter six contains the discussions about the reactivity parameters.

Seventh chapter includes the results and discussions about metal chelation studies. For this three heavy metal ions Cd (II), Hg (II) and Pb (II) were chosen. Chapter eight is the description of corrosion inhibition studies of the molecules under study. Ninth one contains the druggability studies of chitosan and derivatives. Last chapter is a summary and conclusion of the entire work.

LIST OF ABBREVIATIONS

AM1	:	Austin model 1
a_{eq}	:	Equilibrium bond angle
BSSE	:	Basis set superposition error
CASSCF	:	Complete active space self consistent field
CGTO	:	Contracted Gaussian type orbital
CC	:	Coupled cluster
CI	:	Configuration interaction
CIS	:	Configuration interaction Single excitation
CISD	:	Configuration interaction Single and double excitation
CISDT	:	Configuration interaction Single, double and triple excitation
CISDTQ	:	Configuration interaction Single, double, triple and quadruple excitation
CNDO	:	Complete neglect of differential overlap
DFT	:	Density functional theory method
DZ	:	Double zeta
E^2	:	Second order perturbation energy
E_0 (ρ_0)	:	True ground state energy
E_{ads}	:	Adsorption energy
E_{bend}	:	Bond bending energy
EDT	:	Electron density transfer
EHM	:	Extended Huckel method
$E_{nonbond}$	:	Non- bonded interaction energy
$E_{stretch}$	:	Bond stretching energy
$E_{torsion}$	:	Energy of torsional motion
E_{xc}	:	Exchange correlation energy

FMO	:	Frontier molecular orbital
GGA	:	Generalized gradient approximation
GPCR	:	Gene protein coupled receptor
GTO	:	Gaussian type orbital
GVB	:	Generalized Valence bond
HF	:	Hartre Fock
HLG	:	Homo-lumo gap
HOMO	:	Highest occupied molecular orbital
IE	:	Inhibition efficiency
INDO	:	Intermediate neglect of differential overlap
K_{bend}	:	Force constant of bond bending
KS	:	Kohn Sham
$K_{stretch}$	:	Force constant of bond stretching
LDA	:	Local density approximation
l_{eq}	:	Equilibrium bond length
LSDA	:	Local spin density approximation
LUMO	:	Lowest unoccupied molecular orbital
LYP	:	Lee-Yang-Parr
MBPT	:	Many body perturbation theory
MCSCF	:	Multi-configuration self consistent field method
MM	:	Molecular mechanics
MO	:	Molecular orbital
MP_n	:	Moller-Plesset approximation
MP4SDTQ	:	Moller-Plesset approximation (single, double, triple and quadruple)
MRCI	:	Multi reference configuration interaction
NAO	:	Natural atomic orbital
NBO	:	Natural bond orbital
NDO	:	Neglect of differential overlap
NDDO	:	Neglect of diatomic differential overlap
NEC	:	Natural electronic configuration

NPA	:	Natural population analysis
PES	:	Potential energy surface scan
PGTO	:	Primitive Gaussian type orbital
PM3	:	Parameterization method 3
PPP	:	Pariser-Parr-Pople method
PSA	:	Polar surface area
QCI	:	Quadratic configuration interaction calculations
QCISD	:	Quadratic configuration interaction calculations single and double excitation
QCISD (T)	:	Triple excitation Quadratic configuration interaction calculations
RHF	:	Restricted Hartree-Fock method
ROHF	:	Restricted open shell Hartree-Fock method
SAC	:	Symmetry adapted cluster
SAM1	:	Semi *ab initio* method number 1
SE	:	Semi empirical method
SHM	:	Simple harmonic motion
STO	:	Slater type orbital
SV	:	Split valence
UHF	:	Unrestricted Hartree- Fock method
V_{ee}	:	Electron-electron repulsion energy
V_{Ne}	:	Neutron –electron attraction energy
ZDO	:	Zero differential overlap

CONTENTS

In the memory of my dear mother..

1 Chapter Introduction to Computational Chemistry

Theoretical chemistry is the mathematical study of chemical problems or can be defined as mathematical description of chemistry. That is solving chemical problems using mathematical equations. Mathematical formulation of chemistry has its origin from classical physics. Chemistry began as an entirely empirical science dealing with the classification and properties of substances and with their transformation in chemical reactions. As this large body of facts developed into a science it is necessary to focus on the nature and behavior of individual atoms and of their own constituent parts, especially the electrons. This is because of the extremely small mass of electrons which behave as quantum particles and do not obey the rules of classical physics.

In simple terms, quantum theory can be presented as a set of assumptions which are developed through mathematical treatment. Niels Bohr in 1913 developed modern atomic theory. But the advances in quantum theory were not recognized long before Bohr himself. This recognition has taken place in the 1920's. Then required an even deeper explanation for the electron, as it exists in the atom.

About ten years after the development of Bohr’s theory, de Broglie showed that the electron should have wavelike properties of its own. By 1926, de Broglie's theory of the wave nature of the electron had been experimentally confirmed, and the stage was set for its

extension to all matter. But by the same time, three apparently very different theories were developed that attempted to treat matter in general terms. These were wave mechanics by Schrödinger, matrix mechanics by Heisenberg, and a more abstract theory of P.A.M. Dirac. All these were found to be mathematically equivalent, and all continue to be useful.

Among these three alternative treatments, the one which was developed by Schrödinger is the most easily visualized and widely studied. He started from the fundamental treatment that the total energy of the electron is the sum of its kinetic and potential energies. It can be expressed as:

$$E = \frac{mv^2}{2} + \frac{-e^2}{r}$$

The second term is the potential energy term of an electron (charge is denoted by *e*) situated at a distance *r* from a proton (for the nucleus of the hydrogen atom). It is generally easier to deal with equations that use momentum ($p = mv$) rather than velocity in quantum mechanics. So in the next step made substitution as follows:

$$E = \frac{P^2}{2m} - \frac{e^2}{r}$$

Still this is an entirely classical relation and valid for the waves on a guitar string as for those of the electron in a hydrogen atom. The third step is the revolutionary attempt. That is in order to take into account the wavelike character of the hydrogen atom, a mathematical expression applied to both sides of the equation that describes the

position and momentum of the electron at all points in space. A new function, denoted by Ψ, also introduced to the equation of motion of the electron. This is to reflect the fact that the electron itself manifests with greater probability in some locations than at others. Thus got the celebrated Schrödinger equation given below:

$$\left(\frac{mv^2}{2} - \frac{e^2}{r}\right)\Psi = E\,\Psi$$

1. Computational chemistry

Computational chemistry or molecular modelling means using computer technologies or software to solve chemical problems. Computational techniques can be broadly classified into the following categories.

1. Molecular mechanics (MM)
2. Semiempirical (SE) methods
3. Ab –initio methods
4. Density functional theory (DFT) method

Of these four methods MM is the only one which is based on classical physics whereas other three methods rely on quantum mechanics or modern physics. Also the latter three methods are molecular orbital (MO) methods.

1.1. Molecular mechanics (MM)

In molecular mechanics, molecules are considered as balls connected by springs denoting that atoms are connected by bonds. Stretching and bending of these springs can bring about different geometries. But the stretch and bend of springs are limited to some lengths and angles. Thus this model restores a natural geometry. The energy of a molecule is calculated as a function of its resistance toward bond stretching, bond bending, and atom crowding, and to use this energy equation to find the bond lengths, angles, and dihedrals corresponding to the minimum-energy geometry.

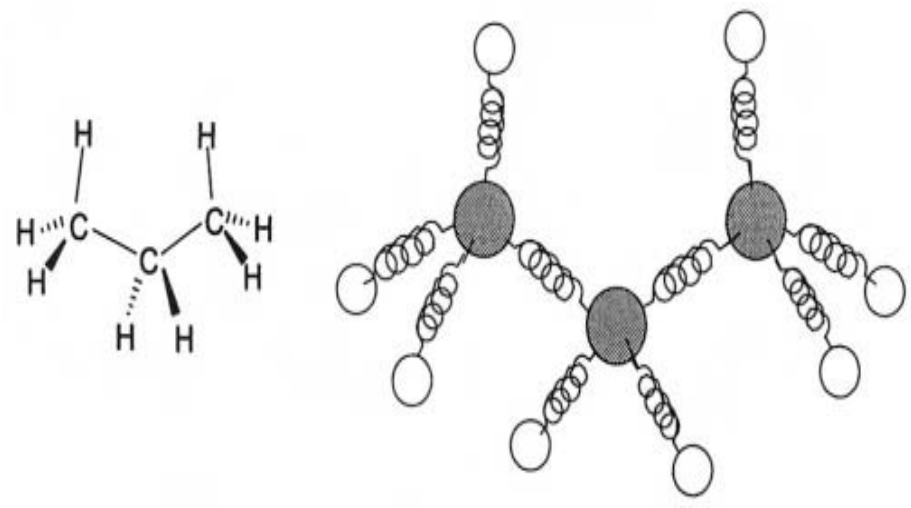

Fig.1.1 Balls and spring model of molecules

This method is otherwise called as force field methods because the form of mathematical expression for the energy, and the parameters in it, constitute a force field. A serious drawback of MM is that it completely ignores electrons. So we cannot calculate electronic

properties like charge distributions or nucleophilic and electrophilic behavior. In this mechanics a molecule is defined by the atoms and the bonds, and to do a MM calculation we must specify each bond as single, double, etc. In an electronic structure calculation like ab initio, semiempirical (SE), and density functional theory, a molecule is defined by the relative positions of its atomic nuclei, the charge, and the multiplicity.

The potential energy of a molecule can be given as sum of energies of bond stretching, angle bending, torsional motion around single bonds, and interactions between atoms or groups which are non-bonded.

$$E = \sum_{bonds} E_{stretch} + \sum_{angles} E_{bend} + \sum_{dihedrals} E_{torsion} + \sum_{Pairs} E_{non-bond}$$

The bond stretching energy is proportional to square of change in the bond length and can be given as the following equation

$$E_{stretch} = k_{stretch}\left(l - l_{eq}\right)^2$$

Where $k_{stretch}$ is the proportionality constant which is one-half the force constant of the spring or bond, l is the length of the bond when stretched and l_{eq} is the equilibrium length of the bond or natural length.

Angle bending energy is also proportional to square of the increase in the angle; we get an analogous equation for bending also

$$E_{bend} = k_{bend}(a - a_{eq})^2$$

Torsional energy term can be expressed as,

$$E_{torsion} = k_0 + \sum_{r=1}^{n} k_r[1 + cos(r\theta)]$$

An easy way to express non bonded interaction term is given by Lennard-Jones 12-6 potential [1, 2] as below

$$E_{nonbond} = k_{nb}\left[\left(\frac{\sigma}{r}\right)^{12} - \left(\frac{\sigma}{r}\right)^{6}\right]$$

Where r is the distance between the centers of non-bonded atoms or groups and σ can be calculated from vander waal radii.

The stretching energy can be improved by the use of cubic or quadratic force field terms, also non- bonded interaction term by more complicated expressions. Thus we can expect more accurate results.

Finding the values or numbers of $k_{stretch}$,l_{eq} , k_{bend} etc. terms in the above equations can be done either by ab initio calculations or by experimental methods. This is known as parametrization of a force field.

Main applications of MM method are;

1. It can calculate the geometries and energies of small to medium-sized molecules. The results are frequently used as a reasonable starting geometry for other methods like ab initio, SE, DFT etc.

2. It can calculate the geometries and energies of polymers, mainly proteins and nucleic acids.

3. It can be used to calculate the geometries and energies of transition states (but not so frequent) as an aid to organic synthesis.

4. It can generate the potential energy function under which molecules move, for molecular dynamics calculations.

Weaknesses of MM method were discussed by Lipkowitz [3]. Draw backs of MM methods can be summarized as;

1. A forcefield parameterized for one class of compounds is insufficient for other classes.

2. Optimized stationary point may not be the correct global minimum.

3. MM completely ignores the solvents and nearby ions. Thus for polar molecules, the geometries and energies are not accurate.

4. Insufficient to differentiate the energies of molecules with small differences.

5. Isomeric compounds cannot be distinguished in terms of their energy differences.

1.2 Semi empirical (SE) methods

SE calculations are neither an empirical method, like molecular mechanics nor a theoretical method, like ab initio calculations. But it stands in contrast to empirical and theoretical methods.

For SE calculations, a Fock matrix will be constructed and diagonalized it in order to get MOs and their energy levels. A core integral H_{rs}^{core} , density matrix elements P_{tu} and electron repulsion integrals$(rs|tu)$,$(ru|ts)$ are needed for calculating Each Fock matrix element.

$$F_{rs} = H_{rs}^{core}(1) + \sum_{t=1}^{m}\sum_{u=1}^{m} P_{tu}\left[(rs|tu) - \frac{1}{2}(ru|ts)\right]$$

An initial guess of the coefficients is needed to calculate the density matrix values P_{tu} ,as for an *ab initio* calculation. A simple Hückel calculation (SHM) or an extended Hückel calculation (EHM) can make the guess. To refine energy levels and coefficients, Fock matrix of F_{rs} elements is diagonalized repeatedly. The basic difference between an ab initio and SE calculations are;

(1) SE method treats only valence or electrons in the sense of the core. In *ab initio* calculation H_{rs}^{core} is the sum of the potential energy and kinetic energy. Kinetic energy is due to electron moving in the force-field of the atomic nuclei whereas potential energy is from attraction of the electron to these atomic nuclei. The electron is moving under the influence of a positive centre (core) composed of atomic nuclei. SE calculations consider at most valence electrons, so each element of the centre becomes

an atomic nucleus and its core electrons. Thus E_{SE} is the valence electronic energy in SE rather than the total electronic energy.

$$E_{SE}^{total} = E_{SE} + V_{cc} = \sum_{i=1}^{n} \in_i + \frac{1}{2}\sum_{r=1}^{m}\sum_{s=1}^{m} P_{rs}\, H_{rs}^{core} + V_{cc}$$

Where V_{CC} denotes the core-core repulsion.

(2) It uses mathematical functions to expand the MOs that are known as the basis set functions. For a SE calculation we need basis functions only for valence electrons. In SCF-type SE methods Slater functions are used instead of approximating Slater functions as sums of Gaussian functions. *Ab initio* calculations use Gaussian functions but Slater functions are more accurate. This is only because calculations of the electron–electron repulsion two-electron integrals are faster in Gaussian functions. For SE, these integrals will be parameterized. To calculate overlap integrals $\langle \phi_r \phi_s \rangle$, mathematical forms of the basis functions ϕ are still needed. Some overlap integrals are evaluated since these methods treat the overlap matrix as a unit matrix. There are some apparent logical contradictions in approximate MO theory that can be used to calculate core integrals and electron-repulsion integrals [4].

(3) Ab initio and SE differs in the evaluation of the core and two-electron repulsion integrals.

In SE, the core integrals and the two-electron repulsion integrals are not calculated from first principles. Many integrals are set to zero. This is done by evaluating their bond distances in an empirical way using atoms involved. In an *ab initio* calculation, this calculation of the two-electron integrals, particularly the three- and four-center calculations are time consuming. From the extent of differential overlap neglected, the ignored integrals can be determined. The differential of the overlap integral *S* is given as *dS*. The expressions are given below:

$$S = \int \phi_r(1)\, \phi_s(1) dv_1$$

$$dS = \int \phi_r\,(1) \phi_s(1) dv_1$$

Different SE methods are available by setting $dS = 0$, i.e. for applying zero differential overlap (ZDO).

(4) The treatment of the overlap matrix in ab initio and SE methods are different. SCF-type SE methods take S = 1 that is overlap matrix to a unit matrix. Then S vanishes in the Roothaan–Hall equations $FC = SC_{\in}$. Thus the equation takes the standard eigenvalue form $FC = C_{\in}$ without orthogonalizing matrix .

1.2.1 Pariser-Parr-Pople (PPP) method

It focused on π electrons only, taking other electrons as a σ framework for holding the atomic p orbitals in their place. The method is specialized in predicting UV spectra of conjugated

compounds, specifically dyes [5, 6]. Accuracy of the results can be improved by incorporating electron correlation through configuration interaction (CI) method. Even though optimization of bond length is permitted usually the calculations were done with a fixed geometry. Thus other methods with neglect of differential overlap (NDO) like INDO/S and ZINDO/S overcome classical PPP method.

1.2.2 Complete neglect of differential overlap (CNDO) method

CNDO calculations use a minimal valence basis set of Slater-type orbitals. In this, usual number of valence AOs will be present corresponding to each atom. The nuclei plus all core electrons represented by H_{rs}^{core} and coefficients of the valence AOs are used to calculateP_{tu}. The two-electron repulsion integrals refer to valence electrons**.** Improved versions like CNDO/2 are available now in addition to ordinary methods like CNDO, CNDO/1.

1.2.3 Intermediate neglect of differential overlap (INDO) method

INDO [7, 8] is superior to CNDO in ZDO approximation. INDO applies ZDO only to those one-center two-electron integrals$(rs|tu)$with ϕ_r, ϕs, ϕt and ϕ_u, all on the same atom. But PPP and CNDO apply it to all different$(r \neq s)$ atomic orbitals in the two-electron integrals. These repulsion integrals should be the most important. Nowadays CNDO and INDO methods are widely used for predicting UV spectra. For these specially parameterized versions called INDO/S and ZINDO/S are also available [9, 10].

1.2.4 Neglect of diatomic differential overlap (NDDO) method

In NDDO [11-13] method, ZDO approximation does not apply to orbitals on the same atom. It is used only for atomic orbitals of different atoms. Currently popular semi empirical methods are developed by Dewar and coworkers. These work on NDDO. Examples are modified NDDO (MNDO), Austin method 1 (AM1) and parametric method (PM3).

AM1 is an improved version of MNDO in which the main change is that the core–core repulsions were modified to overcome the tendency of MNDO to overestimate repulsion between atoms separated by their van der Waals distances. AM1 is the most widely-used SE method. Semi *ab initio* method number 1 (SAM1) is a modification of AM1 in which the two-electron integrals are calculated from contracted Gaussians (an STO-3G basis set) as in standard *ab initio* calculations. Semi empirical calculations are very fast compared to *ab initio* and even to DFT.

1.3 Ab initio methods

This is a quantum mechanical method, the word *ab initio* [14] mean from first principles. It does not include experimental results but the calculations are based on approximate quantum mechanics. Hartree–Fock (HF) calculation is the simplest kind of *ab initio* calculation.

Ab initio methods can be classified into

1. Hartree-Fock approximation

2. Correlation methods

    a) Moller-Plesset approximation (MPn)

    b) Generalized valence bond (GVB) method

    c) Multi-configurational self-consistent field (MCSCF)

    d) Configuration interaction (CI)

    e) Coupled cluster theory (CC)

1.3.1 Hartree-Fock approximation

Hartree Fock method starts from the fact that exact solution to Schrödinger equation of a many electron system is impossible because of the electron-electron repulsion terms. This method is based on two approximations. First one is known as central field approximation. That means Coulombic electron -electron repulsion is taken into account by integrating the repulsion term. This gives the average effect of the repulsion, but not the explicit repulsion interaction.

The second approximation is due to the fact that the wave function must be described by some mathematical function, which is exactly known for only a few one-electron systems. So Hartree's method makes a plausible approximate guess to systems having polyelectrons. Then the wavefunction for an atom will be the product of one-electron wavefunctions.

$$\psi_0 = \psi_0(1)\psi_0(2)\psi_0(3) \ldots\ldots \psi_0(n)$$

This function is called a Hartree product.ψ_0 in the equation is a function of the coordinates of all the electrons in the atom, $\psi_0(1)$ is a function of the coordinates of electron 1, $\psi_0(2)$ is a function of the coordinates of electron 2, etc. These one-electron functions are called atomic orbitals or molecular orbitals if we were dealing with a molecule. The initial guess ψ_0 is known as zeroth approximation to the true total wavefunction. This is so called because we have not yet started to refine it with the Hartree process. In a Hartree process, first generate equation for *electron one* and solve it. For *electron one* the equation will be $\psi_0(2)\psi_0(3)....\ \psi_0(n)$ due to interactions from all the *other* electrons. Electron one is the only moving particle in this equation. Solving this equation gives $\psi_1(1)$ an improved version of $\psi_0(1)$ Similar method is followed to solve electron 2 a one-electron Schrödinger equation with electron two moving in an average field due to the electrons $\psi_1(1)$, $\psi_0(3)$, ..., $\psi_0(n)$. This is continued to electron n moving in a field due to $\psi_1(1)$, $\psi_1(2)$, ..., $\psi_1(n-1)$ Thus first cycle of calculations completes and we get

$$\psi_1 \quad = \quad \psi_1(1)\ \psi_1(2)\ ...\ \psi_1(n)$$

Cycle repeates to get,

$$\psi_2 \quad = \quad \psi_2(1)\ \psi_2(2)\ ...\ \psi_2(n)$$

The process is repeated upto k cycles until getting a wavefunction $_k$ and/or energy calculated from $_k$ which is same as the wavefunction and/or energy from the previous cycle. At this stage the

field of cycle k is "consistent with" this previous field of cycle $k - 1$, and hence the Hartree procedure is called the self-consistent-field-procedure or the *SCF* procedure.

Hartree method has some serious limitations.

1. It does not consider the spin of electrons.

2. Electrons are indistinguishable. This fact is not considered by Hartree method.

3. Electronic wavefunction is actually antisymmetric but Hartree method can not account this fact.

The limitations of Hartree method were corrected by Fock and by Slater. The Hartree wavefunction we discussed is a product of one-electron functions called orbitals, which are essentially spatial orbitals. The Slater wavefunction is composed, not only spatial orbitals, but spin orbitals also. A spin orbital is the product of a spatial orbital and a spin function, α or β.

1.3.2 Basis functions and the Roothaan–Hall equations

For molecular calculations HF equations are not very useful. There are two reasons; one is that this method cannot prescribe a mathematically viable procedure getting the initial guesses for the MO wavefunctions which we need to initiate the iterative process. The second reason is that the complicated wavefunctions make more ambiguity and cannot give a qualitative understanding of the electron distribution. In 1951, by the introduction of MOs as linear

combinations of basis functions Roothaan and Hall solved these problems [15].

$$\psi_1 = c_{11}\varphi_1 + c_{21}\varphi_2 + \cdots + c_{m1}\varphi_m$$

$$\psi_2 = c_{12}\varphi_1 + c_{22}\varphi_2 + \cdots + c_{m2}\varphi_m$$

$$\psi_3 = c_{13}\varphi_1 + c_{23}\varphi_2 + \cdots + c_{m3}\varphi_m$$

$$\cdots\cdots$$

$$\psi_m = c_{1m}\varphi_1 + c_{2m}\varphi_2 + \cdots + c_{mm}\varphi_m$$

The set of basis functions used for a particular calculation is called the *basis set.*

1.3.3 Types of HF calculations

In HF, orbitals are constructed based on the nature of electrons whether they are paired or unpaired. If the molecule has a singlet spin electrons will be paired then we can use same orbital spatial function for both α and β spin electrons of each pair. This method is known as restricted Hartree-Fock method (RHF).

In case of unpaired electrons there are two methods for constructing an HF wave function. One uses two completely separate sets of orbitals for α and β electrons. This method is named as unrestricted Hartree-Fock method (UHF). This will lead to spin contamination or paired electrons have different spatial distribution. It will result in an insignifcant error; the error may be large depending on the chemical system used. Though the limitations, UHF calculation are widely accepted because of its easiness to implement and run.

Restricted open shell Hartree-Fock method (ROHF) is the second way to construct wave functions for open-shell molecules. This method uses same spatial orbital for the paired electrons so there is no spin contamination. But it is more difficult to implement ROHF technique than UHF. Often this may require little more CPU time for execution. But in cases of large spin contamination then ROHF is more advisable.

1.3.4 Basis sets

A basis set is a set of functions (mathematical functions) used to describe the shape of the orbitals in an atom. These mathematical functions are called basis functions and linear combinations of basis functions and angular functions yield molecular orbitals. Semi empirical methods are usually performed on predefined basis sets. But for *ab initio* or density functional theory calculations a basis set must be specified. The type of calculation and choice of basis set determines the accuracy of results.

The basis functions are usually on atomic nuclei. The mathematical representation of atomic orbitals in a molecule is as follows.

$$\psi_i = \sum_i C_{\mu i} \Phi_\mu$$

Where $_i$- the ith molecular orbital

$C_{\mu i}$-the coefficients of linear combination

Φ_μ-μth atomic orbital

The electron distribution around an atom can be represented by hydrogen like functions, slater type functions or Gaussian type functions. Among these Slater and Gaussian types are simple functions. The hydrogen like wave functions can be represented generally as;

$$Y_{nlm} = R_{nl}(r)Y_l^m$$

Here $R_{nl}(r) = r^l e^{\frac{-zr}{na}} \sum b_j r^j$ and j varies from 0 to (n-l-1). These functions are not at all using because they are complicated and time consuming. Usually semi empirical calculations worked on Slater type orbitals whereas *ab initio* calculations employ Gaussian type functions.

A Slater type orbital can be represented as;

$$S_{nlm}(r,\theta,\phi) = \left\{ (2\zeta)^{n+0.5} \Big/ [(2n)!]^{0.5} \right\} r^{n-1} e^{-\zeta r} Y_l^m(\theta,\Phi)$$

The essential difference between hydrogen like orbital and the Slater type orbital (STO) is that STO has no nodes. And also the orbital exponent termζ, is not equal to$\frac{Z}{n}$. As for example a 2S orbital become a mixture of 1S and 2S Slater type functions in a molecular orbital calculation.

STO can represent the real situation of electron density in valence region and beyond. But they are not so good for core electron density. Different types of STO are available. A minimal basis set consists of one STO for every inner and outer shell atomic orbitals of each atom. That means in a minimal basis set the number of basis

functions will be equal to number of AOs in it. For a double zeta (DZ) basis set an STO of minimal basis set will be replaced by two STOs having different orbital exponents. In a split valence (SV) basis set each valence AO uses two STOs. Thus it has minimal basis set for inner shell AOs but DZ for valence shell AOs.

Slater type orbitals are not used nowadays because of the complex integrals from the secular determinants. Instead of STOs, Gaussian type functions (GTO) are now popular. A Gaussian type functions can be represented as follows;

$$G_{nlm}(r,\theta,\phi) = N_n r^{n-1} exp^{-\alpha r^2} Y_l^m(\theta,\Phi)$$

The term exp^{-r^2} is very easy to evaluate. GTOs can not represent the real situation of electron density as good as STOs. Use of a single Gaussian is a poor representation of an atomic wave function. Thus to solve this problem we can use several Gaussians to approximate a Slater function. The individual GTOs are called primitive Gaussian type orbitals (PGTO). And the combined functions are called contracted GTOs (CGTO).

The modern practice is that the use of basis functions as a liner combination of Gaussians. A single Gaussian and a linear combination of three Gaussians have been used to approximate the Slater function as shown. STO-1G means Slater-type orbital approximated by one Gaussian and STO-3G means Slater-type orbital (approximated by) three Gaussians. STO-3G function is the smallest basis function used in standard *ab initio* calculations by commercial programs. Based on the type and number of GTOs used to represent molecular orbitals,

basis sets are classified. Some examples are minimal basis sets, scaling basis sets etc. STO-3G, 3-21G, 6-31G*, and 6-311G* basis sets with variations obtained by adding polarization (*) and diffuse (+) functions, are the most widely-used in *ab initio* calculations.

1.3.5 Basis set super position error (BSSE)

This is not related to the method we chose but depends on the basis functions. It is the energy lowering of a complex of two molecules with respect to the sum of the individual molecule energies. BSSE usually arises when energies of two species with weak interactions like H-bond and van der Waals interactions compared to that specie having no interactions. This result in obtaining van der Waals and hydrogen bond energies that is too large because the basis functions on one molecule act to describe the electron density of the other molecule. With an exact basis set, there would be no superposition error. For minimal basis sets, the error is small which do not have diffuse functions enough to describe an adjacent atom. But when using moderate-size basis sets largest errors will take place.

The method of correcting the energies of A and B with extra functions is called the counterpoise method [16, 17]. In this procedure, the energy of complex molecules is first computed. Then individual energy of molecules is performed using all the basis functions from the complex. For this purpose, many ab initio software programs contain a mechanism for defining basis functions that are centered at a location which is not on one of the nuclei. The interaction energy is expressed

as the energy for the complex minus the individual molecular energies computed in this way.

Mathematically it is given as;

$$E_{interaction} = E_{AB}(AB) - E_{AB}(A) - E_{AB}(B)$$

Here the subscripts denote the basis functions being used and the letters in parentheses denote the molecules included in each calculation.

In theory counterpoise correction is unnecessary for large basis sets. But practically significant improvement in results has shown even for very large basis sets. For the accurate computation of molecular interaction energies by ab initio methods the use of a counterpoise correction is actually suggestive.

1.3.6 Correlation methods

The HF method has serious limitation, it does not account electron correlation instead it takes an average effect of electron repulsions. In order to overcome the errors caused by this defect correlation methods were introduced. These methods also start from HF procedure then correct for the electron correlation. By including correlation we can improve the accuracy of computed energies and molecular geometries.

a) *Moller- Plesset approach*

The Møller-Plesset (MP) approach is based on perturbation theory denoted as MP, MPPT (MP perturbation theory) or MBPT

(many-body perturbation theory) calculations. This method was described by Møller and Plesset in 1934 [18] and developed into a practical molecular computational method by Binkley and Pople [19] in 1975. The basic idea behind perturbation theory is that if we know how to treat a simple system then a more complex version of this system can be treated mathematically as an altered or perturbed version of the simple one. Since the derivation of the MP method is complicated, a general idea is discussed here. MP energy levels may be MP0, MP1, MP2 etc..... These first two designations are not actually used.

In MP2 calculations doubly excited states or doubly excited configurations interact with the ground state. For MP3 calculations doubly excited states interact with one another. That means there are integrals involving two virtual orbitals. Single, double, triple and quadruple excited states are involved in MP4 calculations. MP5 and higher expressions have also been developed. But MP2 and MP4 are by far the most popular MP levels. The MP2 calculations are much slower than HF and can be speeded to some extend by specifying MP2 (FC) meaning MP2 frozen-core. A frozen-core means that the core or nonvalence electrons are "frozen," i.e. not promoted into virtual orbitals. In full MP2 all the electrons will be taken into account in summing the contributions of excited states to the lowering of energy. Most programs like Gaussian and Spartan can perform MP2 by default when MP2 is specified. And "MP2" usually means frozen-core. MP4 calculations are sometimes done by omitting the triply excited terms

(MP4SDQ) but the most accurate and slowest implementation is MP4SDTQ (singles, doubles, triples, and quadruples).

b) *Configuration interaction (CI) method*

The MP and CI methods differ in their mathematical approaches. Configuration interaction wave functions are multiple-determinant wave functions. The construction of wave functions starts with the HF method and then modify with the addition of more determinants by promotion of occupied electrons to unoccupied orbitals. This type of calculations will be very accurate, but their computational cost is very high that means requires more CPU time. N^8 time complexity or more will be taken for calculations. Approximated excited states of the molecule along with the ground-state energy can be obtained from CIS calculations.

CI calculations are classified further on the basis of the number of excitations used to make each determinant. First one is configuration interaction single-excitation (CIS) calculation for this only one electron has been moved for each determinant. Single-and double excitation (CISD) calculations will give ground-state energies corrected for correlation. Triple-excitation (CISDT) and quadruple-excitation (CISDTQ) calculations are also available for very-high-accuracy results. A full CI means configuration interaction calculation includes all possible excitations. This method with an infinitely large basis set can provide an exact quantum mechanical result but its computational cost is very much greater.

c) *Multi-configurational self-consistent field (MCSCF)*

This is another method in which calculations based on multiple determinants, but the orbitals are optimized for use with the multiple-determinant wave function. This also can give accurate quantum mechanical results. When HF wave function produce a poor qualitative description of the system under study then the use of MCSCF or MRCI are recommended.

But these methods require more technical sophistication from user. Active space (choose which configurations are in the calculation) will be manually determined by the user. That means molecular orbitals, bonding and corresponding antibonding orbitals are correlated must be determined. The accuracy of results depends on the user's choice.

If all combinations of the active space orbitals are included in an MCSCF calculation then it is known as a CASSCF (complete active space self-consistent field) calculation. The generalized valence bond (GVB) method is a type of MCSCF with inclusion of a pair of orbitals for each molecular bond.

d) *Multi-reference configuration interaction (MRCI)*

Construction of a CI wave function from an MCSCF method instead of starting with a HF wave function is called MRCI. This wave function from which a calculation starts is called the reference state. This method has more CI determinants than in a conventional CI. Calculations are very costly. MRCI calculation with single and double

CI excitations is termed as MCSCF.1.2. In similar line, CASSCF.1.2 and GVB.1.2 calculations are also available.

e) *Coupled cluster (CC) method*

In this method the wave functions are a linear combination of many determinants. Different types of CC expansions are available like CCSD, CCSDT, and so on. CCSD (T) is a type of CC calculation method including triple excitations. Because the excitations are included in the calculation coupled cluster calculations give variational energies. The accuracy of these CI and CC methods is very similar. The CC calculation is advantageous because it is a size extensive method. When all possible configurations are included, a full coupled-cluster calculation is equivalent to a full CI calculation.

There are other methods with modifications to CI and CC. as for example, Quadratic configuration interaction calculations (QCI). It has an algorithm which is a combination of the CI and CC algorithms. These calculations are advantageous over CC because they provide an optimal amount of correlation for high-accuracy calculations on organic molecules. This method uses less CPU time.

The single- and double-excitation calculation, QCISD is also a popular method. Sometimes, triple excitations uses in calculation, QCISD (T). It can be done by perturbation method. The symmetry adapted cluster (SAC) method is a variation from coupled cluster calculations.

1.4 Density functional theory (DFT) method

In contrast to other quantum mechanical methods density functional theory (DFT) does not depend on the wave function, but on the electron probability density function or electron density function. The electron density or charge density is designated by ρ (x,y,z).

Unlike the wave function, the electron density function is measurable, by methods like X-ray diffraction or electron diffraction [20]. The electron density is a function of position only, that means it is a function of just three variables (*x, y,* z), but the wave function of an *n*-electron molecule is a function of 4*n* variables, three spatial coordinates and one spin coordinate for each electron. Hence the complexity of molecule is not a matter the electron density remains a function of three variables whereas the complexity of the wave function increases with the number of electrons.

The disadvantage of DFT method is that the wave function can be improved systematically by the use of bigger basis sets and higher correlation levels, but in DFT there is so far no known way to systematically improve the functional.

The relationship between wavefunction and electron density can be given as,

$$\rho = \sum_{i=1}^{n} n_i |\psi|^2$$

For multi electron wavefunction ρ will be complicated. Density functional theory can calculate all the properties of atoms and molecules from the electron density.

1.4.1 Kohn –sham approach

Current DFT method is based on Kohn-Sham theorems. This was set by two theorems published by Hohenberg and Kohn.

1.4.2 Hohenberg–Kohn theorems

According to first Hohenberg–Kohn [21] theorem all the properties of a molecule in a ground electronic state can be determined by the ground state electron density function i.e., ρ_0(x, y, z). Or we can in principle calculate any ground state property. For example $E_{0,}$ the energy as,

$$\rho_0(x, y, z) \rightarrow E_0$$

That means E_0 is a functional of$\rho_0(x, y, z)$. A function is a rule that transforms a number into another or the same number whereas a functional is a rule that transforms a function into a number. A functional will be a function of a "definite" function. Then first Hohenberg–Kohn theorem can be restated as any ground state property of a molecule is a functional of the ground state electron density function.

Hohenberg–Kohn second theorem states that any trial electron density function will give energy higher than or equal to the true ground state energy. The theorem can be stated mathematically as,

$$E_v[\rho_t] \geq E_0[\rho_0]$$

Where ρ_t - trail electron density

$E_0[\rho_0]$ - True ground state energy.

A trial density must satisfy the condition;

$$\int \rho_t\,(r)dr = n$$

Where *n* is the number of electrons in the molecule.

There are two basic concepts in the K-S approach to DFT are: first one is to express the molecular energy as a sum of terms, only one of which, a relatively small term, involves the unknown functional. Thus even moderately large errors in this term will not introduce large errors into the total energy. Second is the use of an initial guess of the electron density ρ in the KS equations. This is analogous to the HF equations to calculate an initial guess of the KS orbitals below. This initial guess is then used to refine these orbitals that are similar to that used in the HF SCF method. The final KS orbitals are used to calculate an electron density that can be used to calculate the energy [22].

The equation to get the Kohn- Sham energy is given below as;

$$E_0 = \langle T[\rho_0]\rangle + \langle V_{Ne}[\rho_0]\rangle + \langle V_{ee}[\rho_0]\rangle$$

The nucleus–electron potential energy term in the equation is the sum over all 2*n* electrons of the potential corresponding to attraction of an electron for all the nuclei. But other two terms in the energy equation are unknown. Then the idea of a reference system of

non interacting electrons was introduced by Kohn and Sham. According to this new concept the term $\Delta\langle T[\rho_0]\rangle$ is taken as the deviation of the real kinetic energy from that of the reference system and $\Delta\langle V_{ee}\rangle$ is the deviation of the real electron–electron repulsion energy from classical charge-cloud coulomb repulsion energy.

These two terms 1) sum of the kinetic energy deviation from the reference system and 2) the electron-electron repulsion energy deviation from the classical system is termed as exchange correlation energy functional or the exchange-correlation energy, E_{XC}

$$E_{XC}[\rho_0] \equiv \Delta\langle T[\rho_0]\rangle + \Delta\langle V_{Ne}[\rho_0]\rangle$$

Then we can derive the Kohn-Sham (KS) equation as,

$$\hat{h}^{KS}(1)_i^{KS}(1) = \in_i{}^{KS}{}_i{}^{KS}(1)$$

Where $\hat{h}^{KS}$ is the KS operator. If we knew the density function $\rho_{0(r)}$ and the exchange-correlation energy functional$E_{XC}[\rho_0]$, the KS energy equation will be exact and would give the exact energy. The solution to KS equations is similar to that of HF methods.

To find out the exchange-correlation energy functional $E_{xc}[\rho_r]$ is the main task in DFT method. Local density approximation (LDA) and local spin density approximation (LSDA) are two methods to find$E_{xc}[\rho_r]$. LDA can apply to a uniform (homogeneous) electron gas or one in which the electron density varies only very slowly with position. LDA can accurately calculate the exchange-correlation energy functional$\mathrm{E}_{\mathrm{xc}}^{\mathrm{LDA}}$. LSDA provides better results than LDA

because it accounts spin of electrons. For each α and β electrons separate KS orbitalsψ_{α}^{KS} and ψ_{β}^{KS} are assigned from which electron density ρ^{α} and ρ^{β} can be calculated. LSDA, and has the advantages that it can handle systems with one or more unpaired electrons, like radicals, and systems in which electrons are becoming unpaired, such as molecules far from their equilibrium geometries.

LSDA is equivalent to the LDA for species in which all the electrons are securely paired. And, likeE_{xc}^{LDA},E_{xc}^{LSDA} also can be accurately calculated.

1.4.3 Gradient-corrected functionals and hybrid functional

In order to avoid the shortcomings of uniform electron gas model, modern DFT methods includes gradient or slope of electron density in addition to LSDA for calculating exchange-correlation energy functional. The gradient or slope means the first derivative of electron density with respect to position. These functionals are called gradient corrected, or said to use the generalized-gradient approximation (GGA).

The exchange-correlation energy functional is the sum of an exchange-energy functional and a correlation-energy functional. The equation can be written as$E_{xc} = E_x + E_c$. Both functionals are negative and $|E_x|$ is much bigger than$|E_c|$. Hence it is clear that gradient correction to exchange-energy functional is more effective than that to correlation-energy functional.

Becke 88 functional [23] is a "new and greatly improved functional for the exchange energy" [24]. Its introduction provides much improvement in practical DFT calculations. Gill 1996 (G96) functional is another example of a gradient-corrected exchange energy functional. The Lee–Yang–Parr (LYP) and the Perdew 1986 (P86) functional are examples of gradient-corrected correlation-energy functional.

1.4.4 Hybrid functional

In HF theory the exchange energy is given as,

$$E_x = -\sum_{i=1}^{n}\sum_{j=1}^{n} K_{ij}$$

By substituting this equation in KS orbitals we get HF exchange energy as

$$E_x^{HF} = -\sum_{i=1}^{n}\sum_{j=1}^{n} \langle {}_i{}^{KS}(1)\,{}_j{}^{KS}(2) \left|\frac{1}{r_{ij}}\right| {}_i{}^{KS}(2)\,{}_j{}^{KS}(1)\rangle$$

By the inclusion of an LSDA gradient-corrected DFT expression for $E_{xc} = E_x + E_c$, we get a weighted contribution for${E_{xc}}^{HF}$. It is a HF/DFT exchange-correlation functional, commonly called a hybrid DFT functional. Exchange-energy functional developed by Becke in 1993, is the most popular hybrid functional at present. It is modified later by Stevens *et al.* in 1994 by introduction of the LYP 1988 correlation-energy functional. This exchange-correlation functional, called the Becke3LYP or B3LYP functional [25].

1.5 Objectives of the study

The main objective of the study is the application of computational methods to experimentally known systems. For this we have chosen chitosan as the "material" which is widely studied experimentally. Chitosan is a natural based biopolymer obtained from chitin. Chitin is the second most abundant natural polymer next to cellulose. The outer skeleton of insects and crustaceans like shrimp, crabs and lobster are rich sources of chitin [26]. Its alkaline deacetylation (NaOH, 40-50%) gives chitosan [27-29]. Synthesis, characteristics and applications of chitosan is still an active field of experimental studies.

Chitosan is well-known for its biocompatibility, biodegradability and low-toxicity. Because of the unique properties chitosan find numerous applications in various fields, including food, pharmaceutical, and cosmetic sciences. But the applications are limited due to the high molecular weight, high viscosity and low solubility of chitosan [30, 31]. To improve the properties of chitosan, modified forms are usually employed. Chitosan is easily amenable due to the hydroxyl and amino groups on its backbones. Modifications to chitosan include chemical, physical, and enzymatic methods. As an example,depolymerization is often applied to chitosan to obtain the oligosaccharides and/or monomers [32]. The depolymerization is often achieved via enzymatic modifications using chitonase.

Theoretical or computational developments on chitosan are very rare. The uniqueness of chitosan necessitates advanced researches

in the field. Thus we can predict new applications of chitosan . This study is a simple attempt to understand chitosan reactivity, applications as it is a more eco friendly polymer.

1.6 Programs used for the study

There are a number of computer programs available for the molecular property studies. Examples are Spartan, Gamess, Gaussian etc. [33]. Among these programs Gaussian is more user friendly and popular. It can explore many chemical areas like potential energy surfaces, reaction mechanisms, excitation energies, transition states, thermo chemistry etc. [34-36].

Gaussian is programmed with almost all computational methods currently available. It includes many SE methods, ab initio methods, MM methods, and DFT. We can predict energies of molecules, spectral properties, polarizabilities etc. using Gaussian. 2003 version of Gaussian was used for the entire work. The results were further checked with Gaussian 09 and found to be mostly the same.

The programs Gauss view and Chemcraft were utilized for construction of molecules and visualization [37, 38]. The druggability and toxicity studies of chitosan and derivatives were studied using online resources, molinspiration and OSIRIS property explorer [39,40]. OSIRIS property explorer is a free tool to predict physico-chemical and biological molecular properties. Molinspiration is another free software used for property calculations and bioactivity predictions.

References

1. P. W. Atkins, “Physical Chemistry,” 5th Edn, Freeman New York, 1994, pp.772, 773.

2. W. J. Moore, “Physical Chemistry,” 4th Edn, Prentice-Hall, New Jersey, 1972, p. 158.

3. K. B. Lipkowitz, J. Chem. Ed., 1995, *72,* 1070.

4. M. J. S. Dewar, “The Molecular Orbital Theory of Organic Chemistry,” McGraw-Hill,New York, 1969, chapter 3.

5. Chemie in unserer Zeit, 1993, *12*, 21–31.

6. J. Griffiths, Chemistry in Britain, 1986, *22*,997–1000.

7. J. A. Pople, D. L. Beveridge, and P. A. Dobosh, J. Chem. Phys., 1967, *47,* 2026.

8. R. N. Dixon, Mol. Phys., 1967, *12*, 83.

9. INDO/S: M. Kotzian, N. Rösch, and M. C. Zerner, Theor. Chim. Acta, 1992, *81,* 201.

10. ZINDO/S is a version of INDO/S with some modifications, plus the ability to handle transition metals. The Z comes from the name of the late Professor Michael C. Zerner, whose group developed the suite of (mostly SE) programs called ZINDO, which includesZINDO/S. ZINDO is available from, e.g. Molecular Simulations Inc., San Diego, CA., and CAChe Scientific, Beaverton, OR.

11. J. A. Pople, D. P. Santry, and G. A. Segal, J. Chem. Phys., 1965, *43,* S129.

12. J. A. Pople and G. A. Segal, J. Chem. Phys., 1965, *43,* S136.

13. J. A. Pople and G. A. Segal, J. Chem. Phys.,1966, *44*, 3289.

14. I. N. Levine,“Quantum Chemistry,” 4th edn, Prentice Hall, Engelwood Cliffs, New Jersey, 2000.

15. C. C. J. Roothaan, Rev. Mod. Phys., 1951, *23,* 69; G. G. Hall, Proc. Roy. Soc. (London), 1951, *A205,* 541.

16. T. Clark, "A Handbook of Computational Chemistry," Wiley, New York, 1985, pp. 289–301.

17. J. M. Martin in "Computational Thermochemistry," K. K. Irikura and D. J. Frurip, Eds., American Chemical Society, Washington, D.C., 1998, p. 223.

18. C. Møller and M. S. Plesset, Phys. Rev., 1934, *46,* 618.

19. J. S. Binkley and J. A. Pople, Int. J. Quantum Chem., 1975, *9*, 229.

20. R. F. W. Bader, "Atoms in Molecules," Oxford, New York, 1990. pp 7-8.

21. P. Hohenberg and W. Kohn, Phys. Rev. B, 1964, *136,* 864

22. Errol lewars, **"**Computational chemistry; Introduction to the Theory and Applications of Molecular and Quantum Mechanics," Kluwer academic publishers. p 390

23. A. D. Becke, Phys. Rev. A, 1988, *38,* 3098.

24. M. Head-Gordon, J. Phys. Chem., 1996, *100*, 13213

25. P. J. Stephens, F. J. Devlin, C. F. Chablowski, and M. J. Frisch, J. Phys. Chem., 1994, *98,*11623,

26. P. A .Sanford, In Chitin and Chitosan ; Skjak-Braek, G., Anthonsen,T., Sanford, P., Eds.; Elsevier: Amsterdam, 1989.

27. M. F. A. Goosen, Technomic Publishing Co., Inc.: Lancaster, PA, 1997.

28. L. K. Han, Y.Kimura, H. Okaauda, Int. J. Obes. Relat. Metab.Disord. 1999, *23*, 174.

29. X. F. Liu, Y. L. Guan, D. Z. Yang, Z. Li, K. D. Yao, J. Appl.Polym. Sci. 2001, *79*, 1324.

30. E.I. Rabea, M.E.T. Badawy, C.V. Stevens, G. Smagghe,W. Steurbaut, Bio Macromole. 2003,*4*, 1457-1465

31. Y. Luo, Q. Wang, J. Food Processing & Beverages, 2013, *1*, 1-13.

32. V. K. Mourya, N. N. Inamdar, React. Funct. Polym. 2008, *68*, 1013.

33. D.A Mc Quarrie, J.D. Simon, "Physical chemistry-A molecular approach," VLSE, 2003, New Delhi, p. 427.

34. Mahbobeh Jafari , Mehdi Salehi , Maciej Kubicki, Ali Arab, Ali Khaleghian, Inorganica Chimica Acta 2017, *462*, 329–335.

35. Najmeh Lotfi, Iran Sheikhshoaei , S. Yousef Ebrahimipour , Harald Krautscheid, J. Molecular Structure 2017,*1149*, 432-438.

36. Sonia Benabid , Tahar Douadi , Saïfi Issaadi , Christophe Penverne , Salah Chafaa, Measurement 2017, *99*, 53–63.

37. M.J. Frisch, et al., Gaussian 03, Gaussian Inc., Pittsburgh, PA, 2003.

38. http://www.chemcraftprog

39. http://www.molinspiration.com/cgi-bin/properties.

40. http://www.organic-chemistry.org/prog/peo/.

2 Chapter Literature Review

Chitin is a biopolymer having fibrous structure and is abundant in nature. The outer skeleton of insects and crustaceans like crabs, shrimp and lobster are rich sources of chitin [1]. The chemical structure of chitin is similar to cellulose, with one hydroxyl group substituted with an acetyl amine group in each monomer (Figure 2.1). The extraction can be done by demineralization of calcium carbonate with an acid. This may be done usually by hot reaction with HCl, HNO_3 etc. It is followed by a deproteinization that is removal of proteins. This step usually done by alkaline treatments, eg: NaOH [1, 2]. In the extracted crude form, chitin is highly ordered translucent, crystalline, quite tough and resilient. The solubility and reactivity is very poor.

By removing the acetyl groups chitin structure can be modified. To produce the deacetylated form, chemical hydrolysis is performed in concentrated alkaline solution at elevated temperature (Figure 2.1). When the deacetylation reaches 40-35%, a co-polymer of (1 → 4)-2-amine-2-deoxy-β-D-glucan and (1 → 4)-2-acetamide-2-deoxy-β-D-glucan is formed . It is referred to as chitosan . Characterization of chitosan is based on its degree of acetylation (DA) and molecular weight (MW). Chitosan having DA < 15% and MW between 100 and 1000 kDa is commercially available. chitosan with MW < 50 kDa is low MW, Medium MW 50 – 150 kDa, and High MW > 150 kDa.

Recent studies reports that the cultivation of fungi such as Aspergillus Niger can provide an alternative source for chitosan [3, 4]. Chitin is structurally similar to cellulose with an acetyl amine group on each monomer instead of one hydroxyl group. Molecular structure of cellulose, chitin and chitosan are depicted in Fig.2.1.

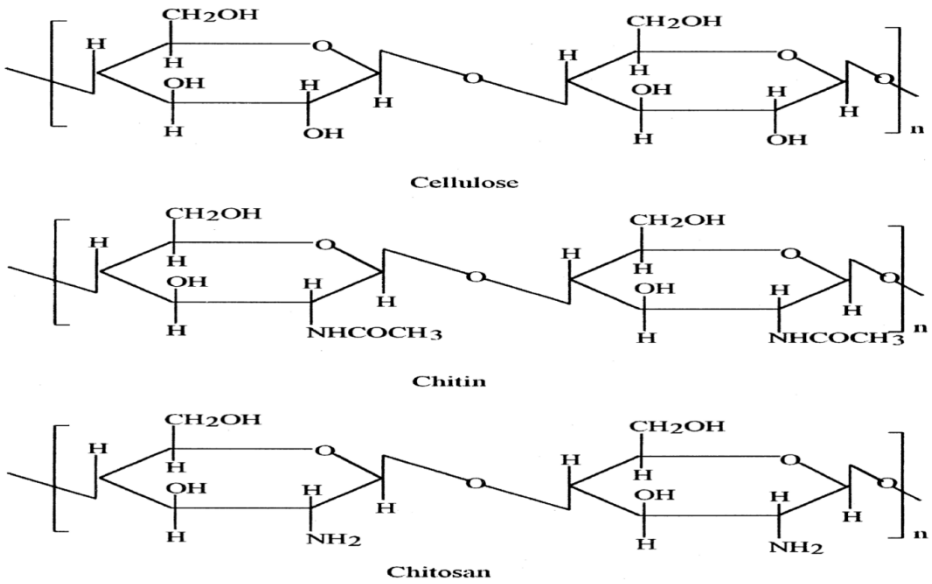

Fig.2.1 Molecular structures of cellulose, chitin and chitosan

Chitosan is a weak base and is insoluble in neutral and alkaline conditions but soluble in solutions below its pKa =~6.3 (dilute aqueous acidic). The solubility is due to conversion of insoluble -NH_2 group into the soluble protonated form -NH_3^+. The solubility of chitosan may vary with its molecular weight, degree of acetylation and biological origin [5]. Chitosan films can be prepared using this property. It is done by dipping or casting, resulting in dense and porous structure [6, 7]. Chitosan film has biofunctional activity used in living tissues as

edible coatings for prolonged shelf-life and to preserve quality of fresh foods [8].

To improve the properties of chitosan its structure can be modified. Mainly three types of modifications are possible they are chemical, physical and enzymatic modifications. Commonly used chemical modifications to chitosan are quaternization, N-alkylation, hydroxylalkylation, carboxyalkylation, thiolation, glycation, etc, [9]. The physical modifications include electromagnetic radiation and sonication. The modified chitosan will show excellent solubility in aqueous solutions at different p^H value, modulated surface charges, higher absorption efficiency, new cross linking sites, find novel applications and can be tailored for particular purpose [10].

2.1. *Derivatives of chitosan*

Schiff bases are an important class of chitosan derivatives that is widely studied and still a hot field of chitosan chemistry. This is because of its ease of formation and improved activities over chitosan . It is reported that Schiff bases show better physiological activities than pure chitosan and found applications in antibacterial, antiphlogistic and antiviral domains [11]. Also Schiff base metal complexes have catalytic property to some degree. Guo et al. reported the antioxidant activity of some Schiff bases of chitosan and carboxymethyl chitosan which was related to the concentrations of active hydroxyl and amino groups in the molecular chains [12]. Tong et al. studied chitosan -based Schiff bases and their Co (II) and Pd (II) complexes with highly

catalytic efficiency on aerobic oxidation of cyclohexane in the absence of reductants or solvents [13].

Dithiocarbamate chitosan was first synthesized by reacting chitosan with carbon disulphide [14]. Extraction of lead ions by dithiocarbamate derivative of chitosan was reported by Sharma. Antifungal activity of dithiocarbamate chitosan was studied by Qin et.al [15]. They are more potent antifungal chitosan derivatives, against some common plant pathogenic fungi.

2.2 Applications

Chitosan find applications in various fields as already mentioned. Many applications of chitosan have been reported in fields like cosmetics, photography, food, nutrition or ophthalmology [16]. It was reported as very potent in agriculture as an antimicrobial compound, in plant defense responses as a potential elicitor, in wastewater treatment as a flocculating agent, in the food industry as an additive, in cosmetics as a hydrating agent and more recently as a pharmaceutical agent in biomedicine [17-22]. Applications of chitosan originated from fungi and crustaceans include antimicrobial activity, non toxic, chelating property, film forming ability, deodorizing property, antistatic activity, polyelectrolyte nature, cost-effectiveness, chemical reactivity, thickening property, wound healing activity and dyeing improvement ability [23].

2.2.1 Antimicrobial properties

Cationic polymers are known for antimicrobial properties. Permeabilization of yeast cells is the first study in this respect; cytochrome *c* and diethylaminoethyl-dextran were used to permeabilize the yeast cell membrane [24-26]. Chitosan itself and by some derivatives can disrupt the bacterial membranes [27]. Polycationic chitosan can interact with the negatively charged membrane in bacteria and alter bacterial surface morphology. This may increases membrane permeability, causing leakage of intracellular substances, or decreases membrane functions, preventing nutrient transport [28]. The effects of Chitosan have not been fully revealed. Its usage as an antimicrobial agent is limited by its low solubility at neutral pH [29].

The antimicrobial activity of chitin and chitosan against target organisms like bacteria, algae, yeasts and fungi has been proved. Both *in vivo* and *in vitro* experiments on interactions with chitosan in different forms as solutions, films and composites were reported [30-35]. The action of chitosan may be bacteriostatic (hinders the growth of bacteria) or bacteriocidal (kills the live bacteria or some fraction therein). But recent studies consider chitosan as bacteriostatic rather than bactericidal [36]. The exact mechanism of antimicrobial activity is not fully understood yet because there are several other factors which can contribute to the antibacterial activity [37].

Three models have been proposed for the interaction between chitosan and bacteria;

i. The most acceptable mechanism is the interaction between negatively charged microbial cell membranes and positively charged chitosan molecules. An electrostatic interaction between the negative residues and the protonated NH_3^+ groups occur in this mechanism [38].

ii. Another mechanism proposed was the interaction of chitosan and microbial DNA. This interaction inhibits synthesis of the mRNA and protein because chitosan can penetrate into the nuclei of the microorganisms [39].

iii. The third mechanism is based on the metals ions chelation with chitosan . This suppresses microbial growth by reducing spore elements and binding to essential nutrients [40, 41]. Chitosan is excellent in metal-binding because the amine groups uptake metal cations by chelation [42]. At high pH this mechanism will be more efficient. Because the amine groups are unprotonated and the electron pair on the amine nitrogen is available for metal ions. The pH dependence of available sites for interacting in polysaccharide backbone is reported on the system chitosan -Cu [43]. At pH < 6 only one NH_2 group and three hydroxyls or H_2O molecules are available for the complexation. While at pH > 6.7 the interaction involve two NH_2 groups. At higher pHs, the hydroxyl groups are deprotonated and the predominant complexation is governed by two $–NH_2$ and two hydroxyl groups dissociated. Wang et al. proposed a recent model the metal is arranged in a manner that one or more chitosan chains are connected via $–NH_2$ and

forming bridges to hydroxyl groups. It thus acts as an electron acceptor [44].

Another significant factor which influences the biological activity of chitosan is its DA and MW. Influence of the MW on the antimicrobial activity is predominant than that of DA [45]. Studies carried out on *E. coli, Bacillus cereus, Staphylococcus aureus, B. subtilis, Salmonella enterica, Pseudomonas aeruginosa, Listeria monocytogenes* and *Klebsiella pneumonia* shown that for LMW chitosan, the effect for reducing microorganism growth and multiplication is greater [46-51]. It is because of the attraction, mobility and ionic interaction of small chains will be easier than that of bigger ones [52].

It is proved that antimicrobial effectiveness of chitosan is improved if the degree of acetylation is lower [53, 54]. *Aspergillus fumigatus, Aspergillus parasiticus, Fusarium oxysporum, Candida albicans* with chitin and chitosan having different DA were analyzed. All these cases proved that the antimicrobial activity is increased with decreasing DA [55-56].

2.2.2 Antifungal Activity

Chitosan is active against fungus also similar to bacteria. It is assumed to be fungistatic rather than fungicidal because it has a potential to control regulatory changes in both fungus and the host [37, 57]. Spore germination, germ tube elongation and radial growth can be effectively inhibited by chitosan [58, 59]. Yeasts and moulds associated with food and plant spoilage were studied widely in this

context. In these plant tissues chitosan can activate several biological processes. The chitinases are induced with action on necrotrophic and biotrophic mycoparasites, vesicular arbuscular mycorrhizal fungi and entomopathogenic fungi [59].

Similar to the effects observed in bacteria cells, antifungic mechanism of chitosan involves cell wall morphogenesis in which chitosan molecules directly interferes the fungal growth [58]. Microscopic studies show that chitosan oligomers can diffuse into hyphae interfering on the enzymes activity which are responsible for the fungus growth [60]. The concentration, DA and local pH influence the intensity of degradation action of chitosan into the fungal cell walls [61]. With increasing the chitosan concentration the percentage of fungus germination decreases in nutrient agar on cultures of *R. solani* and *S. rolfsii*. Influence on the length of the lag phase is observed primarily. The inhibition process shifts the medium toward alkalinity which reduces the effectiveness of the chitosan [61].

2.2.3 Antilipidemic activity

Chitosan is also used as a dietary antilipidemic supplement. Lipid hydrolysis by human digestive enzymes is limited. Chitosan passes along the digestive system acting effectively like a dietary fiber. The anti hyper lipidemic action of chitosan was previously reported [62-64]. The acidic environment of the stomach makes chitosan a positively charged gel due to swelling. These positively charged gels can attract negatively charged molecules of fats, fatty acids and bile

acids to form ionic complexes. Chitosan can also form hydrophobic complexes with neutral lipids such as cholesterol and other sterols.

2.2.4 Metal chelation

Metal chelation is an important and widely studied application of chitosan . Derivatives of chitosan also studied for their metal chelating ability. Metal adsorption property can be easily explained by the presence of free amino groups on the polymer matrix, which can interact with metal ions of the solution by ion exchange or other complexation reactions [66, 67]. The reactive amino group of chitosan selectively binds to virtually all transition metal ions but does not bind to alkali and alkaline earth metal ions [68-73].

Chemical modifications to chitosan improve its adsorption features, such as selectivity and adsorption capacity [74, 75]. The adsorption capacity can be further improved by cross-linking with reagents such as glutaraldehyde, tripolyphosphate salts, ethylene glycol, epichlorohydrin or diglycidyl ether can stabilize chitosan in acid solutions and increase its mechanical properties [76]. Chitosan is characterized as a metal super adsorbent for Cu(II), Cd(II), Pb(II), Hg(II), Cr(VI), Ni(II),U(VI), Pd(II), Pt(IV), Au(III), Mo(V), V(V),As(V), Se(V) [66,77]. The adsorption capacity depends on (i) the type of chitosan (powder, beads), (ii) the chemical modifications possible (cross-linking, grafting reactions), (iii) the different experimental conditions (pH, conditioning, particle size and composition of the solution) etc. [66].

Due to this property they can be used in water purification processes, metal extraction fields etc. some metal complexes show catalytic property also [78]. Use of chitosan as a material for recovery of metal ions was much reported [66, 79-82]. Conventional methods of extraction of metal ions from effluents such as flotation, solvent extraction, precipitation, ion-exchange and electrochemical separation [83] suffer problems like excessive time requirements, high costs and production of highly toxic sledges. Recently alternative methods such as sorption techniques have been applied using activated carbon, clays, fly ash, biomass, etc [84-87]. Uptake of mercury and uranyl ions with glutaraldehyde crosslinked chitosan was reported by Atia et.al [88].

2.2.5 Corrosion inhibition

Corrosion of metals is a severe problem that has technical, economical, environmental, and aesthetical importance. Hence its control is also important in industrial point of view. A best option for protecting metals and alloys against corrosion is the use of inhibitors. There are several organic and inorganic corrosion inhibitors but their toxicity necessitates green corrosion inhibitors or environmental friendly corrosion inhibitors. Such investigations results in the use of polymeric substances that are environmentally friendly, ecologically acceptable, inexpensive, readily available, and renewable materials.

The use of smart coatings for controlled release of active species is a topic that covers corrosion protection. The intrinsic properties of chitosan , such as biocompatibility, antimicrobial activity, biodegradability and excellent film-forming ability, make chitosan as

a potential coating system [89, 90]. But the use of chitosan as corrosion inhibitor is less reported. Chitosan is reported for the controllable release of active agents, as well as for functional coatings [16, 91, 92]. Additionally some recent reports show the use of chitosan and its derivatives as protective coatings [88, 93]. The use of chitosan thin film as a pre-layer reservoir for the immobilization of a corrosion inhibitor near the metallic surface and its prolonged delivery was reported by Zheludkevich et.al [94]. Previously chitosan - mercaptobenzothioazole was investigated as a polymeric coating system for protection of aluminum alloy 2024 [95]. Chitosan was reported as an inhibitor for copper corrosion in acidic medium [96].

References

1. P. A. Sanford, In *Chitin and Chitosan* ; G. Skjak-Braek, T. Anthonsen, P.Sanford, Eds.; Elsevier: Amsterdam, 1989.

2. M. F. A. Goosen, Technomic Publishing Co., Inc.: Lancaster, PA, 1997.

3. W. L. Teng, E. Khor, T. K. Tan, L. Y.Lim, S. C. Tan, Carbohydr.Res. 2001, *332*, 305.

4. P. Pochanavanich, W. Suntornsuk, Lett. Appl. Microbiol. 2002, *35*, 17.

5. R. Shepherd, S. Reader, A. Falshaw, Glycoconjugate J. 1997, *14*, 535.

6. O. B. G. Assis, R. Bernardes Filho, D. C. Viera, S. P. Campana Filho, Int. J. Polymer. Mater. 2002, 51, 633.

7. O. B. G. Assis, V. L. Silva, Polímeros: Ciência & Tecnologia. 2003, *13*, 223.

8. O. B. G. Assis, J. D. C. Pessoa, Braz. J. Food Technol. 2004, *7,* 17.

9. V. K. Mourya, N. N. Inamdar, React. Funct. Polym. 2008, *68*, 1013.

10. Y. Luo, Q. Wang,J.Food Processing&Beverages. 2013,*1*,1.

11. E. Ispir, Dyes Pigments, 2009, *82*, 13.

12. Z.Y. Guo, R.G. Xing, S. Liu, H.H. Yu, P.B. Wang, C.P. Li, P.C. Li, Bioorg.Med.Chem. Lett. 2005, *15*, 4600.

13. J.H. Tong, Z. Li, C.G. Xia, J.Mol.Catal.A.Chem. 2005,*231*,197.

14. R. A. A. Muzzarelli, F. Tanfani, Pure and Applied Chemistry .1982,*54(11),* 2141.

15. Yukun Qin, Song Liu , Ronge Xing, Huahua Yu , Kecheng Li, Xiangtao Menga , Rongfeng Li, Pengcheng Li ,Carbohydrate Polymers .2012, *89* ,388.

16. M.N.V. Ravi Kumar, React. Funct. Polym. 2000, *46*, 1.

17. V.R. Sinha, A.K. Singla, S .Wadhawan, R. Kaushik, R .Kumria, K .Bansal, S. Dhawan, Int. J.Pharm.2004, *274*, 1.

18. N. Velmurugan, G.G. Kumar, S.S. Han, K.S. Nahm, Y.S. Lee, Iran Polym. J. 2009, *18*, 383.

19. K.S.V. Krishna Rao, K. Madhusudana Rao, P.V. Nagendra Kumar, I-D Chung, Iran Polym J. 2010, *19*,265.

20. K. Aiedeh, M. O. Taha, Eur. J. Pharm. Sci. 2001, *13*, 159.

21. T.Ishii, Y. Okahata, T. Sato, Biochim. Biophys. Acta 2001, *1514*,51

22. E. Pascual, M. R. Julia, J. Biotechnol. 2001, *89*, 289.

23. Shahid-ul-Islam, Mohammad Shahid, Faqeer Mohammad, Ind. Eng. Chem. Res. 2013, *52*, 5245.

24. D. A. Yphantis, J. L. Dainko, F. Schlenk, Journal of Bacteriology. 1967, *94*, 1509.

25. M. Durr, T. Boller, A. Wiemken, Archives of Microbiology.1975, *105*, 319.

26. V. Huber-Walchli, A. Wiemken, Archives of Microbiology. 1979,*120*, 141.

27. J. Y. Je, S. K. Kim, Journal of Agricultural and Food Chemistry.2006, *54*, 6629.

28. X. Meng, R. Xing, S. Liu et al., International Journal of Biological Macromolecules.2012, *50*, 918.

29. E. I. Rabea, M. E.-T. Badawy, C. V. Stevens, G. Smagghe, W. Steurbaut, Biomacromolecules.2003, *4(6)*, 1457.

30. C. S. Chen, W. Y. Liau, G. J Tsai, J. Food Prot. 1998, *61*, 1124.

31. L. A. Hadwiger, D. G. Kendra, B. W. Fristensky, W. Wagoner, *Chitosan both activated genes in plants and inhibits RNA synthesis in fungi*, *in:* "Chitin in nature and technology". R. A. A. Muzzarelli, C. Jeuniaux, G. W. Gooday, (Eds.), Plenum, New York (1981).

32. A. M. Papineau, D. G. Hoover, D. Knorr, D. F. Farkas, Food Biotechnol. 1991, *5*, 45.

33. F. Shahidi, J. Arachchi, Y. J. Jeon, Trends Food Sci. Technol. 1999, *10*, 37.

34. N. R. Sudarshan, D. G. Hoover, D. Knorr, Food Biotechnol. 1992, *6,* 257.

35. D. H.Young, H. Kohle, H. Kauss, Plant Physiol. 1982, *70*, 1449.

36. V.Coma, A. Martial-Gros, S. Garreau, A. Copinet, F. Salin, A. Deschamps, J.Food Sci. 2002, *67*, 1162.

37. D. Raafat, K. von Bargen, A. Haas, H. G. Sahl, Appl. Environ. Microbiol. 2008, *74*, 3764.

38. G. J. Tsai, W. H. Su, J. Food. Prot. 1999, *62*, 239.

39. I. Sebti, A. Martial-Gros, A. Carnet-Pantiez, S. Grelier, V. Coma, J. Food Sci. 2005,*70*, 100.

40. R. G.Cuero, G. Osuji, A. Washington, Biotechnol.Lett. 1991, *13*, 441.

41. S. Roller, N. Covill, Int. J. Food Microbiol. 1999, *47*, 67.

42. I. M. Helander, E. L. Nurmiaho-Lassila, R. Ahvenainen, J. Rhoades, S. Roller, Int. J. Food Microbiol. 2001, *30*, 235.

43. E. Guibal, Sep. Purif. Techn. 2004, *38*, 43.

44. X. Wang, Y. Du, L. Fan, H. Liu, Y. Hu, Polymer Bulletin.2005, *55*, 105.

45. S. Sekiguchi, Y. Miura, H. Kaneko, S. I. Nishimura, N. Nishi, M. Iwase, S. Tokura, *Molecular weight dependency of*

antimicrobial activity by chitosan oligomers, *in:* K. Nishinari, E. Doi, (Eds), "Food Hydrocolloids: Structures, Properties and Functions", Plenum Press, New York (1994).

46. Y. J. Jing, Y. J. Hao, H. Qu, Y. Shan, D. S. Li, R. Q. Du, Acta Biologica Hungarica.2007, *58*, 75.

47. B. O. Jung, S. J. Chung, G. W. Lee, J. Chitin Chitosan .2002*, 7*,231.

48. Y. Omura, M. Shigemoto, T. Akiyama, H. Saimoto, Y. Shigemasa, I. Nakamura, T. Tsuchido, Biocontrol. Sci. 2003, *8*, 25.

49. V. E. Tikhonov, E. A. Stepnova, V. G. Babak, I. A. Yamskov, J. Palma-Guerrero, H. B. Jansson, L. V. Lopez-Llorca, J. Salinas, D. V. Gerasimenko, I. D.Avdienko, V. P. Varlamov, Carbohyd. Polym. 2006, *64*, 66.

50. G. J. Tsai, S. L. Zhang, P. L. Shieh, J. Food Prot. 2004, *67*, 396.

51. S. Zivanovic, C. C. Basurto, S. Chi, P. M. Davidson, J. Weiss, J. Food Prot. 2004, *67*, 952.

52. A. B. V. Kumar, M. C. Varadaraj, L. R. Gowda, R. N. Tharanathan, Biochem. J. 2005, *391*, 167.

53. Y. Andres, L. Giraud, C. Gerente, P. Le Cloirec, Environ. Technol. 2007, *28*, 1357.

54. T. Hongpattarakere, O.Riyaphan, Songklanakarin J. Sci. Technol. 2008, *30*, 1.

55. G. J.Tsai, W. H. Su, H. C. Chen, C. L. Pan, Fisheries Sci. 2002, *68*, 170.

56. A. El Ghaouth, J. Arul, J. Grenier, A. Asselin, Phytopathology.1992, *82*, 398.

57. A. S. Sashai, M. S. Manocha, FEMS Microbiol. Rev. 1993, *11*, 317.

58. M. Eweis, S. S. Elkholy, M. Z. Elsabee, Int. J. Biological Macrom. 2006, *38*, 1.

59. O. Stössel, J. L. Leuba, J. Phytopathol. 1984, *111*, 82.

60. L. M. Prescott, J. P. Harley, D. A. Klein, "Microbiology", McGraw-Hill Co., New York (2002).

61. V.Coma, A. Deschamps, A. Martial-Gros, J. Food Sci. 2003, *68*, 2788.

62. P. K. Dutta, S. Tripath, G. K. Mehrotra, Dutta, J. Food Chem. 2009, *114*, 1173.

63. K. M. Shields, Am. J. Health-Syst. Pharm. 2003, *60*, 1310.

64. R. Ylitalo, S. Lehtinen, E. Wuolijoki, P. Ylitalo, T.Lehtima¨ki, Arzneim.-Forsch. 2002, *52*, 1.

65. R. A. A. Muzzarelli, Carbohydr. Polym. 1996, *29*, 309.

66. A.A. Radwan, F.K. Alanazi, I.A. Alsarra, Molecules. 2010, *15*, 6257.

67. R. A. A. Muzzarelli, Natural chelating polymers. Pergamon Press. Oxford, New York, USA. pp. 83 (1973).

68. J. R. Deans, B. G. Dixon, Water Research.1992, *26*, 469.

69. R. A. A. Muzzarelli, Chitin. Oxford: Pergamon Press. (1977).

70. R. A. A. Muzzarelli, In: Chitin in Nat. Technol., [Proc. Int. Conf. Chitin Chitosan], 3rd, Meeting Date 1985, R. A. A. Muzzarelli, C. Jeuniaux, & G. W. Gooday, (Eds.), pp. 321–30, New York, N.Y.:Plenum(1986).

71. C. Peniche-Covas, L. W. Alvarez, W. Arguelles-Monal, Journal of Applied Polymer Science.1992, *46*, 1147.

72. P. Udaybhaskar, Journal of Applied Polymer Science.1990, *39*, 739.

73. P. Chassary, T. Vincent, E. Guibal, React. Funct. Polym. 2004, *60*, 137.

74. A.C.L. Batista, E.R. Villanueva, R.V.S. Amorim, M.T. Tavares, G.M. Campos-Takaki, Molecules. 2011, *16*, 3569.

75. G. Kim, N. Kim, D. Kim, J. Kwon, B.-H. Min, Molecules. 2012, *17*, 13704.

76. A. J. Varma, S. V. Deshpande, J. F. Kennedy, Carbohydrate Polymers.2004, *55*, 77.

77. S.E.S. Leonhardt, A. Stolle, B. Ondruschka, G .Cravotto, C. De Leo, K.D. Jandt, T.F. Keller, Appl Catal AGen. 2010,*379*, 30.

78. S.T. Lee, F.L. Mi, Y.J. Shen, S.S. Shyu, Polymer .2001, *42*, 1879.

79. M.L. Arrascue, H.M. Garcia, O. Horna, E. Guibal, Hydrometallurgy. 2003,*71*,191.

80. G. Ca´rdenas, P. Orlando, T. Edelio, International Journal of Biological Macromolecules. 2001,*28*,167.

81. Y. Kawamura, H. Yoshida, S. Asai, H. Tanibe, Water Science and Technology. 1997, *35(7)*, 97.

82. Y. Kawamura, H. Yoshida, S. Asai, H. Tanibe, Journal of Chemical Engineering of Japan .1998,*31 (1),* 115.

83. V.I.E.Ajiwe, I.E. Anyadiegwu, Separation and Purification Technology. 2000, *18*, 89.

84. L. Dambies, E. Guibal, A. Roze, Colloids and Surfaces. 2000, *170*, 19.

85. P. Malakul, K.R. Srinivasan, H.Y. Wang, Industrial and Engineering Chemistry Research .1998, *37,* 4296.

86. N.L.D. Filho, Y. Gushikem, W.L. Polito, Analytica ChimicaActa .1995, *306*, 167.

87. G. Absalan, M.A. Mehrdjardy, Separation and Purification Technology .2003,*33 (1)*, 95.

88. A. A. Atia, M. D. Ahmed, K. Z. Elwakeel, Reactive & Functional Polymers.2005, *65*, 267.

89. B. Ghosh, M. W. Urban, Science.2009, *323*, 1458.

90. C. Peniche, W. Arg¨uelles-Monal, F. M. Goycoolea, "Monomers, Polymers and Composites from Renewable Resources", Elsevier, Amsterdam (2008).

91. M. Rinaudo, Prog. Polym. Sci. 2006, *31*, 603.

92. J. Berger, M. Reist, J. M. Mayer, O. Felt, N. A. Peppas ,R. Gurny, Eur. J. Pharm. Biopharm. 2004, *57*, 19

93. Y. Yuan, B. M. Chesnutt, L. Wright, W. O. Haggard ,J. D. Bumgardner, J. Biomed. Mater. Res., Part B.2008, *86*, 245.

94. M. L. Zheludkevich, J. Tedim,C. S. R. Freire, S. C. M. Fernandes, S. Kallip,A. Lisenkov,A. Gandini, M. G. S. Ferreira, J. Mater. Chem. 2011, *21*, 4805.

95. Jorge Carneiro, Joao Tedim, Susana C. M. Fernandes, Carmen S. R. Freire,Alessandro Gandini, M´ario G. S. Ferreira, Mikhail L. Zheludkevicha; ECS Electrochemistry Letters.2013, *2 (6),* C19.

96. Mahmoud N. El-Haddad, International Journal of Biological Macromolecules 2013, *55* 142.

3 Chapter Materials and Methods

The present work is surface activity study of chitosan monomer and some of its derivatives. For this at first chitosan monomer has to be modelled. A monomer of chitosan was built up with Gauss view program. This geometry was optimized to minimum energy. Derivatives were constructed from the optimized minimum energy structure of chitosan monomer.

Schiff bases of chitosan including both aliphatic and aromatic substituents. Their N-reduced/alkylated forms also modeled and studied. Aliphatic Schiff bases: citral (CC),pyruvate (PyC) and glyoxylic acid (GC) derivatives. Aromatic Schiff bases: salicylaldehyde (SC), pyridoxal (PC) and pyridyl methyl (PMC) derivatives. Corresponding N-reduced forms are CCR,PyCR,GCR,SCR,PCR and PMCR respectively. The properties of these derivatives were studied and compared with that of chitosan. Properties such as polarizability, reactivity were examined. All of the derivatives show better reactivity than chitosan monomer. The variation in the properties depends on the groups attached to each derivative.

Citral is a natural open chain aldehyde found in the oil of lemon grass, orange, lemon etc. Citral has application in the field of cosmetics and scents. Adsorption behavior of Pb (II) and Hg (II) ions

onto CC were reported by Alikutty et.al [1]. Fig.3.1 shows a monomer of CC.

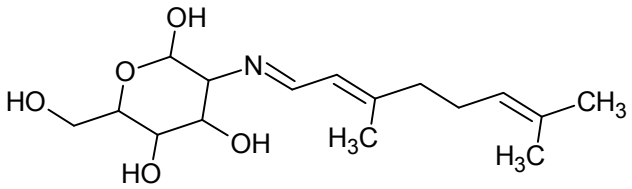

Fig.3.1 Molecular structure of CC

A long chain of aliphatic group is attached to chitosan monomer in CC. in CCR the imine group (-N=C<) will be reduced and we get an N-alkylated product.

Derivatives of Chitosan with ketoacids were effective for removal of Co^{60} from nuclear plant wastewaters. It is also better for uranium removal from dilute solutions and from saline waters [2,3]. Another report shows that pyruvic acid –it is the simplest of α-keto acids-modified chitosan had higher adsorption capacities for metal ions of Cu, Zn and Co [4]. Second derivative of chitosan is from pyruvate. It can form imine with chitosan. The following figure depicts the structure of PyC.

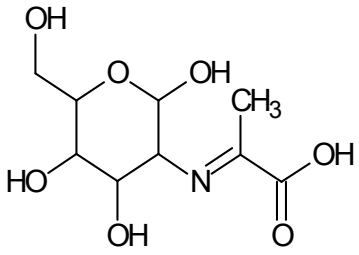

Fig.3.2 Structure of PyC

PyC has –COOH group attached to chitosan moiety. Alkaline reduction of this Schiff base also yields an N-alkylated product PyCR.

Glyoxylic acid or oxoacetic acid occurs naturally. It is widely used to introduce carboxymethyl group to chitosan. From glyoxylic acid, water soluble N-carboxymethyl chitosan can be prepared. N-carboxy methyl chitosan is a costly functional ingredient of cosmetic hydrating creams due to its durable moisturizing effect on the skin [5]. It is also a good adsorbent of metal ions. Adsorption capacity of N-carboxy methyl chitosan towards Au (III) ions was reported [6]. A review of carboxy methyl chitosan and its applications were reported by Mourya et.al [7]. Figure 3.3 shows the molecular structure of GC.

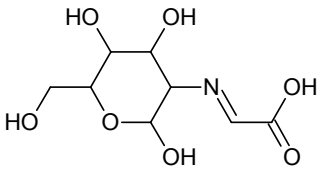

Fig.3.3 GC structure

Salicylaldehyde is a key precursor to a variety of chelating agents. An aromatic group is introduced to chitosan when reacting with salicylaldehyde [4]. The structure of SC is depicted in fig.3.4.

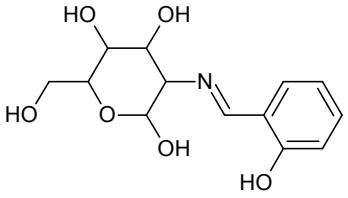

Fig.3.4 Molecular structure of SC

Pyridine derivatives were introduced into the polymer backbone of chitosan in order to improve the polymer properties including the solubility, physicochemical and biological properties. The introduction of pyridine derivatives into the chitosan backbone has recently gained interest because it can be applied in metal absorption antimicrobial activity, gene delivery sensor application and biomedical application [8]. Here 2-pyridinecarbaldehyde was introduced to chitosan to get pyridyl methyl chitosan (PMC) Schiff base and N-reduced (PMCR).

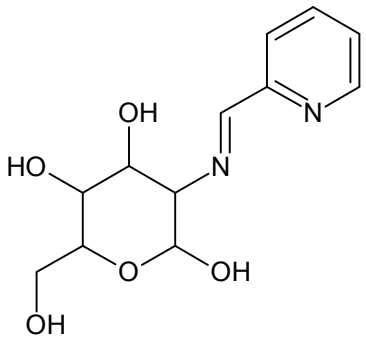

Fig.3.5 Structure of PMC

Chitosan –pyridoxal derivatives were synthesized by reacting chitosan with pyridoxal hydrochloride and then reducing the product formed with sodium cyanoborohydride [9]. The derivative showed enhanced adsorption capacities for Cu (II), Pb (II) and Fe (III) than chitosan .

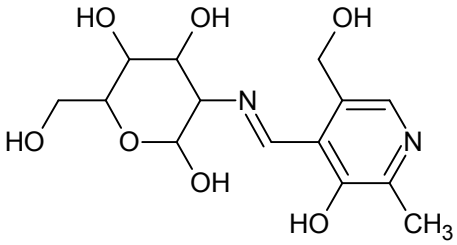

Fig 3.6 Structure of PC

An aromatic ring with more substituents is attached to chitosan in PC. The fig.3.6 shows the molecular structure of PC.

Applications of chitosan and the above derivatives also studied. Metal chelation, corrosion inhibition and druggability of the derivatives were studied and compared with chitosan monomer.

3.1 Methods

3.1.1 Geometry optimization

The process of finding out the energy minimum structure (conformation) of the required molecule is known as geometry optimization. This can be achieved with a potential energy surface (PES) scanning process. PES is a plot of energy against some geometric parameters like bond lengths, bond angles, dihedral angles etc. If energy is plotted against only one variable then we get a 2D surface. And for a plot with energy against two variables the result will be 3D. So as the variables increased the plot become more and more complicated [10].

The procedure starts with initial wave function and calculates energy then move to a new geometry having lower energy. This

process repeats until geometry with lowest energy which is close to the initial structure is obtained. In the energy minimization process some gradient points in the PES with respect to electronic energy will be found out. Gradient can be defined as a vector constituted by 3N-6 first partial derivatives of energy with respect to the variables on which energy is dependent. The point on the PES where gradient is zero is called a stationary or critical point. These points may constitute a minimum, maximum or a saddle point.

Saddle point will be energy maximum in one direction and energy minimum in other directions. Saddle points are actually a transition state between two equilibrium states. The lowest energy point or trough in the PES corresponds to the global minimum structure. Other minima are called local minimum structures. A typical plot of PES is depicted in fig.3.7.

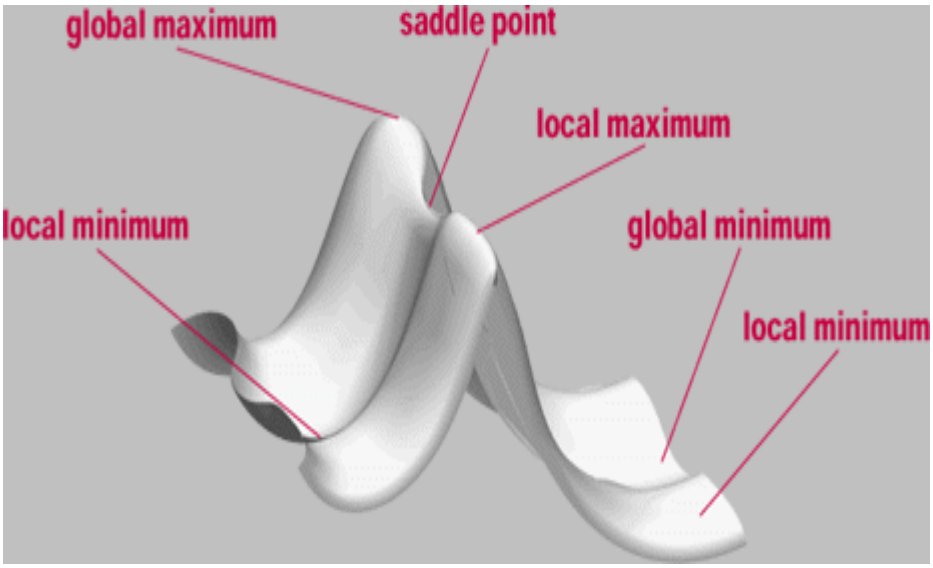

Fig.3.7 Schematic representation of PES

3.1.2 Frequency calculation

We have carried out frequency calculation along with every optimization process. A frequency calculation result has two benefits. First of all we can find out the infrared and Raman intensities. And the second is that it is possible to check whether the obtained geometry from the optimization is local or global minimum or a transition state. For a local or global minimum structure we get all the calculated frequencies are real and positive. But for transition state structure, the some of the frequencies will be complex and printed as negative values. This is called as imaginary frequency. Well behaved transition state structure of a reaction has one imaginary frequency.

3.1.3 Natural bond orbital (NBO) analysis

Natural bond orbital (NBO) method is a localization method that can closely describe the chemical concepts. The method was developed by Weinhold and co-workers [11]. Orbitals that are closely associated entirely with a single atom are termed as core orbitals. In NBO procedure these core orbitals and other orbitals associated with a single atom like lone pairs are at first localized and called as natural atomic orbitals (NAOs). Next, orbitals involving bonding or antibonding between pairs of atoms are localized by using only the basis set AOs of those atoms. Remaining Rydberg-like orbitals can be identified and all other orbitals are made orthogonal to one another. As a result, all NAOs and Rydberg orbitals are described using the basis-set AOs of a single atom and all NBOs are described using the basis-set AOs of two atoms. In cases where resonance or other delocalization effects exists, additional work is required. Therefore NBO analysis can

provide an orbital picture that is as close as possible to a classical Lewis structure for a molecule.

NBO method is very useful for the assignment of hybridization both to the atomic lone pairs and to each atom's contributions to its bond orbitals. Hybridization is a widely accepted chemical concept even though it has no formal basis in the absence of high-symmetry constraints. The NBO localization analysis will give the percent s and p character (and d, f, etc.) from the coefficients of the AO basis functions from which the NAO or NBO is formed. The partial atomic charges also can be evaluated using NBOs with natural population analysis (NPA).

Hyperconjugation is a useful chemical concept that can rationalize certain chemical phenomena in terms of filled-orbital–empty-orbital interactions. NBO analysis can be used to quantify this phenomenon. Since the NBOs do not diagonalize the Fock operator (or the Kohn–Sham operator, if the analysis is carried out for DFT instead of HF), when the Fock matrix is formed in the NBO basis, off-diagonal elements will in general be non-zero. Second-order perturbation theory indicates that these off-diagonal elements between filled and empty NBOs can be interpreted as the stabilization energies. Thus NBO approach can be used to other analyses focusing on structural changes or changes in partial atomic charges in the investigation of hyperconjugative effects. Since NBO procedure is based on orbitals some limitations can be expected in cases where chemical species are poorly represented as Lewis structures.

Natural bond orbital (NBO) analysis is a technique introduced to understand chemical interaction of hyper conjugation and electron

density transfer (EDT) from filled lone pairs of electron (Lewis base) into the unfiled antibonds (Lewis acid) in hydrogen bonding systems[11]. A filled bonding or lone pair orbital can act as a donor and an empty or filled bonding, antibonding or lone pair orbital can act as an acceptor. These interactions may strengthen or weaken bonds. The NBO method demonstrates the bonding concepts like Lewis structure, bond type, atomic charge, hybridization, charge transfer, bond order, and resonance weights. This analysis is useful in understanding delocalization of electron density from occupied Lewis-type or donor NBOs to properly unoccupied non- Lewis type or acceptor NBOs within the molecule. The stabilization of orbital interaction is proportional to the energy difference between interacting orbits. Therefore, the interaction having strongest stabilization takes place between effective donor and effective acceptors.

Estimation of energetic importance of NBOs' was done by second order Perturbation theory [12]. The interaction between bonding and anti bonding orbitals can be quantitatively described in terms of the NBO approach that is expressed by means of $E^{(2)}$ second-order perturbation interaction energy [13-15]. This energy represents the measure of the off-diagonal NBO Fock matrix element. The energy of stabilization $E^{(2)}$ is associated with i (donor) and j (acceptor). Delocalization can be calculated from the second order perturbation approach [16] as given below

$$E^{(2)} = -q_i \frac{(F_{i,j})^2}{\epsilon_j - \epsilon_i}$$

$E^{(2)}$-- Energy of hyper conjugative interaction (stabilization energy).

$\in_j - \in_i$ – Energy difference between donor and acceptor i and j NBO orbitals

$(F_{i,j})$ – Fock matrix element between i and j NBO orbitals.

3.1.4 Polarizability and hyper polarizability

The distribution of charge within the molecule affects properties like atomic charges, dipole moment and polarizability tensor. Quantum computation methods promise an inexpensive way to evaluate the NLO properties of materials by theoretical calculations based on the polarizability calculations. Electric dipole moment, the isotropic polarizability and the first hyperpolarizability can be used to understand the microscopic NLO mechanism of molecules. Polarizability is the measure of the change in electron distribution of a molecule in response to an applied electric field, or otherwise can be induced by electric interactions with solvents or ionic reagents. The charge density in a molecule can be measured from permanent electric dipole moment. The magnitude and direction of dipole moment is being sensitive to shape and molecular size. It acts as an indicator of physical, chemical and biological properties exhibited by molecule.

The molecule having polarizability values $\alpha_{XX} = \alpha_{YY} = \alpha_{ZZ}$ said to be isotropic. If the molecule is anisotropic, then polarizability is $\alpha_{XX} \neq \alpha_{YY} \neq \alpha_{ZZ}$. The intensity of Raman scattering may be proportional to the derived polarizability components. To express the scattering intensity in terms of the derived polarizability tensor, the quantities (α') and the anisotropy invariant (γ) are necessary. The quantity (α') is the mean value of the three principle components of (α') and (γ)

measures the anisotropy of the tensor. The definitions [17] for the isotropic polarizability are given as:

$$\alpha' = \frac{1}{3}\left(\alpha_{xx} + \alpha_{yy} + \alpha_{zz}\right)$$

Hyper polarizability can be expressed as;

$$\beta_{total} = \sqrt{\beta_x^2} + \sqrt{\beta_y^2} + \sqrt{\beta_z^2}$$

The polarizability anisotropic invariant is given as follows,

$$\gamma^2 = \frac{1}{2}\left[(\alpha_{xx} - \alpha_{yy})^2 + (\alpha_{yy} - \alpha_{zz})^2 + (\alpha_{zz} - \alpha_{xx})^2 + 6\,(\alpha_{xy}{}^2 + \alpha_{yz}{}^2 + \alpha_{xz}{}^2)\right]$$

3.1.5 Reactivity parameters

HOMO and LUMO analysis gives an idea into stability and hence reactivity of molecules. HOMO gives the electron donating capacity whereas LUMO energy represents electron acceptance of the molecules. The global reactivity parameters such as hardness (η), softness ($S = \frac{1}{\eta}$) , chemical potential etc. can be evaluated from these two orbitals. The maximum hardness or absolute hardness (η) of a system having N electrons and total energy E is given as [18]:

$$\eta = \left(\frac{\partial^2 E}{\partial N^2}\right)_{v(r)} \approx \frac{1}{2}(IE - EA) \approx \frac{1}{2}(E_{LUMO} - E_{HOMO})$$

Where IE is the vertical ionization energy given as -E_{HOMO} and EA is vertical electron affinity as - E_{LUMO}[19]. Global softness is the reciprocal of hardness ($S = \frac{1}{\eta}$). As the harness value increase the

stability of molecules increase and therefore reactivity decreases. Electron affinity can be calculated from the equation;

$$\chi = -\mu = \left(\frac{\partial E}{\partial N}\right)_{v(r)} \approx \frac{1}{2}(IE + EA) \approx -\frac{1}{2}(E_{LUMO} - E_{HOMO})$$

The global electrophilicity index (ω) is given as:

$$\omega = \frac{\mu^2}{2\eta}$$

These reactivity descriptors are used to predict the reactivity of chitosan and derivatives in the present study.

References

1. P. Alikutty, V. M. Abdul Mujeeb, M. A. Zubair, K. Muraleedharan, P. Mujeeb Rahman, Polym. Bull. 2014,*71*,1919.

2. R. A. A. Muzzarelli, Carbohydrate Polymer.1984, *5(2),* 85.

3. R. A. A. Muzzarelli, In: Chitin in Nat. Technol., [Proc. Int. Conf. Chitin Chitosan], 3rd, Meeting Date 1985, R. A. A. Muzzarelli, C. Jeuniaux, & G. W. Gooday, (Eds.), pp. 321–30, New York, N.Y.: Plenum(1986).

4. Q. Ma, Z. Zou, Y. Gao, Xiandai Huagong. 2000, *20(10)*, 44.

5. R. Lapasin, S. Stefancic, F. Delben, Agro-Food Ind. High Tech. 1996, *7*, 12.

6. W.S.W. Ngah, K.H. Liang, Ind. Eng. Chem. Res. 1999, *38*, 1411.

7. V.K Mourya, N.N. Inamdar, A. Tiwari, Adv. Mat. Lett. 2010*,* *1(1)*, 11.

8. C. A. Rodrigues, M. C. Laranjeira, F. De, T. Valfredo, E. Sadler, Polymer. 1998, *39(21)*, 5121.

9. C. L. Lasko, B. M. Pesic, D. J. Oliver, Journal of Applied Polymer Science.1993, *48(9)*, 1565.

10. Errol lewars, **"**Computational chemistry; Introduction to the Theory and Applications of Molecular and Quantum Mechanics," Kluwer academic publishers. p 10.

11. A. E. Reed, L. A. Curtiss, F. Weinhold, Chem. Rev. 1988, *88*, 899.

12. R. John Xavier, P. Dinesh, Spectrochimica Acta Part A: Molecular and Biomolecular Spectroscopy .2014, *128*, 54.

13. A.E. Reed, F. Weinhold, J. Chem. Phys. 1985,*83*,1736.

14. A.E. Reed, R.B. Wainstock, F. Weinhold, J. Chem. Phys. 2004, *84,677*.

15. A.E. Reed, F. Weinhold, J. Am. Chem. Soc. 1980,*102*, 7211.

16. P.V.R. Schieyer, N.L. Allinger, T. Clark, J. Gasteiger, P.A. Kolmann, H.F. Schaefer, R.R. Schreiner, "The Encyclopedia of Computational Chemistry," John Willy and Son, Chichester, 1998.

17. M. Silverstein, G. Clayton, C. Morill, "Spectrometric Identification of Organic Compounds," Wiley, New York, 2001.

18. Z. Zhou, H.V Navangul, J.Physc.Org.Chem. 1990, *3*,784.

19. T.Koopmans, Physica.1934, *1,*104.

4 Chapter Modeling and Optimization of Chitosan Monomer and Derivatives

4.1 Structure of chitosan monomer

Structure of chitosan monomer was modeled with Gauss view software. Geometry was optimized with DFT method. B3LYP/6-31G (d) level of theory was adopted for the optimization. A monomer of chitosan has four –OH and an $–NH_2$ functionalities arranged in the heterocyclic ring. The lowest energy conformation of heterocyclic ring is chair form. And all the functionalities are in the equatorial position of the chair conformation [1]. The only possible variation that may cause different conformation for chitosan monomer is the dihedral angle χ (O1C2C6O5). There are three possible orientations gauche-gauche (χ= -60°), gauche-trans (χ= 60°) or trans-gauche (χ= 180°) [2] for this type of saccharides.

Chitosan monomer is optimized with these three possible conformations. Fig. 4.1 depicts these possibilities.

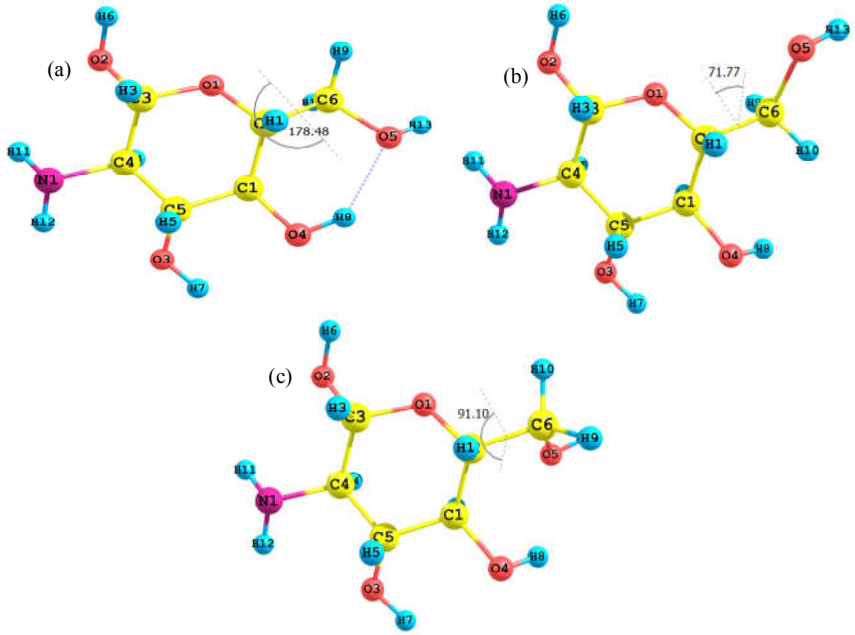

Fig.4.1. Three possible conformations of chitosan monomer at B3LYP/6-31G (d) level

Energy values of the conformations are given in Table 4.1. This shows that conformer (a) is more stable having lower energy value. For (a) the χ is equal to -178.48 degrees. Thus it is close to the trans – gauche conformation and which is preferable for the chitosan monomer. It has a hydrogen bonding between O5 and H8 atoms. Conformer (b) has χ 71.77 and (c) has -91.10 degrees. They deviated much from gauche-trans and gauche-gauche conformations respectively. All these are staggered conformations and have small difference in their energy values. Hydrogen bonding observed in conformer (a) is the reason for its extra stability.

Table 4.1 Energies of chitosan monomer structure at B3LYP/6-31G (d)

Conformations	E (Hartrees)	E (Kcal/mol)
a	-667.2827	-418719.89
b	-667.2748	-418714.94
c	-667.2779	-418716.88

The stable conformation is used for further studies. A potential energy surface scan was carried out at B3LYP/6-31G (d) to obtain the global energy minimum structure of chitosan monomer by varying the dihedral angle χ. The dihedral angle χ is varied from -180 degrees to +180 degrees with 30 degrees intervals.

Ten optimized structures were obtained after PES scan. The PES scan plot is given below in Fig 4.2. Structures with χ = -150 and +150 degrees are energy minima structures.

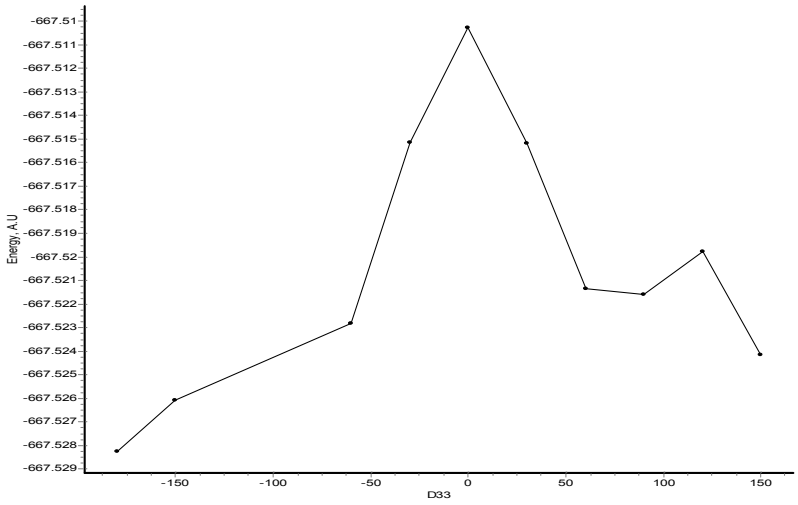

Fig.4. 2 PES of chitosan monomer at B3LYP/6-31G (d)

The plot shows that lowest energy conformation has χ = -180 degrees. That is trans-gauche conformation is more preferable to chitosan monomer. This geometry was again optimized to obtain the exact dihedral angle for the orientation of O5. This lowest energy structure has χ angle - 177.86 degrees. It is very close to trans-gauche conformation.

The structure of chitosan monomer was analyzed with another basis set 6-311++G (d,p). The stable form of chitosan monomer with both 6-31G (d) and 6-311++G (d,p) is trans-gauche. The bond angles and bond lengths of chitosan monomer optimized at both basis sets are compared in table 4.2 below. Most of the bond lengths are very close to each other. Some of them C2-C1, C1-C5, C4-N1 shows same bond distance for both basis sets. Bond angles also do vary not much when higher basis set is used.

Table 4.2 Bond angles and bond lengths of optimized chitosan monomer

Bond lengths and angles	6-31G(d)	6-311++G(d,p)
C3-O1	1.430	1.429
O1-C2	1.425	1.427
C2-C1	1.540	1.540
C1-C5	1.526	1.526
C5-C4	1.526	1.525
C4-C3	1.529	1.528
C3-O2	1.394	1.395
C4-N1	1.461	1.461
C5-O3	1.422	1.425
C1-O4	1.421	1.425
C2-C6	1.527	1.526
C6-O5	**1.432**	**1.435**
O5-H8(H-bond)	1.952	-
C3O1C2	113.17	113.91
O1C2C1	108.50	110.13
C2C1C5	109.80	110.17
C1C5C4	111.75	111.82
C5C4C3	108.75	108.70
C4C3O1	111.07	111.20

Most of the bond parameters have same value in both methods. Some bond lengths show higher value for 6-311++G (d,p) than 6-31G(d) method. C5-O3, C1-O4 and C6-O5 have greater bond distance in the higher basis set. The hydrogen bonding between O5 and H8 is not observed in B3LYP/6-11++G (d,p) method. This may be due to the variation in bond lengths of C1-O4 and C6-O5. Other bonds are similar in both. Thus 6-31G (d) method is suitable for the optimization of

chitosan monomer. Derivatives of chitosan were also optimized and studied with B3LYP/6-31G (d) method.

4.2 Citral derivatives

Citral is a long chain aliphatic aldehyde containing two isolated double bonds. Its imine with chitosan monomer was modeled. For this, minimum energy structure of chitosan monomer was used. Citral-chitosan Schiff base derivative was modeled and optimized at B3LYP/6-31G (d) method. The optimized structure of CC is reduced to get the N-alkylated derivative of chitosan, CCR. The structure was then optimized to get lowest energy conformation.

Orientation of the citral group determines the stability of conformations. The orientation of citral group is important for the stability of the derivative. In the stable structure C4N1C7 bond angle is 117.09 degrees. The dihedral angle O1C2C6O5 is -178.29 degrees for CC. Optimized lowest energy conformation of CC and CCR are depicted in fig.4.3. and 4.4 respectively. Bond parameters of both CC and CCR were given in table 4.3.

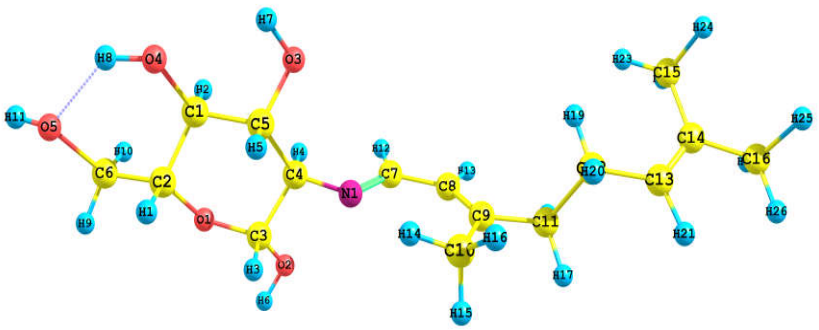

Fig 4.3 Optimized CC geometry at B3LYP/6-31G (d) level of theory

The bond lengths for the two double bonds C8-C9 and C13-C14 is 1.350 and 1.342 angstroms respectively. A closer observation of the bond angles and bond lengths of CC and CCR is shown in the following table 4.3. It is useful to understand the structural deviations that might take place on Schiff base formation.

Table 4.3 Bond lengths and bond angles of CC and CCR at B3LYP/6-31G (d) level of theory

Bond lengths and angles	**CC**	**CCR**
C3-O1	1.429	1.431
O1-C2	1.424	1.423
C2-C1	1.537	1.538
C1-C5	1.529	1.526
C5-C4	1.535	1.530
C4-C3	1.537	1.536
C3-O2	1.390	1.393
C4-N1	**1.448**	**1.461**
C5-O3	1.418	1.421
C1-O4	1.422	1.421
C2-C6	1.527	1.527
C6-O5	1.432	1.432
O5-H8 (H bond)	1.951	1.955
N1-C7	**1.279**	**1.476**
C3O1C2	113.92	113.96
O1C2C1	109.59	109.94
C2C1C5	110.5	110.01
C1C5C4	111.75	112.03
C5C4C3	108.95	107.41
C4C3O1	111.53	111.25

The table shows that the bond parameters of CC have no significant deviation from that of chitosan monomer. But the bond length C4-N1 is shortened from 1.461 to 1.448 angstroms. This is because of the adjacent imine bond. The adjacent bond C5-O3 also decreased from 1.421 to 1.418. The C-C bonds near to the imine bond are lengthened. C3-C4 and C4-C5 are increased because of the new bond formation. Other bond lengths have no significant deviation. Bond angles also show no remarkable deviation.

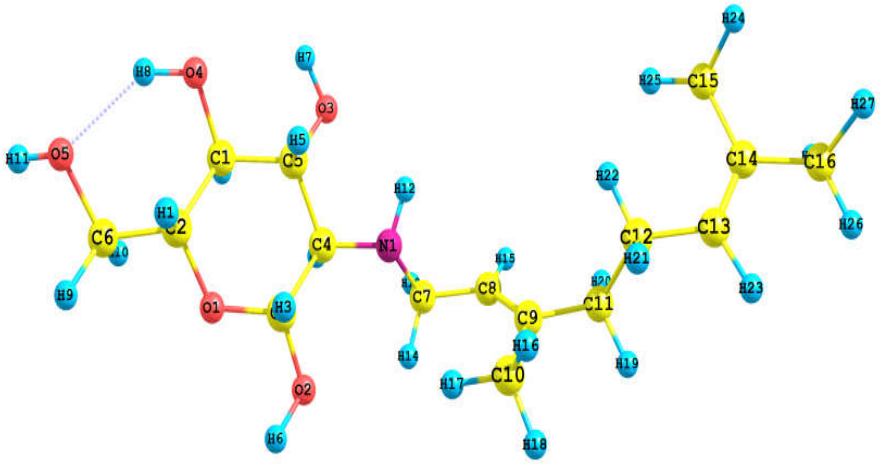

Fig.4.4 Optimized structure of CCR at B3LYP/6-31G (d)

The bond lengths N1-C7 are 1.491, C8-C9 1.356 and C13-C14 is 1.356 Å for CCR. Reduction of –C=N bond causes the elongation of N1-C7 bond from 1.280 to 1.491 angstroms. The bond angle C4N1C7 is 116.30 degrees. It shows that the structure of CC and CCR are not varied.

The shortening of bond lengths near the C=N of CC is restored in CCR. The dihedral angle O1C2C6O5 is found to be -178.34 degrees

which is not more deviated from that of chitosan monomer and CC. also the H-bond between O4 and O5 is found in CCR. Hence the structural or conformational variation to the citral derivatives is not significant. Both the Schiff base of citral and its N-reduced derivative possesses the trans-gauche conformation as that of chitosan monomer.

4.3 Glyoxylic acid derivatives

Schiff base formed between glyoxylic acid and chitosan monomer (GC) and its N-reduced derivative (GCR) were modeled computationally and optimized in similar line as that for CC and CCR. Optimized geometries GC and GCR are depicted in Fig 4.5 and 4.6 respectively. There is a carboxylic acid group in the GC structure. Bond lengths and angles of GC and GCR are listed in table below.

Table 4.4 Bond parameters of GC and GCR at B3LYP/6-31G (d) level of theory

Bond lengths and angles	**GC**	**GCR**
C3-O1	1.426	1.427
O1-C2	1.425	1.425
C2-C1	1.537	1.539
C1-C5	1.529	1.525
C5-C4	1.535	1.528
C4-C3	1.537	1.535
C3-O2	1.389	1.390
C4-N1	**1.450**	**1.469**
C5-O3	**1.417**	**1.421**
C1-O4	1.420	1.420
C2-C6	1.527	1.527
C6-O5	1.432	1.432
O5-H8 (H bond)	1.949	1.949
N1-C7	**1.267**	**1.470**
C3O1C2	113.10	114.47
O1C2C1	109.56	109.879
C2C1C5	110.51	109.56
C1C5C4	111.37	111.76
C5C4C3	109.22	108.59
C4C3O1	111.12	110.71

The bond length of C4-N1 is 1.267 angstroms for GC and the angle C4N1C7 is 117.91 degrees. The imine bond length is smaller than that of CC. This may be due to the effect of carboxylic acid group which is an electron withdrawing group. The bond angle C4N1C7 is close to that in CC. Other variations are similar to that found in CC. As for example, variations in the bond lengths of C4-N1 and C5-O3. Both of them shows bond length shortening from that of chitosan monomer. These bonds are closer to the imine bond newly fromed.

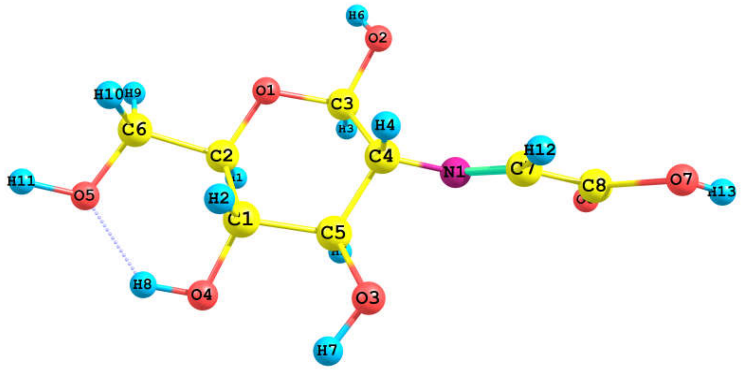

Fig.4.5 Optimized structure of GC at B3LYP/6-31G (d) level of DFT

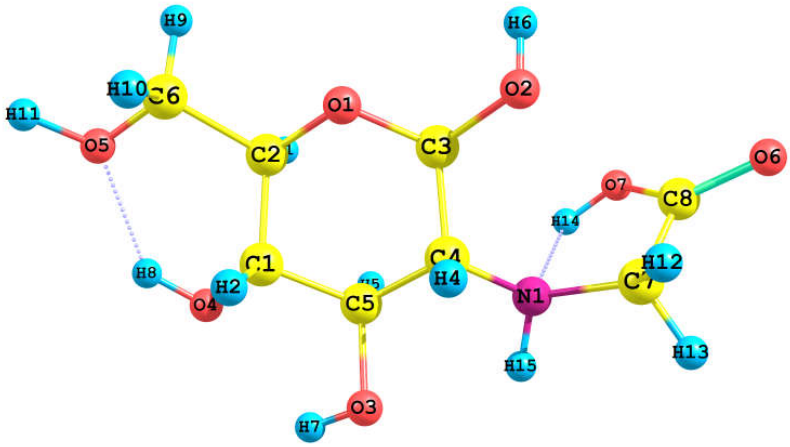

Fig.4.6 Optimized structure of GCR at B3LYP/6-31G (d) level of DFT

In case of GCR the bond N1-C7 has length 1.472 angstrom and bond angle C4N1C7 is 116.97 degrees. That means neighboring bonds are elongated when reduction to Schiff base occurred. This trend is observed in case of CC and CCR. Similarly C4-N1 and C5-O3 has changed from 1.450 to 1.469 and 1.417 to 1.421 angstroms respectively when GC is reduced to GCR. The orientation of glyoxylic acid group has slightly changed in GCR from 117.91 to 116.97 degrees.

4.4 Pyruvate derivatives

Pyruvate forms a Schiff base with chitosan using its α-keto group. The structure of PyC and PyCR were built up with Gaussview software. Optimized and found out the lowest energy structure using B3LYP method in similar lines as discussed above. Fig 4.7 and 4.8 shows the optimized lower energy structure of PyC and PyCR derivatives.

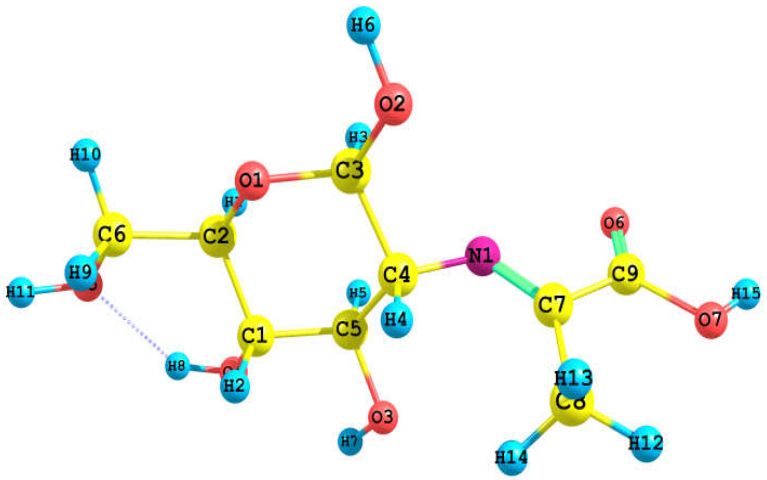

Fig.4.7 Optimized structure of PyC

As that for GC, PyC also has a carboxylic acid group in their structure. The imine bond length is 1.274 angstroms. It is slightly higher than that of GC. The presence of –Me group on the imine carbon may be the reason for increase in bond length. Bond lengths and angles of PyC and PyCR are given in table below for comparison.

Bonds adjacent to the –N=C< are deviated in PyC. C3-O1 is changed to 1.428 from 1.43. Other bonds which are deviated from chitosan parent have given below. The corresponding bond lengths of chitosan monomer are given in brackets, C2-C1; 1.537 (1.540), C5-C4; 1.535(1.526), C4-C3; 1.537(1.529), C3-O2; 1.360(1.394), C4-N1; 1.450(1.461), C5-O3; 1.419(1.422) show some deviation on Schiff base formation.

Table 4.5 Bond characteristics of PyC and PyCR at B3LYP/6-31G (d) level of DFT

Bond lengths and angles	PyC	PyCR
C3-O1	1.428	1.431
O1-C2	1.424	1.425
C2-C1	1.537	1.538
C1-C5	1.528	1.527
C5-C4	**1.535**	**1.542**
C4-C3	1.537	1.534
C3-O2	**1.360**	**1.390**
C4-N1	**1.450**	**1.457**
C5-O3	1.419	1.419
C1-O4	1.421	1.422
C2-C6	1.527	1.527
C6-O5	1.432	1.432
O5-H8 (H bond)	1.945	1.961
N1-C7	**1.274**	**1.454**
C3O1C2	113.83	114.37
O1C2C1	109.48	109.68
C2C1C5	110.43	109.89
C1C5C4	111.61	111.27
C5C4C3	109.13	107.91
C4C3O1	111.39	109.99

The C4N1C7 bond angle of PyC is 120.84 degrees which is greater than that in CC and GC. That is orientation of pyruvate group is slightly distorted in PyC compared to CC and GC. On reduction of PyC to get PyCR, some of the bond properties are changed. C4-C5 bond is lengthened to 1.542 angstroms which is greater than that in

PyC and the parent chitosan monomer. C4-C3 is shortened to some extent from 1.537 to 1.534. C3-O2 bond is shortened in Schiff base but in PyCR it is close to that in chitosan monomer.

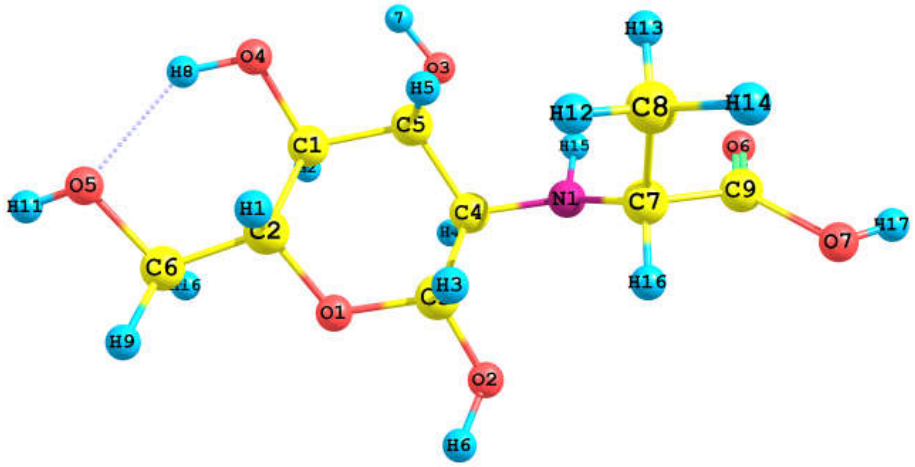

Fig.4.8 Optimized structure of PyCR

C4-N1 and N1-C7 are elongated in PyCR because of the rupture of –N=C< bond of PyC. Bond angle C4N1C7 is 118.46 degrees which is less than that of PyC. This value is close to that in GCR and CCR.

4.5 Pyridoxal derivatives

Pyridoxal hydrochloride forms Schiff base with chitosan structure. The Schiff base (PC) and its N-reduced form (PCR) were modeled and optimized to minimum energy structure. The figures are depicted in 4.9 and 4.10 respectively. Pyridoxal hydrochloride introduces an aromatic ring to chitosan monomer. This aromatic ring has –OH,-CH_3 and –CH_2OH functionalities.

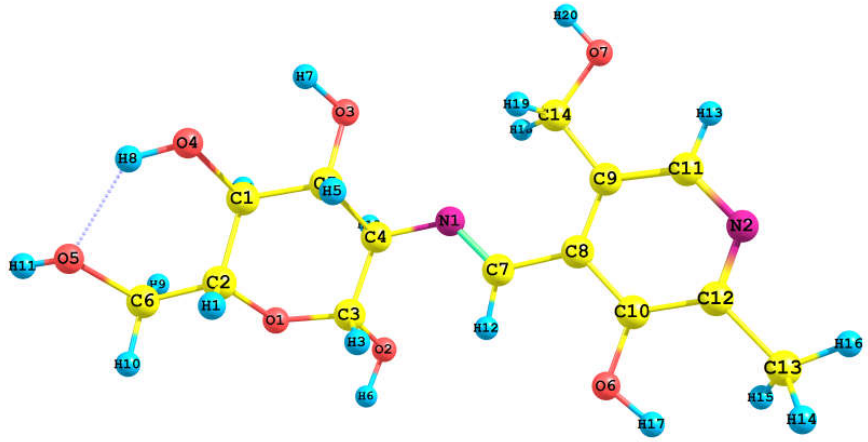

Fig 4.9 Optimized geometry of PC

Bond lengths and bond angles of PC and PCR are given in table 4.6. The formation of PC causes changes to some bond lengths of chitosan monomer similar to that in the above discussed Schiff bases. These are highlighted in the table. The bonds which are closer to the new –N=C< bond are deviated. C1-C5, C5-C4 and C4-C3 are lengthened in PC. And C2-C1 and C4-N1 are shortened in Schiff base. When PC is reduced to PCR C4-N1 bond length is restored. Other bonds remain close to that in PC.

Table 4.6 Bond properties of PC and PCR at B3LYP/6-31G (d) level of DFT

Bond lengths and angles	PC	PCR
C3-O1	1.428	1.429
O1-C2	1.424	1.424
C2-C1	**1.534**	**1.539**
C1-C5	1.529	1.530
C5-C4	**1.542**	**1.530**
C4-C3	1.541	1.543
C3-O2	1.394	1.393
C4-N1	**1.454**	**1.460**
C5-O3	1.417	1.418
C1-O4	1.421	1.422
C2-C6	1.527	1.527
C6-O5	1.432	1.432
O5-H8 (H bond)	1.950	1.951
N1-C7	**1.278**	**1.470**
C3O1C2	114.23	111.67
O1C2C1	109.06	110.27
C2C1C5	110.67	110.68
C1C5C4	112.13	110.50
C5C4C3	108.76	107.80
C4C3O1	111.68	111.12

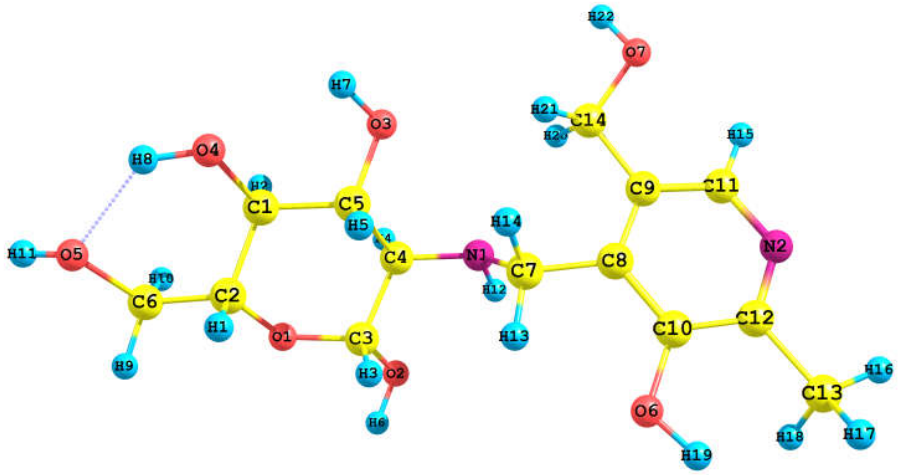

Fig.4.10 Optimized geometry of PCR

The bond length N1-C7 is 1.278 for PC and 1.476 angstrom for PCR. Orientation of pyridoxal group can be understood from the bond angles. The bond angle C4N1C7 is 117.30 degrees for PC and 114.275 degrees for PCR. The value of PC is comparable with that of CC and GC. But that of PCR is smaller than that in CCR and GCR.

4.6 Pyridine carbaldehyde derivatives

Chitosan monomer with 2-pyridinecarbaldehyde forms a Schiff base which contains a pyridyl methyl group attached to chitosan . The Schiff base of pyridine –carbaldehyde and chitosan monomer is abbreviated as PMC and its N-reduced form as PMCR. Their optimized lower energy structures are given in figures 4.11 and 4.12.

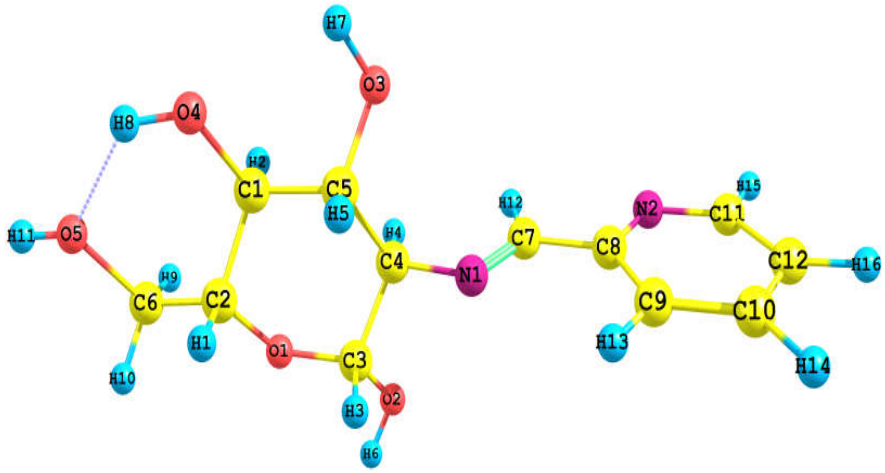

Fig.4.11 Optimized geometry of PMC

In PMC also bond lengths near to imine bond are varied. Some of them are lengthened and others shortened. The values are highlighted in table 4.7. The imine bond in PMC has a length of 1.291. Reduction of PMC to PMCR changed this bond length to 1.466 angstrom.

Table 4.7 Bond properties of PMC and PMCR at B3LYP/6-31G (d)

Bond lengths and angles	PMC	PMCR
C3-O1	1.428	1.431
O1-C2	1.424	1.423
C2-C1	1.537	1.538
C1-C5	1.529	1.525
C5-C4	**1.535**	**1.531**
C4-C3	1.537	1.537
C3-O2	1.390	1.393
C4-N1	**1.449**	**1.462**
C5-O3	**1.417**	**1.422**
C1-O4	1.421	1.421
C2-C6	1.527	1.527
C6-O5	1.432	1.432
O5-H8 (H bond)	1.951	1.958
N1-C7	**1.273**	**1.466**
C3O1C2	113.85	114.33
O1C2C1	109.59	109.83
C2C1C5	110.52	109.82
C1C5C4	111.61	112.23
C5C4C3	108.93	107.59
C4C3O1	111.35	111.14

The C4-N1 bond has changed from 1.461 to 1.449 in PMC but it is restored in PMCR. The C5-O3 bond also restored in PMCR which is shortened in PMC from 1.422 to 1.417.

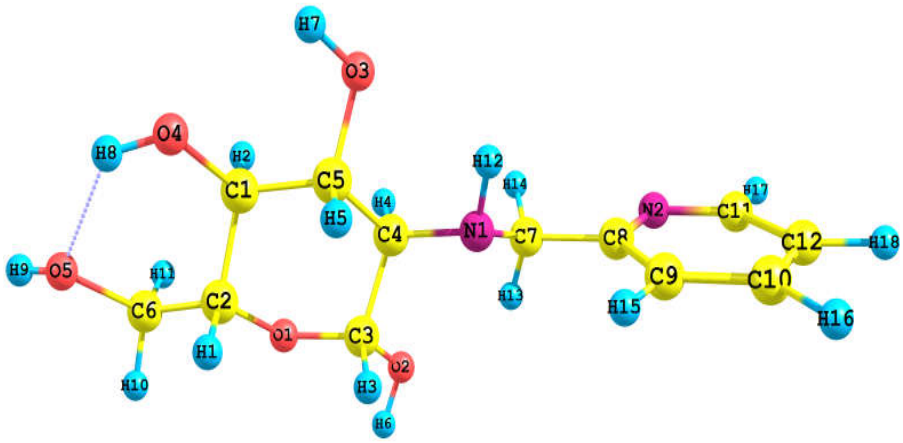

Fig.4.12 Optimized geometry of PMCR

N1-C7 bond of PMC has a length of 1.273 but in PMCR it has length 1.466. The bond angle C7N1C4 helps to observe the orientation of pyridine ring to chitosan monomer. Its value is 119.26 for PMC and 112.09 for PMCR. This value of PMCR is smaller than all of the above discussed derivatives.

4.7 Salicylaldehyde derivatives

Salicylaldehyde can form Schiff base with chitosan . The Schiff base and its N-reduced derivative can be abbreviated are SC and SCR respectively. Structures are given in fig.4.13 and 4.14.

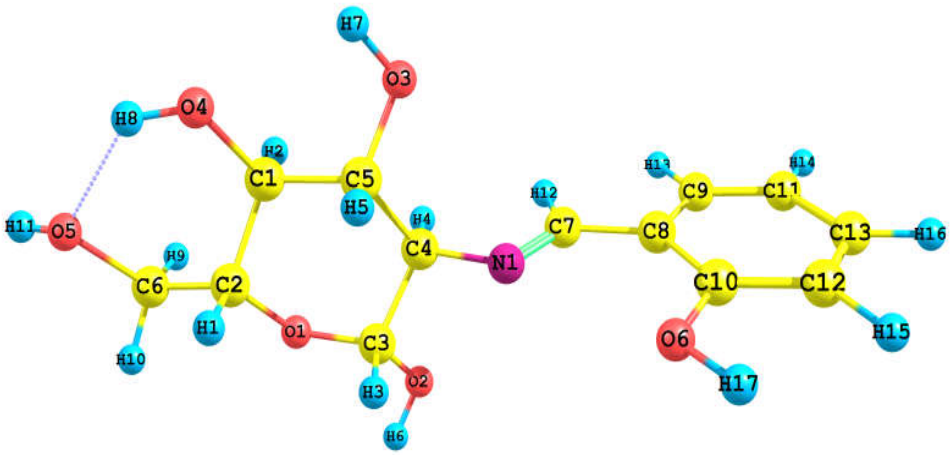

Fig 4.13 Optimized geometry of SC

Important bond parameters of SC and SCR are given in table 4.8. In case of SC also, changes occurred to some bond lengths on formation of new imine bond. C2-C1 bond is shrinked to 1.536 angstrom from 1.540. C5-C4 and C4-C3 bonds are elongated as that from chitosan monomer. But C3-O2 and C4-N1 are shortened on Schiff base formation.

Table 4.8 Bond lengths and angles of SC and SCR

Bond lengths and angles	SC	SCR
C3-O1	1.429	1.426
O1-C2	1.423	1.424
C2-C1	1.536	1.535
C1-C5	1.528	1.531
C5-C4	1.534	1.535
C4-C3	1.536	1.537
C3-O2	1.390	1.395
C4-N1	**1.448**	**1.463**
C5-O3	1.418	1.423
C1-O4	1.422	1.423
C2-C6	1.527	1.527
C6-O5	1.432	1.432
O5-H8 (H bond)	1.951	1.954
N1-C7	**1.273**	**1.475**
C3O1C2	113.84	113.28
O1C2C1	109.54	109.44
C2C1C5	110.49	111.18
C1C5C4	111.88	111.69
C5C4C3	109.16	107.52
C4C3O1	111.61	112.36

When SC is reduced to SCR these bonds are again varied. Some of them restore original bond length as that in parent chitosan monomer. C3-O2 and C4-N1 are examples these are close to the imine bond newly formed in SC. C2-C1 and C5-C4 have bond lengths close to that in SC. But C1-C5 is again elongated to 1.531 angstrom.

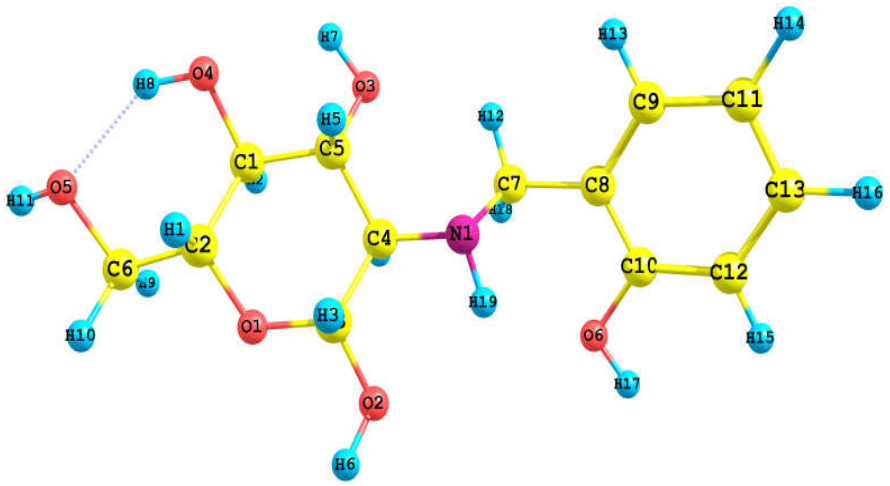

Fig 4.14 Optimized geometry of SCR

Another bond undergoes changes on reduction of Schiff base is N1-C7. Bond lengths of C7-N1 for SC are 1.292 and 1.489 angstroms for SCR. That shows on reduction to the SCR, the bond adjacent to –N=C< are elongated. The angle which directs the salicylaldehyde group is C4N1C7. In SC it has value 118.27 and 116.07 degrees for SCR.

4.8 Conclusion

Structures of chitosan monomer and all derivatives were optimized in similar manner. The variation in the bond parameters on formation of derivatives was also examined. The C-N bond is shortened in Schiff bases as that of parent chitosan. Bond angles and dihedral angles were also studied.

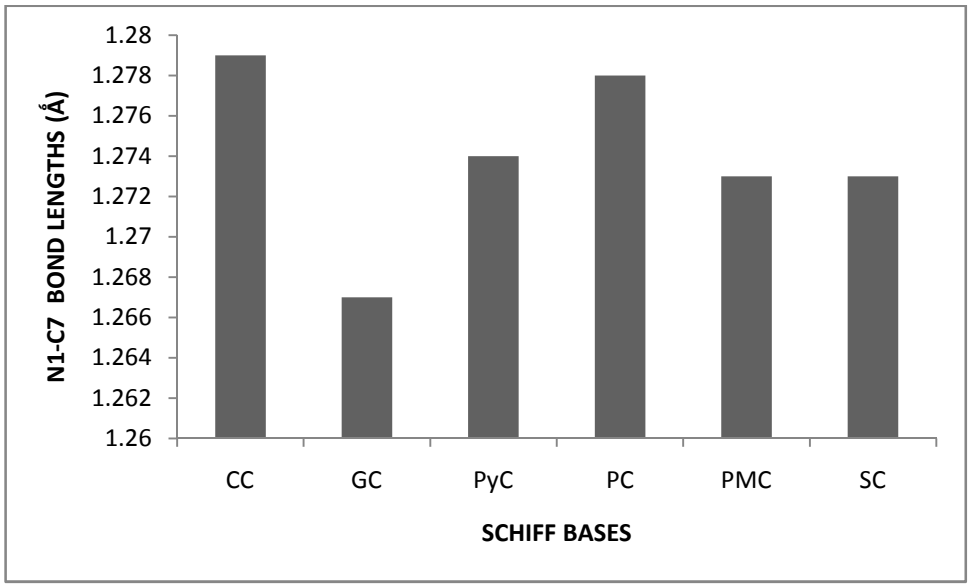

Fig.4.15 Plot of N1-C7 bond lengths of Schiff bases of chitosan monomer

The variation in the N1-C7 bond lengths of the Schiff bases is shown in the plot above. Citral chitosan Schiff base has the longest bond because of the presence of adjacent double bond. The conjugation reduces pi bond character. GC has the shortest bond length because of the presence of -COOH group. PyC also has carboxylate group but there is a methyl group also present. Hence N1-C7 bond is not as short as that of GC.

References

1. N.C Braier, R.A Jishi, J.molecular structure (theochem). 2000, *499*, 51.

2. R. H. Marchessault, S. PBrez, Biopolymers. 1979, *18*, 2369.

5 Chapter Natural Bond Orbital Analysis

Natural population analysis (NPA) and natural bond orbital (NBO) analysis of chitosan monomer and its derivatives were carried out at B3LYP level of DFT method. The most stable conformations of chitosan derivatives were selected for NBO analysis.

5.1 Chitosan monomer

NBO analysis of the optimized lowest energy structure of chitosan monomer is carried out at B3LYP/6-31G (d) level of DFT. Significant donor-acceptor interactions are given below in table 5.1. The lone pairs of O2, O5 and N1 contribute to the stability of molecule through hyper conjugative interaction. Delocalization from the lone pair of O2 to the antibonding sigma orbital of C3-O1 has energy 13.02 Kcal/mol. This is the highest delocalization effect in chitosan monomer.

Table 5.1 Important donor-acceptor interactions in chitosan monomer

Donor	**Acceptor**	$E^{(2)}$ **(Kcal/mol)**
LP (2) O 2	σ* C 3 - O 1	13.02
LP (2) O 5	σ*O4 - H 8	9.89
LP (1) N 1	σ*C 4 - H 4	8.72

Transition from lone pair of O5 to the antibonding sigma orbital of O4-H8 is a non bonded hyper conjugation effect. It has delocalization energy 9.89 Kcal/mol. The hydrogen bonding formed between O5 and O4 is due to this delocalization (Fig 4.1). Another important donor-acceptor interaction is from lone pair of nitrogen to the antibonding sigma orbital of C4-H4 which has energy 8.72 Kcal/mol.

5.2 Citral derivatives

NBO results of citral derivatives of chitosan monomer are discussed here. Important donor-acceptor interactions in CC are given below in table 5.2.

Table 5.2 Donor-acceptor interactions in CC

Donor	**Acceptor**	$E^{(2)}$ **(Kcal/mol)**
π N 1 - C 7	π* C 8 - C 9	8.40
π C8 - C 9	π *N 1 - C 7	18.44
LP (1) N 1	σ*C 7 - H 12	12.07
LP (2) O 2	σ*C 3 - O 1	14.37
LP (2) O 5	σ*O 4 - H 8	8.39
π *N1 - C7	π *C 8 - C 9	35.93

Since CC has a conjugated double bond (fig 4.3) the first two delocalizations are expected. Filled pi orbital of N1-C7 contributes to unfilled pi orbital of C8-C9 with a delocalization energy of 10.45. The delocalization from pi orbital of C8-C9 to the antibonding pi orbital of N1-C7 is greater with energy 18.44 Kcal/mol. The imine bond thus

gets more stabilization. Delocalization of lone pair of nitrogen to the anti bonding sigma of neighboring C7-H12 bond has higher energy 12.07 Kcal/mol.

Another n-σ* charge transition occurs from O2 to C3-O1 with energy 13.87 Kcal/mol. This is observed in chitosan monomer also. Both energies are nearly same and this indicates that the structure of chitosan is not varied on Schiff base formation with citral. Charge transition from π* of N1-C7 to π* of C8-C9 has the highest delocalization energy. The situation can be explained on the basis of primary and secondary hyper conjugative interactions. The primary hyper conjugative interactions due to the various types of orbital overlaps such as σ-π*, n-π*, n-σ*, π*-π* whereas secondary hyper conjugative interactions due to the orbital overlap of σ-σ*. Theoretical calculations can predict all interactions however, only π-π*and n-π* interactions are observed in experimental results [1]. The hyper conjugation effect between the conjugated double bonds in CC is responsible for this π*-π* transition. It can provide extra stability to the molecule.

Similarly the delocalization effects of CCR also studied at B3LYP/6-31G (d) level of theory. The important results are given in table 5.3.

Table 5.3 Donor-acceptor interactions in CCR

Donor	**Acceptor**	$E^{(2)}$ **(Kcal/mol)**
LP (2) O 2	σ*C 3 - O 1	11.60
LP (2) O 5	σ*O 4 - H 8	9.97

In CCR (Fig.4.4) the double bond conjugation is not present because of the reduction of imine bond. There are two important n-σ*charge transitions occurred. One is from lone pair of O2 to antibonding sigma of C3-O1. But its energy is lower than that of chitosan monomer and CC. Another one is from the lone pair of O5 to O4-H8 antibonding orbital. That indicates the hydrogen bond between O4 and O5 in which O5 act as the donor and O4 is the hydrogen bond acceptor.

5.3 Glyoxylic acid derivatives

Glyoxylic acid –chitosan Schiff base (GC) and its N-reduced form (GCR) are analyzed at B3LYP/6-31G (d) level of DFT mehod. Donor-acceptor interactions of GC are shown below in table 5.4.

Table 5.4 Donor-acceptor interactions of GC

Donor	Acceptor	$E^{(2)}$ (Kcal/mol)
π N 1 - C 7	π* C8 - O 6	12.93
LP (2) O 2	σ* C 3 - O1	14.84
LP (2) O 5	σ*O4 - H 8	08.39
LP (1) N 1	σ* C7 - H12	12.30
LP (1) O 6	RY*(1) C8	15.63
LP (2) O 6	σ* C7 - C8	20.86
LP (2) O 6	σ* C8 - O7	34.77
LP (2) O 7	π* C8 - O6	46.03
π*C8 - O 6	π* N1 - C7	74.38

Significant delocalizations involved in GC are shown above in table 5.4. Structure of GC is depicted in fig.4.5. π-π* transition from N1-C7 to C8-O6 has delocalization energy 12.93 kcal/mol. This is due to the conjugative delocalization between the imine and carboxylic acid double bonds. Lone pair of O2 transfer some charge to C3-O1 which is commonly observed in chitosan monomer and derivatives. This is increased in GC when compared to chitosan , CC and CCR. The hydrogen bond found between O5 and O4 oxygens of chitosan part is important in GC also with an energy 8.39 kcal/mol.

Lone pair of nitrogen is a donor for the antibonding sigma orbital of C7-H12 bond. It has delocalization energy 12.3 Kcal/mol. The carboxylic acid oxygen O6 is a donor for beyond vacant orbitals of C8 atom. The delocalization or conjugation effect of the two carboxylic acid oxygens was notable with delocalizaion energies 34.77 and 46.03 kcal/mol. The π*-π* transition occurs from C8-O6 to N1-C7

with energy 74.38 Kcal/mol. This corresponds to the primary hyperconjugative delocalization of the conjugated double bonds of GC.

Similarly for GCR some important donor-acceptor interaction was observed from NBO analysis results. They are shown in table 5.5. Structure depicted in fig 4.6.

Table 5.5 Donor-acceptor interactions of GCR

Donor	**Acceptor**	$E^{(2)}$ **(Kcal/mol)**
LP (2) O 2	σ*C 3 - O 1	15.88
LP (2) O 5	σ*O 4 - H 8	8.35
LP (1) N 1	σ*O 7 - H 15	14.40
LP (1) O 6	RY*(1) C 8	17.10
LP (2) O 6	σ*C 7 - C 8	21.09
LP (2) O 6	σ*C 8 - O 7	33.44
LP (2) O 7	π*C 8 - O 6	37.46
π*C8 - O 6	σ*C 8 - O 6	12.25

Almost all the delocalizations that we are observed in GC are common with GCR also except those arose due to the imine bond in GC. The energy will be varied to some extent. π*-π* transition is not present because there is no conjugated double bond in GCR.

5.4 Pyruvate derivatives

Schiff base fromed between pyruvate and chitosan monomer was optimized to lower energy (fig 4.7). Its N-alkylated derivative also modeled and optimized at B3LYP level of DFT. NBO analysis results

shows the donor-acceptor interactions that leads to the stability or instability of the molecules. Significant donor-acceptor delocalizations are shown below in table 5.6.

Similar to other chitosan derivatives PyC also has some usual hyperconjugate effects. Transitions from lone pair of O2 to antibonding orbital of C3-O1 and lone pair of O5 to antibonding of C4-H8 are typical for chitosan monomer and derivatives. For PyC, transition from O2 to C3-O1 has some higher delocalization energy (15.01 kcal/mol).

Table 5.6 Important donor-acceptor interactions in PyC

Donor	**Acceptor**	$E^{(2)}$ **(Kcal/mol)**
πN1 - C 7	π*C 9 - O 6	12.20
LP (2) O 2	σ*C 3 - O 1	15.01
LP (2) O 5	σ*O 4 - H 8	8.56
LP (1) N 1	σ*C 7 - C 8	13.56
LP (1) O 6	RY*(1) C 9	15.66
LP (2) O 6	σ*C 7 - C 9	21.41
LP (2) O 6	σ*C 9 - O 7	34.54
LP (2) O 7	π*C 9 - O 6	45.23
π*C 9 - O 6	π*N1 - C7	44.56

Delocalization of charge from lone pair of O5 to O4-H8 corresponds to the hydrogen bond formed between O5 and O4. Its energy is close to that of chitosan monomer and other derivatives discussed below.

In PyCR, the following delocalizations shown in table 5.7 are important. Because of the absence of imine bond in PyCR π* to п* charge delocalization is impossible. Other transitions are similar to those in PyC.

Table 5.7 Donor-acceptor interactions in PyCR

Donor	**Acceptor**	$E^{(2)}$ **(Kcal/mol)**
LP (1) N 1	σ*C 7- C8	11.31
LP (1) O 6	RY*(1) C9	17.08
LP (2) O 6	σ*C7 - C9	19.43
LP (2) O 6	σ* 9 - O7	34.05
LP (2) O 7	π*C9 - O6	47.22
LP (2) O 2	σ*C3 - O1	13.47
LP (2) O 5	σ*O 4 - H 8	7.96

An important transition observed in both PyC and PyCR are from lone pair of O6 to rydberg orbital of C9. It has delocalization energy 15.66 in PyC and 17.08 Kcal/mol in PyCR. Other transitions are typical to chitosan monomer.

5.5 Pyridoxal derivatives

Pyridoxal –chitosan Schiff base and its N-alkylated derivatives were subjected to NBO analysis. Important results are given below in table 5.8. Unlike the above mentioned derivatives PC has an aromatic ring which is from pyridoxal part. Delocalizations involve that from aromatic ring also can contribute to electronic nature of PC. Structure of PC is shown in fig 4.9.

Table 5.8 Delocalization interactions in PC

Donor	Acceptor	$E^{(2)}$ (Kcal/mol)
π C10 - C12	π* N1 - C7	16.41
π C10 - C12	π* C 9 - C11	18.39
πC10 - C12	π* C11 - N 2	24.29
π C9 - C11	π* C10 - C12	19.94
πC 9 - C11	π*C 12 - N 2	20.86
πC12- N2	π*C4 - C 6	15.47
πC12 - N2	π*C9 - C11	21.46
LP (1) N1	σ*C7- H12	12.28
LP (1) N2	σ*C 10 - C12	11.07
LP (2) O6	π*C 8 - C10	26.96
LP (2) O2	σ*C 3- O 1	12.79
LP (2) O5	σ*O 4- H 8	8.36
π*C8 - C10	π*C9- C11	140.92
π*C12- N 2	π*C9- C11	105.80

Charge transfer from lone pair of O2 to antibonding orbital of C3-O1 has lower energy compared to that of chitosan monomer. The hydrogen bonding between O5 and O4 has energy 8.36 Kcal/mol. Two π* to π* transitions occurred in PC within the aromatic ring. They have high delocalization energy.

In case of PCR the following transitions (table 5.9) occur. Hydrogen bond between O5 and O4 has energy 8.33 Kcal/mol. The

transition from O2 to antibonding orbital of C3-O1 has energy 14.55 kcal/mol.

Delocalizations in the aromatic ring are observed with higher energy. These include π-π* and π*-π* transitions. π*-π* transitions have greater delocalization energy above hundred Kcal/mol. The hyper conjugative effects of PCR are given below.

Table 5.9 Delocalization interactions in PCR

Donor	**Acceptor**	$E^{(2)}$ **(Kcal/mol)**
πC 8 - C 9	π*C10 - C12	18.73
πC 8 – C 9	π*C11 - N2	25.09
πC 10 - C12	π*C8 - C9	21.54
πC 10 - C12	π*C11 - N 2	20.11
πC 11 - N2	π*C 8 - C9	14.64
πC 11 - N2	π*C10 - C12	22.03
LP (1) N 2	σ*C10 - C12	11.04
LP (2) O 6	π*C8 - C9	25.78
LP (2) O 2	σ*C3 - O1	14.55
LP (2) O5	σ*O4 - H8	8.33
π*C 8 - C9	σ*C 10 - C12	206.62
π*C11 - N2	π*C8 - C9	285.24
π*C11 - N2	σ*C 10 - C12	111.96

Donor-acceptor interactions are found to be those similar to PC. Aromatic delocalization effects are stronger in PCR than PC.

5.6 Pyridine carbaldehyde derivatives

Pyridine carbaldehyde can form Schiff base with chitosan . Thus we can introduce a pyridyl methyl group into the chitosan . The

optimized lower energy structure of pyridyl methyl Schiff base (PMC) and its N-reduced form (PMCR) were subjected to NBO analysis. Important donor-acceptor interactions are given below in table 5.10. Structure of PMC is depicted in fig 4.11.Similar to the above derivatives donor-acceptor interactions are closely observed for PMC and PMCR.

Table 5.10 Delocalization interactions in PMC

Donor	**Acceptor**	$E^{(2)}$ **(Kcal/mol)**
πN 1 - C 7	π*C 8- N 2	10.14
πC 8 - N 2	π*N 1 - C 7	12.05
πC 8 - N 2	π*C 9- C 10	13.44
πC 8 - N 2	π*C 11 - C 12	25.32
πC 9- C 10	π*C 8- N 2	26.09
πC 9- C 10	π*C 11 - C 12	18.03
πC 11 - C 12	π*C 8 - N 2	16.79
πC 11 - C 12	π*C 9- C 10	19.83
LP (2) O2	σ*C 3 - O 1	13.00
LP (2) O 5	σ*O 4 - H 8	10.05
LP (1) N 1	σ*C 7 - H 12	11.43
π*C 8 - N 2	π*N 1 - C 7	55.77
π*C 8 - N 2	π*C 9- C 10	164.73
π*C 8 - N 2	π*C 11 - C 12	194.15

PMC has additional nitrogen that is in conjugation with N1 of chitosan part. The first two π-π* transitions indicates this delocalization. The next coming six transitions are expected for the pyridine ring. Delocalization from lone pairs of O2 and O5 are common for all chitosan monomer and other derivatives. Their energies are nearly same with that of chitosan monomer itself. Interaction from lone pair of N1 to antibonding sigma orbital of C7-

H12 occurs with an energy of 11.43 Kcal/mol. π*-π* transitions with greater $E^{(2)}$ values occurs in PMC.

Similarly for PMCR the following important charge transfer occurs. Delocalizations that take place inside the pyridine ring are shown in the first six transitions.

Table 5.11 Delocalization interactions in PMCR

Donor	**Acceptor**	$E^{(2)}$ **(Kcal/mol)**
πC 8 - N 2	π*C 9 - C 10	13.19
πC 8 - N 2	π*C 11 - C 12	27.84
πC 9 - C 10	π*C 8 - N 2	28.22
πC 9 - C 10	π*C 11 - C 12	17.51
πC 11 - C 12	π*C 8 - N 2	16.11
πC 11 - C 12	π*C 9 - C 10	22.42
LP (1) N 2	σ*C 8 - C 9	10.14
LP (2) O 2	σ*C 3 - O 1	14.03
LP (2) O 5	σ*O 4 - H 8	8.10
π*C8 - N 2	π*C 9 - C 10	266.71
π*C8 - N 2	π*C 11 - C 12	275.90

Other transitions are common. One is from O2 to C3-O1 having delocalization energy 14.03 kcal/mol. Hydrogen bond delocalization from O5 to O4 has energy 8.10 kcal/mol. Two π*- π* transitions takes place with high energy. One is from C8-N2 to C9-C10 having 266.71 kcal/mol. Other is from antibonding orbital of C8-N2 to C11-C12. These two are observed in PMC also but energy is less.

PMC has an additional π*- π* transition occurs which is absent in PMCR because of the lack of imine bond.

5.7 Salicylaldehyde derivatives

NBO results of salicylaldehyde derivatives of chitosan (SC and SCR) are given below. For SC the following hyper conjugative transitions are important (table 5.12). First transition corresponds to the delocalization from aromatic ring to imine bond of SC. Next six delocalizations from π-π* represents the aromatic ring delocalization of salicylaldehyde benzene ring. Structure of SC depicted in fig 4.13.

Table 5.12 Delocalization interactions in SC

Donor	**Acceptor**	$E^{(2)}$ **(Kcal/mol)**
π C 8 – C 9	π*N 1– C 7	18.46
π C 8 – C 9	π*C 10 – C 12	23.24
π C 8 – C 9	π*C 11 – C 13	17.74
π C 10 – C 12	π*C 8 – C 9	15.80
π C 10 – C 12	π*C 11 – C 13	22.86
π C 11 – C 13	π*C 8 – C 9	22.93
π C 11 – C 13	π*C 10 – C 12	17.38
LP (2) O 2	σ*C 3 – O 1	13.67
LP (2) O 5	σ*O 4 – H 8	10.16
LP (1) N 1	σ*C 7 – H 12	11.34
LP (2) O 6	π*C 10 – C 12	27.95
π*C 8 – C 9	π*N 1 – C 7	111.47

Delocalization from lone pair of O2 to antibonding sigma orbital of C3-O1 is significant in SC also with energy equal to 13.67 Kcal/mol. It is almost equal to that of chitosan monomer indicates that the derivatization has not changed the chitosan part. The hydrogen

bond which is found in chitosan monomer is present here also. It has delocalization energy 10.16 Kcal/mol. Lone pairs of N1 and O6 transfers charge to neighboring anti bonding orbitals of sigma and pi respectively. A π*-π* transition takes place from C8-C9 to N1-C7.

In case of SCR, the following transitions are important. First six corresponds to aromatic ring delocalization. Their energies are similar to that for SC. Structure of SCR is shown in Fig 4.14.

Table 5.13 Delocalization interactions in SCR

Donor	**Acceptor**	$E^{(2)}$ **(Kcal/mol)**
π C 8 – C 9	π*C 10 – C 12	22.90
π C 8 – C 9	π*C 11 – C13	18.93
πC 10 – C 12	π* C 8 – C 9	17.02
πC 10 – C 12	π*C 11 – C13	20.81
πC 11 – C 13	π* C 8 – C 9	20.16
πC 11 – C 13	π*C 10 – C12	17.61
LP (2) O 2	σ*C 3 – O 1	12.05
LP (2) O 5	σ*O 4 – H 8	10.01
LP (2) O 6	π*C 10 – C 12	23.81
π*C 10 – C 12	π* C 8 – C 9	170.88
π*C 11 – C 13	π* C 8 – C 9	260.66

Two typical delocalizations from lone pairs of O2 and O5 are notable here also with nearly same delocalization energy. Delocalization from O6 to antibonding pi orbital of C10-C12 has energy 23.81 Kcal/mol which is smaller when compared to that of SC. Two π*-π* transitions are significant in SCR from C10-C12 to C8-C9

and C11-C13 to C8-C9 with energies 170.88 and 260.66 Kcal/mol respectively.

5.8 Conclusion

NBO analysis of chitosan monomer and its derivatives were carried out and discussed. Some of the interactions like LP (2) O 2 to σ*C3 – O 1 and LP (2) O 5 to σ*O 4 – H 8 are common with parent chitosan monomer and derivatives. Donor –acceptor interactions of aromatic ring, pi- conjugation etc. can be compared quantitatively from the results.

References

1. Z. Demircioglu, C. A. Kastas, O. Buyukgusng, Spectrochimica Acta Part A: Molecular and Biomolecular Spectroscopy. 2015,*139*,539.

6 Chapter Reactivity Studies

6.1 Natural charges and reactivity

Local and global reactivity of chitosan monomer and its twelve derivatives are studied at B3LYP/6-31G (d) level of DFT. Local reactivity can be understood from the natural charges obtained from NBO analysis.

The charge distribution on different atoms of chitosan monomer is given in table 6.1. Mulliken charges and natural charges obtained from NBO analysis at B3LYP method are compared. The trend in the values of mulliken and natural charges are similar when 6-31G (d) basis set was used.

Table 6.1 Charges on different atoms of chitosan monomer at B3LYP level of theory

Atoms	B3LYP/6-31G(d)	
	Mulliken charges	**Natural charges**
N	-0.742	-0.92061
O1	-0.520	-0.61662
O2	-0.622	-0.75367
O3	-0.654	-0.77104
O4	-0.676	-0.79235
O5	-0.636	-0.78773
C1	0.123	0.04261
C2	0.104	0.03747
C3	0.369	0.41278
C4	-0.007	-0.12041
C5	0.129	0.07314
C6	-0.055	0.10634

Mulliken atomic charges of different atoms of chitosan monomer are given in table. Nitrogen of the free $–NH_2$ group has greater negative charge than oxygen atoms. Chitosan monomer has five oxygen atoms. Out of these five, only O5 is primary whereas O2, O3 and O4 are secondary –OH groups attached to heterocyclic ring. O1 is the ring oxygen. For B3LYP/6-31G (d) method, O4 shows higher negative charge than O3. O2 has the lowest negative charge among the oxygen atoms. It is in between N1 and O1. When the charges on carbon atoms are considered, C3 attached to O2 has the highest positive charge. C4 and C6 have slight negative charge.The natural charges on different atoms at B3LYP/6-31G (d) method shows similar trend as that of Mulliken charges.

Natural charge values indicate the local reactivity of different sites of molecules. Negative value shows the nucleophlicity and positive values shows the electrophilicity. Nitrogen and oxygen atoms of chitosan monomer show negative charges and they are ready to bind with electrophiles like metal ions. In chitosan the free nitrogen of amino group has the highest negative charge and it is more reactive than oxygens. Next is O4. The primary –OH has third position in the series then O3. The two oxygens which are closer to nitrogen have comparatively low reactivity. Heterocyclic oxygen is the least nucleophilic oxygen. All the carbon atoms except C4 show positive charge. This is because C4 is bonded to nitrogen.

6.1.1 Citral derivatives

Natural atomic charges on different atoms of CC and CCR are given in table 6.2. From the table it is clear that the negative charge of nitrogen is decreased in CC when compared to chitosan monomer. This is due to the double bond formation in between N and C7 atom. But the negative potential of C4 attached to nitrogen increased due to the electron donating effect of the substituent group. Negative charge on oxygen atoms also slightly decreased in CC than that of chitosan monomer.

Table 6.2 Natural charges on different atoms of CC and CCR at B3LYP/6-31G (d)

Atoms	**CC**	**CCR**
N	**-0.46947**	**-0.70099**
O1	-0.61118	-0.61266
O2	-0.73535	-0.74266
O3	-0.75447	-0.76235
O4	-0.78412	-0.78480
O5	-0.77298	-0.77379
C1	0.04351	0.04632
C2	0.04184	0.04244
C3	0.42200	0.41842
C4	-0.13254	-0.11919
C5	0.08318	0.07629
C6	-0.10553	-0.10495

Natural charges on oxygen and carbon atoms of CC show similar trend as that in chitosan monomer. Negative charges on oxygen atoms are slightly decreased. In case of CCR, charge on nitrogen increased because of the destruction of imine bond of Schiff base. But its reactivity is lower than oxygen atoms. In CCR also O4 has higher negative charge and hence reactivity.

6.1.2 Glyoxylic acid derivatives

Since glyoxylic acid group is an electron withdrawing group, the electron density at nitrogen atom may be reduced than that of CC. Natural charges of different atoms of GC and GCR are given in table. 6.3. As expected the negative charge of nitrogen is decreased to -0.3694 units which is less than that of CC. for the N-alkylated from (GCR) it is equal to -0.7440. This is higher than CCR.

Table 6.3 Natural charges on different atoms of GC and GCR

Atoms	GC	GCR
N	**-0.3694**	**-0.7440**
O1	-0.6081	-0.6050
O2	-0.7354	-0.7465
O3	-0.7559	-0.7641
O4	-0.7822	-0.7736
O5	-0.7731	-0.7698
C1	0.0440	0.0429
C2	0.0407	0.0381
C3	0.4212	0.4149
C4	-0.1413	-0.1141
C5	0.0823	0.0747
C6	-0.1059	-0.1141

Charges on oxygen atoms of GC are further decreased from that of CC. Similarly for GCR, negative charge of oxygen atoms is close to that of GC. This shows that the Schiff base formation affects the charge of nitrogen atom only. Carbon atoms C4 and C6 of glyoxylic acid derivatives have small negative polarity in chitosan and its derivatives. For GCR, nitrogen is more reactive than CCR. N and O2 have closer values in CCR.

6.1.3 Pyruvate derivatives

PyC and PyCR also have a carboxylic acid group in their structure. The imine bond length is 1.274 angstroms. It is slightly higher than that of GC. The presence of –Me group on the imine carbon may be the reason for increase in bond length.

Natural charges on the different C, H, O and nitrogen atoms of PyC and PyCR were given in table 6.4. As for CC and GC, PyC also has decreased negative charge on nitrogen atom because of the Schiff base formation. Even though the pyruvate has a carboxylate group the charge of nitrogen in PyC is greater than GC. That means the +I effect of $-CH_3$ has significant effect on determining the reactivity of nitrogen atom.

Table 6.4 Natural atomic charges of PyC and PyCR

Atoms	PyC	PyCR
N	**-0.39284**	**-0.71117**
O1	-0.60685	-0.60457
O2	-0.73726	-0.74457
O3	-0.76298	-0.76731
O4	-0.77441	-0.77536
O5	-0.76969	-0.76929
C1	0.04012	0.03986
C2	0.03759	0.03830
C3	0.42065	0.41698
C4	-0.14456	-0.11577
C5	0.08399	0.07567
C6	-0.11401	-0.11372

For PyCR nitrogen has a charge of -0.71117 units. Oxygen and carbon atoms PyC and PyCR have comparable values. Among the three aliphatic derivatives of chitosan , nitrogen of CC has greater negative charge and hence more reactive towards electrophiles, like metal ions. All of the three N-reduced derivatives show greater reactivity on nitrogen atoms than their corresponding Schiff bases. But it is lower than chitosan monomer. The double bond of imine group decreases the reactivity of nitrogen considerably.

6.1.4 Pyridoxal derivatives

Natural charge values (table 6.5) shows that nitrogen of PC has charge of -0.46154 and that for PCR is -0.70914. This indicates that the delocalization from pyridoxal part has an effect on the charge of

nitrogen. For GC and PyC, nitrogen shows lower negative charge than that for PC. But CC nitrogen is slightly more reactive than PC.

Table 6.5 Natural atomic charges on PC and PCR

Atoms	PC	PCR
N1	**-0.46154**	**-0.70914**
O1	-0.60683	-0.60880
O2	-0.73668	-0.74633
O3	-0.75384	-0.76148
O4	-0.77426	-0.77459
O5	-0.76846	-0.76860
C1	0.03943	0.04273
C2	0.03808	0.03923
C3	0.42011	0.41659
C4	-0.13172	-0.11757
C5	0.08328	0.07621
C6	-0.11389	-0.11356

Charges on other atoms, C and oxygen, has no significant variation due to the substituents attached on pyridine ring.

6.1.5 Pyridine carbaldehyde derivatives

The natural charge values of nitrogen atoms of PMC and PMCR are -0.4489 and -0.739 units respectively. Negative charge of Nitrogen on PMC is lower than that of PC but higher than the aliphatic derivatives of chitosan . The increase in charge of PC is due to the presence of hydroxyl groups in the ortho positions of pyridoxal ring. In PMC also O4 is more nucleophilic. C4 and C6 of PMC and PMCR also show negative polarity.

Table 6.6 Natural charge values of PMC and PMCR

Atoms	PMC	PMCR
N	**-0.44894**	**-0.71398**
O1	-0.61517	-0.60894
O2	-0.74380	-0.74371
O3	-0.76213	-0.76262
O4	-0.79156	-0.77537
O5	-0.78732	-0.76893
C1	0.04170	0.04245
C2	0.03725	0.03906
C3	0.41764	0.41583
C4	-0.13837	-0.11524
C5	0.07888	0.07577
C6	-0.10691	-0.11360

6.1.6 Salicylaldehyde derivatives

Natural charge values of SC and SCR are given in table 6.7 shows the natural charges on different C, O and nitrogen atoms of SC and SCR derivatives of chitosan monomer. As for the above discussed derivatives, SC has lower reactivity on nitrogen atom due to the double bond formation. O4 is more reactive in SC and SCR.

Table 6.7 Natural charges of SC and SCR

Atoms	SC	SCR
N	**-0.43138**	**-0.71441**
O1	-0.61680	-0.61389
O2	-0.74301	-0.75343
O3	-0.76417	-0.77158
O4	-0.79235	-0.79419
O5	-0.78731	-0.78741
C1	0.04186	0.04109
C2	0.03735	0.03800
C3	0.41666	0.41519
C4	-0.14063	-0.11818
C5	0.07774	0.07395
C6	-0.10675	-0.10677

The variation in natural charges of different atoms of chitosan monomer and derivatives was closely examined. For all these derivatives, negative charge on nitrogen atoms is very much decreased in Schiff bases. For N-reduced derivatives it is increased, but not more than the parent chitosan monomer. The natural charge values are slightly varied. So the effect of the substituent groups to the chitosan moiety cannot be understood from the natural charge values only.

6.2 Frontier molecular orbitals and global reactivity

The highest occupied and lowest unoccupied molecular orbitlas (HOMO and LUMO) of molecules are termed as frontier molecular orbitals (FMOs). These orbitals are responsible for the

chemical stability of molecules [1]. HOMO represents the electron donating ability whereas LUMO represents the electron acceptance.

The global reactivity parameters such as hardness (η), softness ($S = \frac{1}{\eta}$) , chemical potential etc. can be evaluated from these two orbitals. The maximum hardness or absolute hardness (η) of a system having N electrons and total energy E is given as [2]:

$$\eta = \left(\frac{\partial^2 \mathrm{E}}{\partial \mathrm{N}^2}\right)_{\mathrm{v(r)}} \approx \frac{1}{2}\,(\mathrm{IE} - \mathrm{EA}) \approx \frac{1}{2}\,(\mathrm{E_{LUMO}} - \mathrm{E_{HOMO}})$$

Where IE is the vertical ionization energy given as -$\mathrm{E_{HOMO}}$ and EA is vertical electron affinity as - $\mathrm{E_{LUMO}}$[3]. Global softness is the reciprocal of hardness ($S = \frac{1}{\eta}$). As the hardness value increases the stability of molecules increase and therefore reactivity decreases. Electron affinity can be calculated from the equation;

$$\chi = -\mu = \left(\frac{\partial E}{\partial N}\right)_{v(r)} \approx \frac{1}{2}(IE + EA) \approx -\frac{1}{2}(E_{LUMO} + E_{HOMO})$$

The global electrophilicity index (ω) is given as:

$$\omega = \frac{\mu^2}{2\eta}$$

These reactivity descriptors are used to predict the reactivity of chitosan monomer and derivatives in the present study. Before calculating these parameters the HOMO-LUMO gap of chitosan and derivatives were observed. Table 6.8 shows the HLG gap.

Table 6.8 HOMO –LUMO gap (HLG) of chitosan monomer and its derivatives

Molecules	**E_H**	**E_L**	**$\Delta E=E_L-E_H$**	**ΔE (eV)**	**E_L+E_H**
Chitosan	-0.2287	0.0412	0.2700	7.34	-0.1876
CC	-0.2171	0.0287	0.1883	5.12	-0.2456
CCR	-0.2097	0.0269	0.2385	6.44	-0.1829
GC	-0.2571	-0.0554	0.2017	5.49	-0.3125
GCR	-0.2375	0.0310	0.2685	7.30	-0.2065
PyC	-0.2502	-0.0461	0.2041	5.55	-0.2963
PyCR	-0.2069	0.0163	0.2232	6.07	-0.1906
SC	-0.2137	-0.0298	0.1839	5.01	-0.2435
SCR	-0.2066	-0.0085	0.1981	5.40	-0.2151
PC	**-0.2174**	**-0.0437**	**0.1740**	**4.73**	**-0.2614**
PCR	-0.2114	0.0055	0.2059	5.52	-0.2169
PMC	-0.2393	-0.0455	0.1938	5.28	-0.2898
PMCR	-0.2189	-0.0103	0.2086	5.68	-0.2292

From the HOMO-LUMO energy difference the absolute reactivity parameters of chitosan and derivatives were calculated. The energy gap of chitosan monomer and its derivatives are represented in the figure given below. Pyridoxal Schiff base derivative has the lowest energy gap. That means electronic transition is more feasible in PC and it must more reactive among the other derivatives. N-reduced derivatives have higher energy gap compared to corresponding Schiff bases.

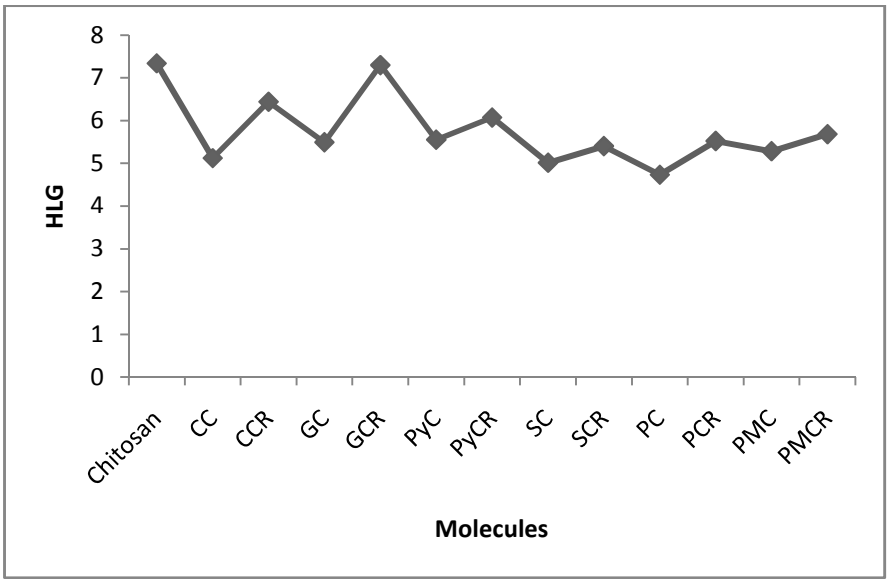

Fig.6.1 HOMO-LUMO energy gap of chitosan and derivatives

Reactivity descriptors are calculated from the data given in table 6.8. Values of absolute hardness (η), softness (S), electron affinity (χ) and global electrophilicity (ω) of the studied molecules are given in table below. The table 6.9 shows that all of the chitosan derivatives have global hardness value less than that of chitosan monomer or their softness is greater than chitosan . Normally a higher value of softness or lower value of hardness indicates the increase in global reactivity of molecules. Hence the result shows that chitosan derivatives are more reactive than parent chitosan .

Table 6.9 Global reactivity parameters of chitosan and derivatives

Molecules	η	S	χ	ω
Chitosan	3.67	0.27	2.55	0.886
CC	2.56	0.39	3.34	2.179
CCR	3.22	0.31	2.99	1.388
GC	2.75	0.36	4.26	3.299
GCR	3.65	0.27	2.81	1.082
PyC	2.78	0.36	4.03	2.921
PyCR	3.04	0.33	2.59	1.103
PC	**2.37**	**0.42**	**3.56**	**2.674**
PCR	2.76	0.36	2.95	1.576
PMC	2.64	0.38	3.85	2.807
PMCR	2.84	0.35	3.12	1.714
SC	2.51	0.39	3.30	2.169
SCR	2.70	0.37	2.93	1.589

The result shows that for all derivatives hardness is lower than chitosan monomer. So derivatives will be more reactive. Also the reactivity of N-reduced derivative is lower than the corresponding Schiff base derivatives. As already mentioned PC is more reactive then SC. The order of reactivity can be given as PC > SC > CC > PMC > SCR > GC > PCR > PyC > PMCR > PyCR > CCR > GCR.

Aromatic derivatives show higher reactivity than aliphatic derivatives. But CC show better reactivity compared to GC and PyC.

6.3 Conclusion

Local and global reactivity of chitosan monomer and its derivatives were studied. Local reactivity is obtained from the natural charge values. Global reactivity is calculated from the HOMO and LUMO energies. Nitrogen of the $–NH_2$ group of chitosan monomer is more nucleophilic. On Schiff base formation its nucleophilicity is reduced. Global reactivity studies proved that all of the derivatives are more reactive than parent chitosan monomer.

References

1. S. Gunasekaran, R.A. Balaji, S. Kumaresan, S. Srinivasan. Can. J. Ana. Sci Spectrosc. 2008,*53*,149.

2. Z. Zhou, H.V Navangul, J.Physc.Org.Chem. 1990, *3*,784.

3. T.Koopmans, Physica.1934, *1,*104.

7 Chapter Metal ions Interaction Studies

Metal ions can chelate with chitosan and derivatives as mentioned earlier. Chitosan and its modified forms are effectively used as metal ions adsorbent [1-5]. The mode of interaction of metal ion with chitosan is still ambiguous. Using computational techniques we have tried to understand the adsorption between chitosan and derivatives with metal ions. As a primary attempt we considered only monomer unit of chitosan biopolymer. Heavy metal ions Cd (II), Hg (II) and Pb (II) were chosen to study interaction with chitosan monomer and derivatives.

Earlier chapters discussed the optimization of Chitosan monomer and derivatives at B3LYP/6-31G (d) level of DFT. The basis set used was rather compact and is not sufficient beyond argon of periodic table. So LanL2DZ basis set is selected to study the heavy metal ions interaction with chitosan monomer and derivatives. This basis set is usually reported for heavy metals [6]. For this chitosan monomer and derivatives were optimized to lower energy structure at B3LYP/LanL2DZ level. These optimized structures were further used for metal ion interaction studies.

7.1 Cd (II)-Chitosan monomer *interaction*

B3LYP/LanL2DZ level of DFT was used for the study of complexation between chitosan and cadmium ions. Stable conformation of chitosan monomer was chosen for the metal interaction studies. The stability of complexes can be understood from

the *Eads* values which are calculated from the following equation [7]. Adsorption energies were expressed in Kcal/mol units.

$$Eads = E_{Complex} - [E_{adsorbent} + E_{Metal\ ion}]$$

Before studying the metal coordination, chitosan monomer is optimized at B3LYP/LanL2DZ level of DFT. Three complexes were formed between chitosan monomer and cadmium ion. These optimized complexes were subjected to stability check using Gaussian 03 at B3LYP/LanL2DZ level of theory.

For the complex (a), O3 and N1 are the adsorbing sites for metal ion. O3 and N1 bind with metal ion with the bond lengths 2.145 and 2.258 respectively. Fig.7.1 depicts the geometry of Cd(II)-chitosan complex (a). Stabilization energy of the complex (a) is -190.07 Kcal/mol. The hydrogen bond found in chitosan monomer is preserved in this complex with length 1.844 Å. *Eads* values of Cd (II)-chitosan complexes are shown in table 7.5.

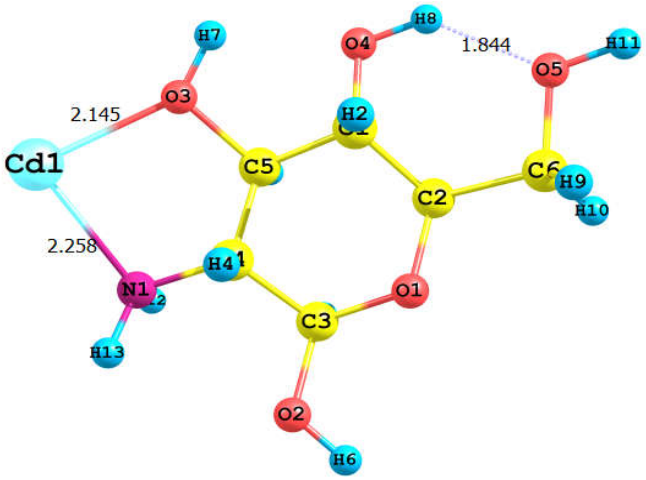

Fig.7.1 Cd (II)-chitosan complex (a)

The complex (b) has *Eads* value -212.66 Kcal/mol. In this O3 and O4 are the coordinating sites of metal ion with 2.088 and 2.189 Å as bond lengths respectively. H atom of O3 is transferred to nitrogen and hence the charge on it was decreased. Hydrogen of O4 is partly shifted to O5. These are reasons for the high stability of the complex. Fig.7.2 shows the optimized structure of Cd (II)-chitosan complex.

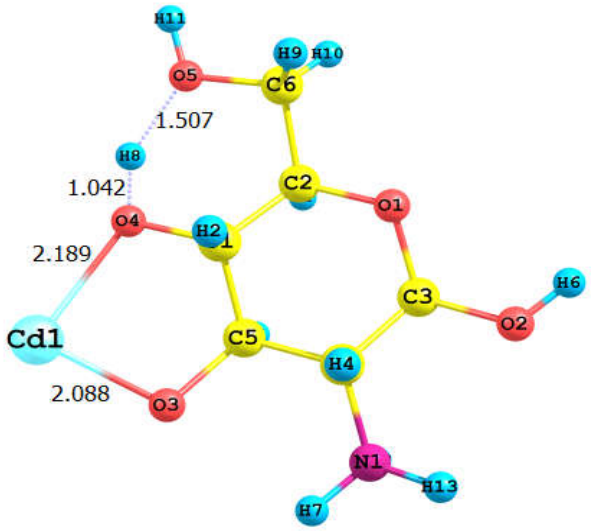

Fig.7.2 Cd (II)-chitosan complex (b)

The third complex (c) was formed between N1 and O2 of chitosan monomer and metal ion. The bond lengths of metal adsorbing sites are 2.240 Å for N1 and 2.191 Å for O2. H-bond between O4 and O5 is preserved in this complex also at a distance of 1.862 Å. This complex is the least stable of the three Cd (II)-chitosan complexes having stabilization energy of -181.85 Kcal/mol.

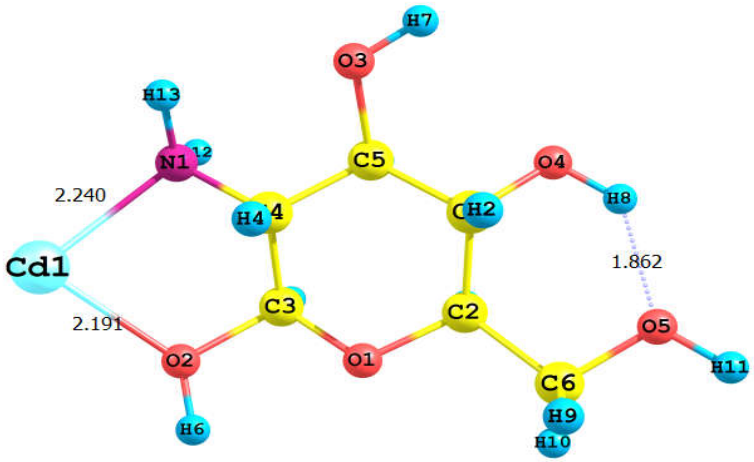

Fig 7.3 Cd (II)-chitosan complex (c)

Natural electronic configuration (NEC) of Cd (II) ion on different Cd (II)-chitosan complexes were analyzed from NBO results. Normal electronic configuration of Cd (II) is 5S(0)4d(10)5p(0).

Table 7.1. Natural electronic configuration of cadmium ion in different complexes.

Complexes	Cd(II) NEC
a	[core]5S(0.29)4d(9.99)5p(0.02)
b	[core]5S(0.31)4d(9.99)5p(0.03)
c	[core]5S(0.33)4d(9.99)5p(0.02)

Important delocalization efffects of complex (a) are listed below. Delocalization from lone pair of O5 to antibonding sigma of O4-H8 is responsible for the hydrogen bond formation.

Table 7.2 Donor-acceptor interactions in complex (a)

Donor	Acceptor	$E^{(2)}$ (Kcal/mol)
LP (2) O2	σ^* C3 – O 1	13.62
LP (2) O3	**σ^* N -Cd**	**13.82**
LP (2) O5	σ^* O 4 – H 8	12.21

Delocalization from lone pair of O2 to antibonding sigma orbital of C3-O1 has an energy 13.62 which is close to that in chitosan monomer. Lone pair of O3 to antibonding orbital of N-Cd stabilizes the metal coordination.

The complex (b) has the following delocalizations shown in Table 7.3. Highest delocalization energy is observed for transition from lone pair of O5 which corresponds to the hydrogen bonds in the complex. This interaction gives extra stability to the complex.

Table 7.3 Donor-acceptor interactions in complex (b)

Donor	Acceptor	$E^{(2)}$ (Kcal/mol)
LP (2) O2	σ^* C 3 – O 1	14.81
LP (2) O4	**σ^* O 3-Cd**	**12.42**
LP (2) O5	σ^* O 4- H 8	47.24
σ^* O 4- H 8	RY*(1) H 8	11.79

Charge transfer from O2 to antibonding sigma of C3-O1 has energy 14.81 Kcal/mol. Another effect is from lone pair of O4 to

antibonding sigma of O3-Cd orbital that also stabilizes the complex. For complex (c), two interactions are significant. They are shown in table 7.4

Table 7.4 Donor-acceptor interactions in complex (c)

Donor	**Acceptor**	$E^{(2)}$ **(Kcal/mol)**
LP (2) O 2	**σ *(1) N -Cd**	**12.04**
LP (2) O 5	σ *(1) O 4 - H 8	9.75

Table 7.5 shows the frontier molecular orbitals. HOMO and LUMO can predict the stability of complexes. The energy values of all the complexes are listed in table 7.5.

Table 7.5 HOMO-LUMO energy gap in Cd (II)-chitosan complexes

Complexes	***Eads***	E_L	E_H	$\Delta E=E_L-E_H$ ***(Hartrees)***	ΔE ***Kcal/mol***
Chitosan	-	0.0235	-0.2187	0.2422	151.98
a	-190.07	-0.4794	-0.5079	0.0285	17.88
b	-212.66	-0.4299	-0.5302	0.1003	62.94
c	-181.85	-0.4828	-0.5013	0.0185	11.61

As the stability of complexes increased the energy gap will be higher. In complex (b) HOMO-LUMO energy gap is greater than that in (a) and (c).

From the shape of HOMO and LUMO of complexes we can predict the charge transfer transitions. HOMO and LUMO of all the complexes is given in fig.7.4 below.

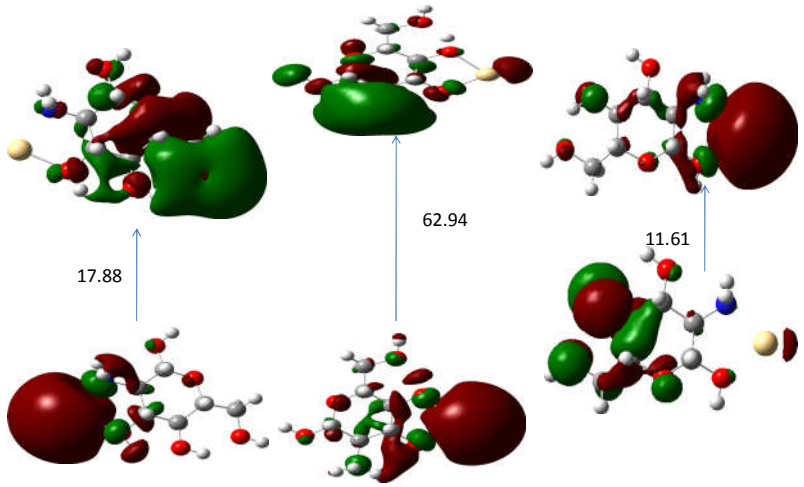

Fig.7.4 HOMO-LUMO representation of all the three Cd(II)-chitosan complexes

If the shape of HOMO and LUMO are different there is a possibility of charge transfer transition. For all the three complexes the charge density of HOMO and LUMO are different. That indicates the charge transfer occurs in them.

7.2 Hg (II)-chitosan complexes

Chitosan can be effectively used for the retention of Hg (II) ions [8, 9]. The present study focuses on the interaction of Hg (II) ions with chitosan monomer. Studies were carried out at B3LYP/LanL2DZ level of density functional theory. Metal ion was placed at different adsorbing sites of chitosan . Possible complexes formed between chitosan and Hg (II) ions were given below.

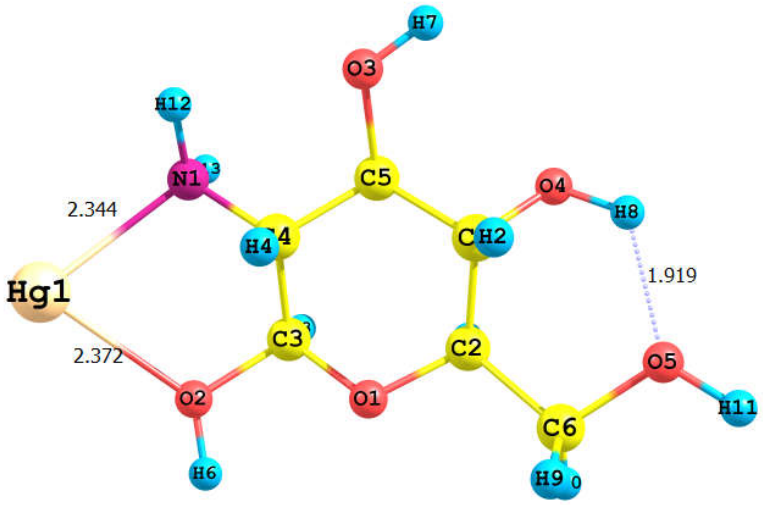

Fig.7.5 Hg (II)-chitosan complex (a)

Complex (a) is formed by the bonding of Hg (II) with nitrogen and O2 of chitosan monomer. Bond lengths between metal ion and adsorbing sites are 2.344 and 2.372 Å respectively for nitrogen and oxygen atoms. The hydrogen bond between H8 and O5 of chitosan is preserved in complex also with bond distance of 1.919 angstrom. *Eads* energy is -190.45 Kcal/mol.

Another complex (b) is formed in which metal ion is bonded to N1 and O3 of chitosan monomer. 2.379 and 2.329 Å are the bond lengths between adsorbing sites and metal ion. *Eads* for complex (b) is 198.45 Kcal/mol. Hydrogen bond with length of 1.832 Å is found between H8 and O5 of chitosan .

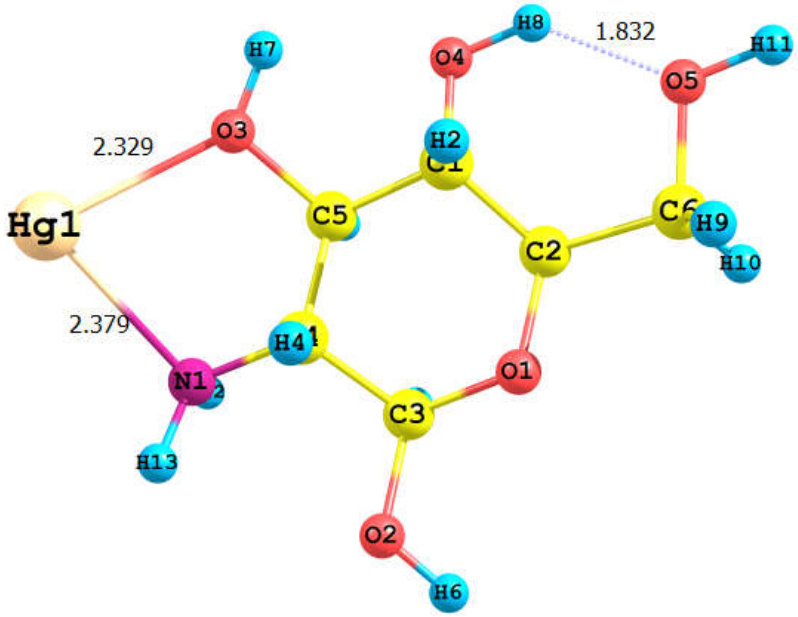

Fig.7.6 Hg (II) -chitosan complex (b)

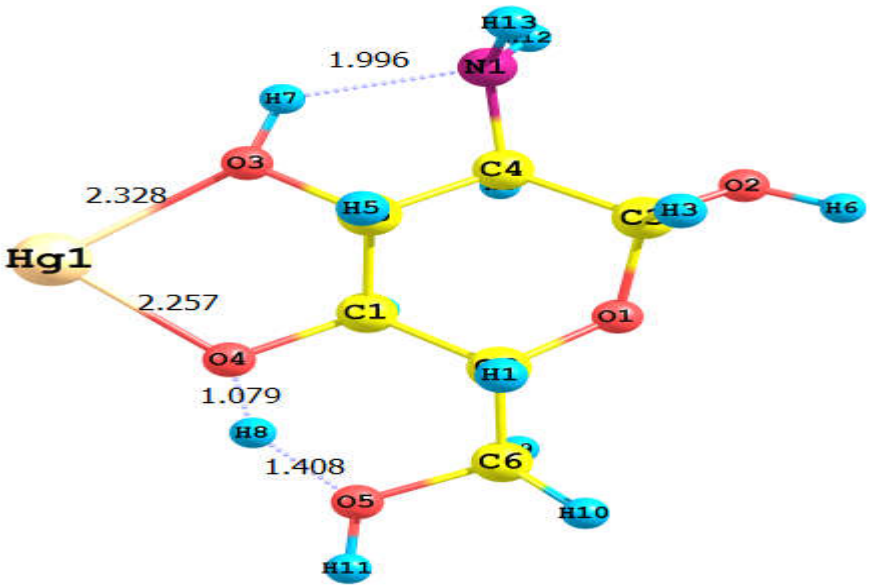

Fig .7.7 Hg (II)-chitosan complex (c)

The third complex (c) is formed when Hg (II) is bonded to O3 and O4 of chitosan monomer. It is the stablest of all other complexes. Table 7.8 shows that *Eads* values of all the three mercury-chitosan complexes are close to each other.

Natural electronic configuration of mercury ion in all complexes was observed from NBO results. The stability of complexes can be explained on the basis of the d electron delocalization.

Table 7.6 Natural electronic configuration of Hg (II) ion in Hg (II)-chitosan complexes

Complexes	**NEC of Hg(II)**
a	[core]6S(0.58)5d(9.99)6p(0.01)
b	[core]6S(0.59)5d(9.99)6p(0.01)7p(0.01)
c	[core]6S(0.52)5d(9.99)6p(0.02)

Extend of delocalization is higher in complex (b) and hence its stability. In case of (c) the s contribution is lower compared to others therefore it is highly stable.

Important donor-acceptor interactions that lead to stability of complexes are given below. In (a), delocalization from O3 to σ* C 1 - C 5 has $E^{(2)}$ value 8.19 Kcal/mol. Delocalization from O4 to σ*C 1 - C 2 has energy 8.20 Kcal/mol and from O5 to σ* O 4 - H 8 has 6.29 Kcal/mol. Another important transition is from σ* N -Hg to Rydberg orbital of metal ion with delocalization energy 5.86 Kcal/mol. The

extent of delocalization is not so significant in this complex. Thus it is least stable.

For (b), the highest delocalization occurs from lone pair of O2 to σ* C 3 - O 1 with energy value 13.16. Transition from lone pair of O3 to σ* N -Hg orbital has delocalization energy 9.87 Kcal/mol. Delocalization of electrons from lone pair of O5 to σ* O 4- H 8 is also noticed with energy 7.87 Kcal/mol. Donor- acceptor interaction between O3 and antibonding of nitrogen-metal ion is the stabilization factor of complex (b).

In complex (c), the donor-acceptor interactions are much stronger than the above complexes. Some significant interactions are given below in table 7.7.

Table 7.7 Donor-acceptor interactions in complex (c)

Donor	**Acceptor**	$E^{(2)}$ **(Kcal/mol)**
LP (2) O 2	σ^*C 3 - O 1	19.54
LP (2) O 5	σ^*O 4 - H 8	67.30
LP (1) N	σ^*O 3- H 7	10.71
σ^*O 4- H 8	RY*(1) H 8	13.11
LP (2) O 3	**LP*(6)Hg**	**10.46**
LP (2) O 4	**LP*(6)Hg**	**13.62**

The typical charge transfer from lone pair of O2 to antibonding sigma orbital of C3-O1 has higher energy than that in chitosan monomer and other complexes. The hydrogen bond also is highly

stabilized with delocalization energy of 67.30 Kcal/mol. Lone pairs of O3 and O4 also transfer charges to vacant orbitals of mercury ion, these interactions causes the formation of complex (c). All delocalization have higher energy and is favorable to the formation of the complex (c). Hence it is most stable among the other complexes.

HOMO-LUMO energies are valuable for the prediction of reactivity and conductance property of complexes. The table below shows this energy difference of all Hg (II)-chitosan complexes.

Table 7.8 HOMO-LUMO energy gap of Hg (II) –chitosan complexes

Complexes	***Eads***	E_L	E_H	$\Delta E=E_L-E_H$ ***(Hartrees)***	ΔE ***Kcal/mol***
chitosan	-	0.0235	-0.2187	0.2422	151.98
a	-190.45	-0.4977	-0.5168	0.0191	11.99
b	-198.54	-0.4957	-0.5193	0.0236	14.81
c	**-199.55**	**-0.4875**	**-0.5278**	**0.0403**	**25.29**

Complex (c) has the maximum energy gap which is quite expected. That is as the HOMO and LUMO energy gap increased, the stability of complexes increased. Frontier molecular orbitals of complexes Hg (II)-chitosan complexes (a) - (c) is depicted in the following figure.

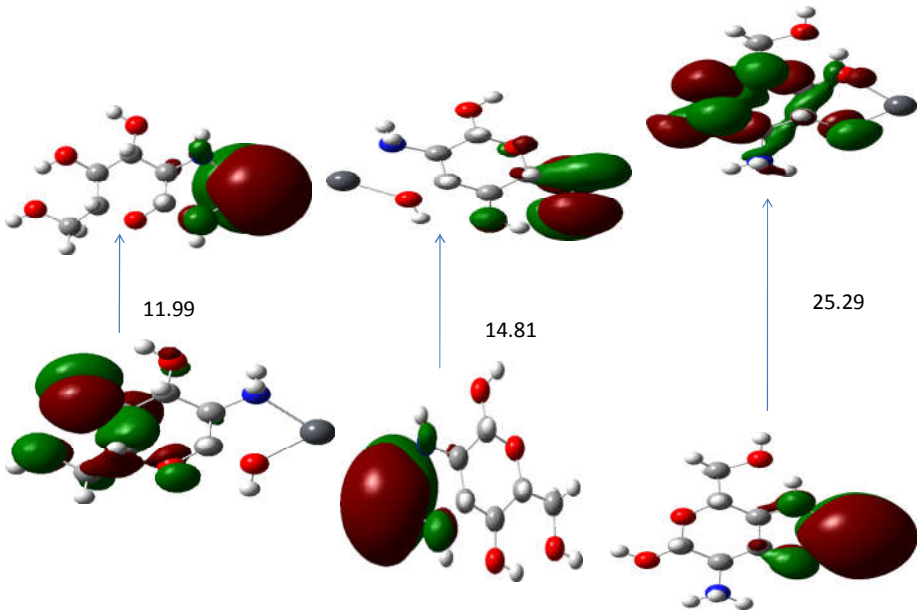

Fig 7.8 HOMO and LUMO representations of Hg (II)-chitosan complexes

The figure shows that complex (b) has different type HOMO and LUMO. In HOMO charge is concentrated at chitosan side that is on ligand part and LUMO is on mercury attached side. As the energy gap is increased the stability of complex also increased. Here complex (a) is less stable so as its HOMO-LUMO gap is small. For complex (b), stability is higher than that of complex (a) and its HLG is greater than (a).

7.3 Pb (II)-chitosan complexes

Removal of Pb (II) ions from aqueous solutions using chitosan biopolymer and its derivatives is previously reported [10, 11]. Here we

have attempted to study how Pb (II) ions interact with chitosan and to which site the metal ion can bind strongly. The whole studies were carried out with chitosan monomer at gaseous phase.

The metal ion was introduced to the optimized chitosan monomer at B3LYP/LanL2DZ level of DFT. Depending upon the position of metal ion in chitosan three possible complexes (a-c) were formed. Each complex was studied separately in order to understand the type of bonding, extend of delocalization etc.

In complex (a), Pb (II) was bonded to O2 and nitrogen of chitosan monomer. The bond lengths were 2.222 and 2.357 Å for O2 and N1 with Pb (II) respectively.

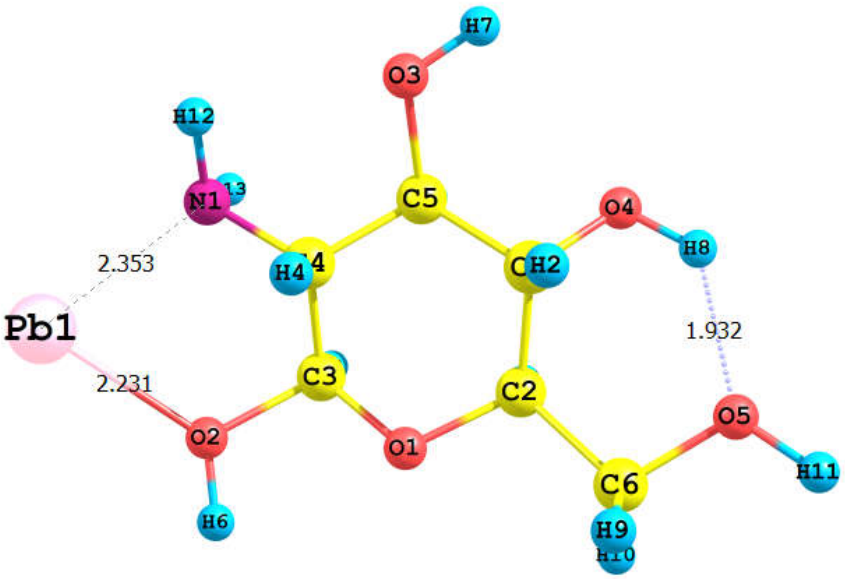

Fig.7.9 Chitosan –Pb (II) complex (a)

For complex (b), Pb (II) is bonded to N1 and O3 of chitosan monomer. In this bond lengths are 2.396 and 2.185 Å respectively for nitrogen and oxygen atoms. The hydrogen bond in chitosan monomer is preserved in both complexes. That is between O5 and H8 of chitosan monomer at a distance of 1.849 Å. Complex (b) is more stable than (a) in terms of *Eads*. Charge distribution on different atoms of chitosan and Pb (II) ion follows the similar trend as that of complex (a).

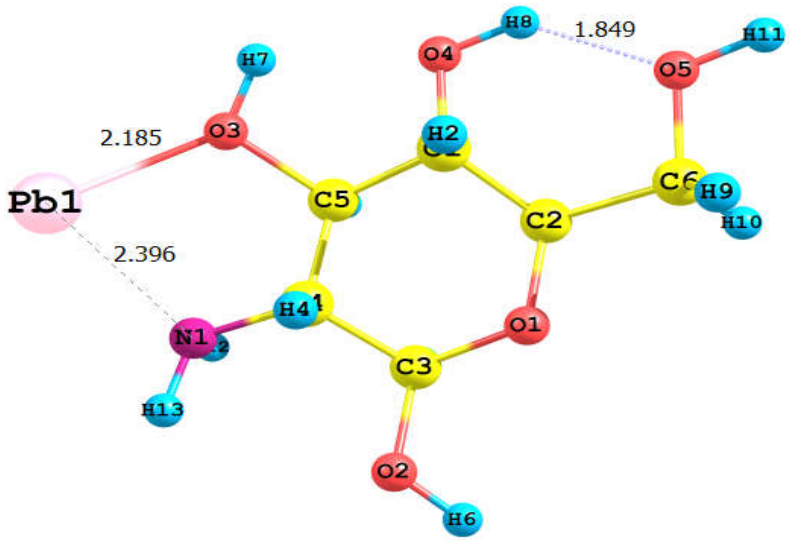

Fig.7.10 Pb (II)-chitosan complex (b)

Complex (c) is the most stable complex among all other chitosan –Pb (II) complexes. Its Eads value is -208.46 Kcal/mol. In this O3 and O4 are coordinated to metal ion with bond distances 2.036 Å and 2.272Å respectively. Hydrogen bonds were formed between O4, H8 and O5 atoms.

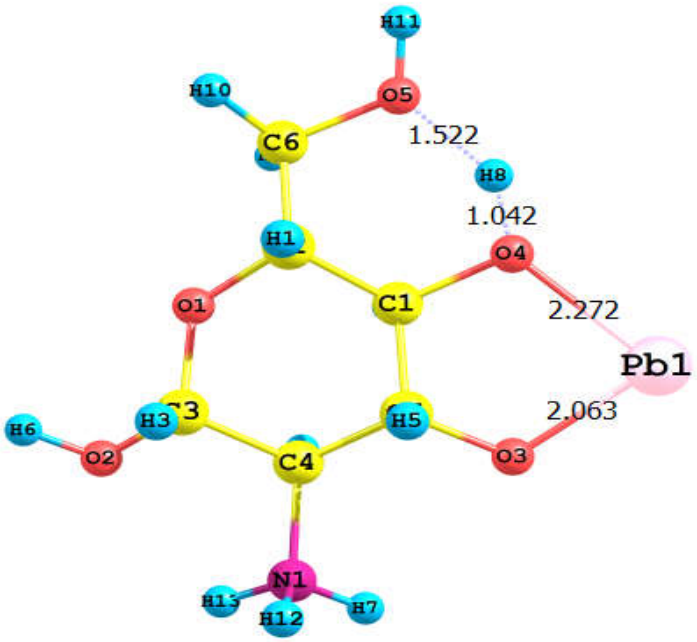

Fig.7.11 Pb (II)-chitosan complex(c)

The natural electronic configuration (NEC) of Pb (II) in different complexes is given in table 7.9. The electronic configuration of Pb (II) is [core] 6S (2) 6p (0) as we know. On coordination to chitosan some changes must be occurred to this situation that will account for the stability of complexes. For (c), Pb (II) has higher value in 6p than others. This means that charge transfer from the chitosan to metal ion is more in complex (c). This is one of the reasons for the extra stability of complex (c). The s electrons also delocalized to p in this complex.

Table 7.9 Natural electronic configuration of Pb (II)-chitosan complexes

Complexes	NEC of Pb(II)
a	[core]6S(1.95)6p(0.32)
b	[core]6S(1.95)6p(0.34)
c	[core]6S(1.92)6p(0.44)

NBO results of all the complexes were analyzed. The highest $E^{(2)}$ values are discussed below. In complex (a), lone pair of O2 delocalizes to nonbonding orbital of Pb at 26.92 Kcal/mol. That explains the shorter bond length of Pb-O2 compared to that of Pb-N1. Table 7.10 gives the important donor-acceptor interactions in complex (b). For (b) electron delocalization from O3 to nonbonding Pb is 30.59 Kcal/mol. In both (a) and (b) metal to ligand delocalization is not so prominent.

Table 7.10 Donor-acceptor interactions in chitosan -Pb(II) complex (b)

Donor	Acceptor	$E^{(2)}$ (Kcal/mol)
LP (2) O 2	σ* C 3 - O 1	14.10
LP (2) O 3	**LP*(2)Pb**	**30.59**
LP (2) O 5	σ* O 4 - H 8	12.04

Donor-acceptor interactions of complex (c) is shown in table 7.11. In (c), two delocalizations are important with high $E^{(2)}$ values. One is from lone pair of O2 to σ^* O4-H8 with high energy 45.38 Kcal/mol. And the second one is from lone pair of O3 to nonbonding

of metal ion at 54.40 Kcal/mol. This high value of $E^{(2)}$ corresponds to the extra stability of complex (c).

Table 7.11 Donor-acceptor interactions in chitosan -Pb (II) complex (c)

Donor	Acceptor	$E^{(2)}$ (Kcal/mol)
LP (2) O 2	σ* C 3 - O 1	14.45
LP (2) O 5	σ* O 4- H 8	45.38
LP (3) O 3	**LP*(2)Pb**	**54.40**
LP (2) O 4	**LP*(2)Pb**	**12.95**
LP (2) O 4	LP*(4)Pb	11.14

Frontier molecular orbitals of complexes are discussed as it is important in the stability. Values of HOMO and LUMO of complexes in comparison with free chitosan are given in table 7.12.

Table 7.12 HOMO-LUMO energy gap in Pb (II)-chitosan complexes

Complexes	Eads	E_L	E_H	$\Delta E=E_L-E_H$ *(Hartrees)*	ΔE *Kcal/mol*
chitosan	-	0.0235	-0.2187	0.2422	151.98
a	-165.66	-0.4400	-0.4884	0.0484	30.37
b	-175.01	-0.4358	-0.5081	0.0723	45.37
c	**-208.46**	**-0.364**	**-0.5414**	**0.1774**	**111.32**

The energy gap is greater for complex (c) which is more stable Pb (II) complex. Next is chitosan -Pb (II) complex (b). Its energy gap

is 45.37 Kcal/mol. The lowest stable complex (a) has lower energy gap. This is expected because as the energy gap is increased the complex/system will be more stable.

The HOMO-LUMO figures are depicted in Fig 7.12. In all the three complexes, charge density in HOMO is located away from metal coordinated sites. The LUMO charge density is located around the metal adsorbed sites. That is shift from HOMO to LUMO means the transfer of charge from ligand part (ie,chitosan) to metal ion.

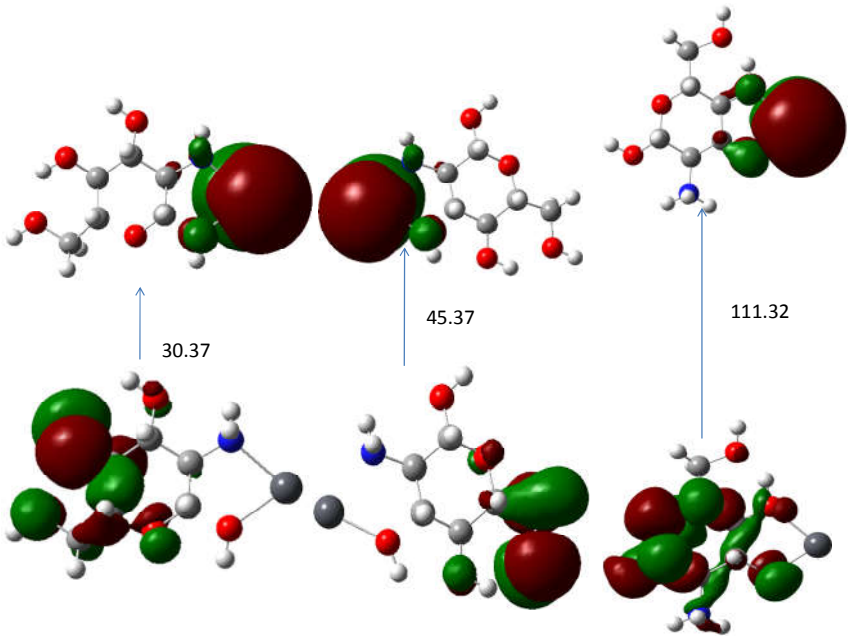

Fig.7.12. HOMO-LUMO representation of Pb (II)-chitosan complexes

For the three metal ions Cd(II),Hg(II) and Pb(II) three important chitosan complexes were analyzed above. The O3 and O4 site of chitosan is most probable adsorption site. It is favorable for

metal interaction because of its structural reasons also in addition to electronic factors.

The adsorption energy shows that all the three complexes of Hg (II) and chitosan have comparable energies. But for Cd(II) and Pb(II) ions only O3,O4 site shows better adsorption. Thus Hg will be more reactive towards chitosan .

7.4 Comparison between metal ions-chitosan complexes

A comparison between these three metal ions interaction with chitosan is essential. For this the energy of adsorption is tabulated in table 7.13. The complexation tendency of metal ions with chitosan can be explained on the basis of HSAB principle. According to Pearson's HSAB principle hard acids combines with hard bases and form ionic compounds. Soft acids react with soft bases and form covalent complexes. The amino groups are softer than hydroxyl groups. Also the metal ions Hg (II) and Cd (II) are soft acids whereas Pb(II) is a border line acid or harder than mercury and cadmium ions.

Table 7.13 E_{ads} of different metal ions with chitosan monomer

Adsorption site of chitosan monomer	E_{ads} **(Kcal/mol) Cd(II)-chitosan**	E_{ads} **(Kcal/mol) Hg(II)-chitosan**	E_{ads} **(Kcal/mol) Pb(II)-chitosan**
N1,O2	-181.85	-190.45	-165.66
N1,O3	-190.07	-198.54	-175.01
O3,O4	-212.66	-199.55	-208.46

Table shows that O3 and O4 of chitosan monomer can chelate with metal ions strongly than other sites. N1 and O2 is the least possible site for metal ions. Lead ion can form a stronger complex at O3 and O4 site than mercury ions. This is because of the hard-hard interaction. Among Hg (II) and Cd (II), cadmium ion is harder due to the small ionic radii. And thus it can form a more stable complex at O3 and O4 than mercury ion.

The nitrogen sites are less preferable for Pb (II) ions than mercury and cadmium ions. Mercury is found to be more suitable for the amino neighboring sites of adsorption. Mercury-chitosan complexes have close value for the *Eads.* This is the case of chitosan monomer only. We can extend the result to polymer system. In chitosan polymer the N and O3 sites are the only available locations for metal chelation. Thus the selectivity is based on the adsorption energy of this site. Lead ion forms less stable complexes than cadmium and mercury ions. Hence we can summarize the selectivity of metal ions to chitosan as Hg (II) > Cd (II) > Pb (II).

7.5 Metal ions and PC complexes

Of the twelve derivatives optimized, pyridoxal derivative is most reactive and is selected for metal adsorption studies. The three metal ions Cd(II),Hg(II) and Pb(II) were included in the study. Pyridoxal chitosan has a pyridine ring with a primary and secondary –OH groups. These groups increase the metal adsorption efficiency. The most stable complexes of the metal ions with PC are discussed here. In PC, N1 is more nucleophilic than N2 and other oxygen atoms. All the

three metal ions preferentially adsorbed in the neighborhood of nitrogen of chitosan monomer.

7.5.1 Cd(II)-PC complexes

Three possible sites of PC is checked for Cd(II) adsorption. O2, O3, O4 and N1 of PC can effectively bind with cadmium ion. The following figures depict Cd(II)-PC complexes.

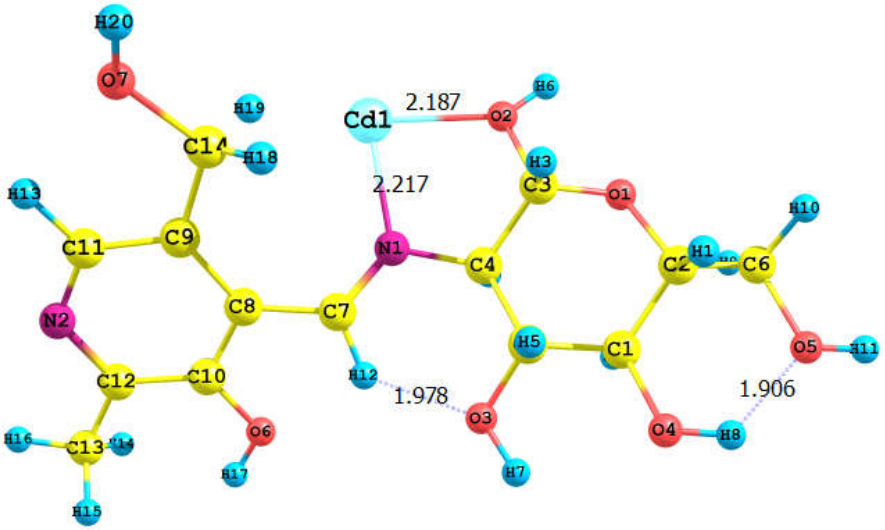

Fig.7.13 Cd(II)-PCcomplex (a)

Cadmium is bonded to the N1 and O2 atoms of PC monomer with bond lengths 2.217 and 2.187 Å respectively. Adsorption energy is -205.82 Kcal/mol. Natural electronic configurations of cadmium ion in the Cd(II)-PC complexes are given in table 7.14. Contribution from PC to metal ion goes to 6p orbital of cadmium ion. 5S orbital is empty in cadmium ions but in the complex it has some electronic charge. This

is due to the ligand-metal ion charge transfer that stabilizes the complex.

Table 7.14 Natural electronic configuration of different Cd(II)-PC complexes

Complexes	NEC of Cd(II) ion
a	[core]5S(0.40)4d(9.99)6p(0.02)
b	[core]5S(0.38)4d(9.99)6p(0.02)
c	[core]5S(0.65)4d(9.99)5p(0.02)6p(0.01)

The donor-acceptor delocalizations in Cd(II) –PC complex (a) is given below in table 7.15. Delocalizations with energy greater than 10 Kcal/mol are only shown in table. First four interactions corresponds to the π-π* transitions in the pyridoxal ring. Their energy has a range from 20 to 30 Kcal/mol.

Table 7.15 Donor-acceptor interactions in Cd(II)-PC complex (a)

Donor	Acceptor	$E^{(2)}$ (Kcal/mol)
π C 8 - C 10	π* N 1 - C 7	31.20
π C 8 - C 10	π* C 9 - C 11	18.59
π C 8 - C 10	π* C 12 - N 2	19.74
π C 9 - C 11	π* C 8 - C 10	20.32
π* C 9 - C 11	π* C 12 - N 2	16.28
π *C 12 - N 2	π* C 8 - C 10	17.68
π* C 12 - N 2	π* C 9 - C 11	24.98
LP (1) N 2	σ* C 9 - C 11	11.28
LP (1) N 2	σ* C 10 - C 12	12.72
LP (2) O 6	π* C 8 - C 10	32.48
LP (2) O 7	σ* C14 - H 19	13.08
π* N 1 - C 7	π* C 8 - C 10	39.17
π* C 8 - C 10	π* C 9 - C 11	97.18
π* C 8 - C 10	π* C 12 - N 2	251.42
LP (2) O 2	**LP*(6)Cd**	**16.10**
LP (1) N 1	**LP*(6)Cd**	**26.83**

The next three interactions are π-π^* transitions of the aromatic pyridoxal ring part. These interactions are responsible for the stability of molecule. The last shown two interactions corresponds to charge transfer from ligand to metal ion. That will stabilize the complex. Delocalization from π C 8 - C 10 to π^* N 1 - C 7 has energy 31.20 Kcal/mol. This interaction will increase the metal interacting ability of N1. All others show the delocalization inside the aromatic ring of PC. That includes primary (π-π^*) and secondary (π^* - π^*) hyperconjugation effects.

The second Cd(II)-PC complex is formed with O3 and N1 of PC. Fig.7.14 depicts the (b) complex. Important bond lengths are also shown in figure.

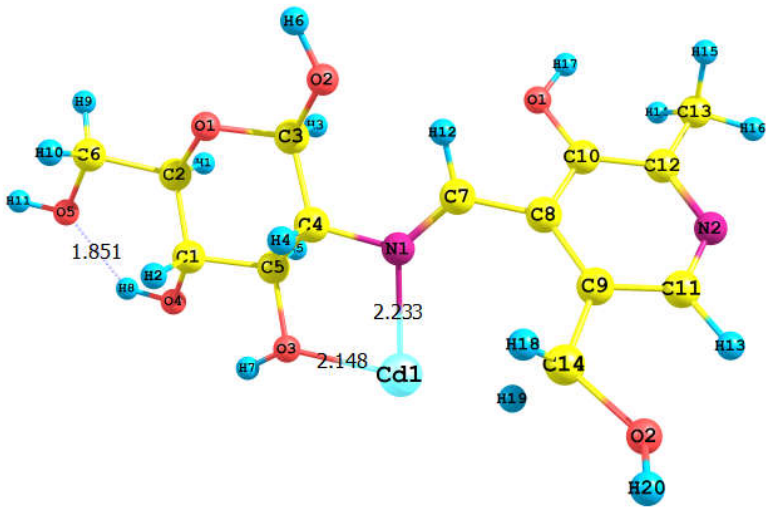

Fig.7.14 Cd(II)-PC complex (b)

It is the stablest of the three Cd(II)-PC complexes with energy 213.23 Kcal/mol.

Table 7.16 Donor-acceptor interactions in Cd(II)-PC complex (b)

Donor	Acceptor	$E^{(2)}$ (Kcal/mol)
πC 8 - C 9	π*N 1 - C 7	23.13
πC 8- C 9	π*C 10 - C 11	18.40
πC 8 - C 9	π*C 9 - N 2	20.47
πC 10- C 12	π*C 8 - C 10	21.31
πC 10- C 12	π*C 12 - N 2	16.12
πC 12 - N 2	π*C 8 - C 10	17.60
πC 12 - N 2	π*C 10- C 12	25.77
LP (1) N 2	σ*C 10 - C 12	11.36
LP (1) N 2	σ*C 10 - C 12	12.65
LP (2) O 6	π*C 8 - C 9	30.31
LP (2) O 7	σ*C 14 - H 18	13.30
LP (2) O 5	σ*O 4 - H 8	11.93
π*N 1 - C 4	π*C 4 - C 5	26.14
π*C 8 - C 9	π*C 10 - C 11	107.72
π*C 8 - C 9	π*C 11 - N 2	271.60
LP (2) O 3	LP*(1) H 7	12.22
LP (3) O 3	LP*(1) H 7	379.60
LP (3) O 3	RY*(1) H 7	20.23
LP (1) N 1	**LP*(6)Cd**	**26.01**
LP (2) O 3	**LP*(6)Cd**	**18.79**
LP*(1) H 7	σ*C 5 - O 3	30.44
LP*(1) H 7	RY*(1) H 7	41.30

In complex (c), Cd (II) is bonded to O3 and O4 of PC. Structure of complex is shown in Fig.7.15. Important bond lengths also shown in the figure.

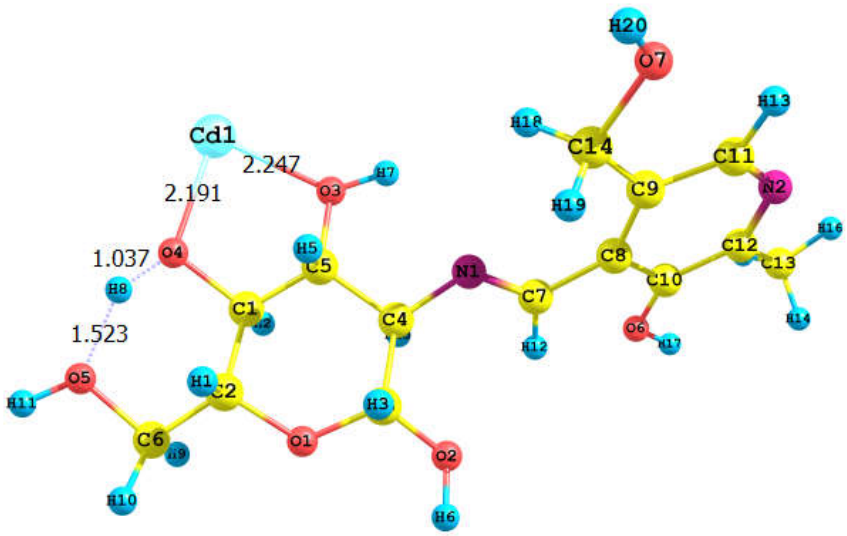

Fig 7.15 Cd(II)-PC complex (c)

Donor-acceptor interactions of Cd(II)-PC complex (c) is tabulated in 7.17. It includes primary and secondary hyperconjugative interactions as described for complexes (a) and (b).

Table 7.17 Donor-acceptor interactions in Cd(II)-PC complex (c)

Donor	Acceptor	$E^{(2)}$ (Kcal/mol)
πC8- C9	LP (1) C 10	68.26
πC8- C9	π*N1 - C7	19.32
πC8- C9	π*C 12- N 2	23.17
πC12 - N 2	LP*(1) C12	62.97
πC11 - N2	π*C 8 - C 9	15.23
LP (1) C10	LP*(1) C12	881.94
LP (1) C10	π*C 8- C 9	49.37
LP*(1) C 12	π*C11 - N 2	62.64
LP (1) N2	σ*C 9 - C11	10.72
LP (1) N2	σ*C10 - C 12	11.80
LP (1) O6	σ*C10 - C 12	7.27
LP (2) O6	LP (1) C 10	59.48
LP (2) O2	σ*C 3- O1	15.91
π*N 1 - C 7	π*C 8 - C 9	49.26
π*C11 - N 2	π*C 8- C 9	215.75
σ C1 - O 4	LP*(1) H8	10.41
CR (1) O 4	LP*(1) H8	10.03
LP (2) O 4	LP*(1) H8	12.61
LP (3) O 4	LP*(1) H8	327.92
LP (2) O 5	LP*(1) H8	55.97
LP (2) O 4	**LP*(6)Cd 44**	**11.69**
LP*(1) H 8	σ*C1 - O 37	11.72
LP*(1) H 8	RY*(1) H 8	23.57

Table 7.18 shows the HOMO-LUMO energy gap of all the three Cd(II)-PC complexes. Complex (b) has the greater energy gap

hence it is more stable than other two complexes. Energy gap or band gap is related to the stability and conductance of molecules.

Table 7.18 HOMO-LUMO energy gap of Cd (II)-PC complexes

Complexes	***Eads (Kcal/mol)***	E_L	E_H	$\Delta E=E_L-E_H$ ***(Hartrees)***	ΔE ***Kcal/mol***
PC	-	-0.0569	-0.2309	0.174	109.19
a	-205.82	-0.4163	-0.4667	0.0504	31.63
b	**-213.23**	**-0.4011**	**-0.4655**	**0.0644**	**40.41**
c	-207.08	-0.41984	-0.43264	0.0128	8.032

Pictorial representation of HOMO and LUMO is given in Fig 7.16.

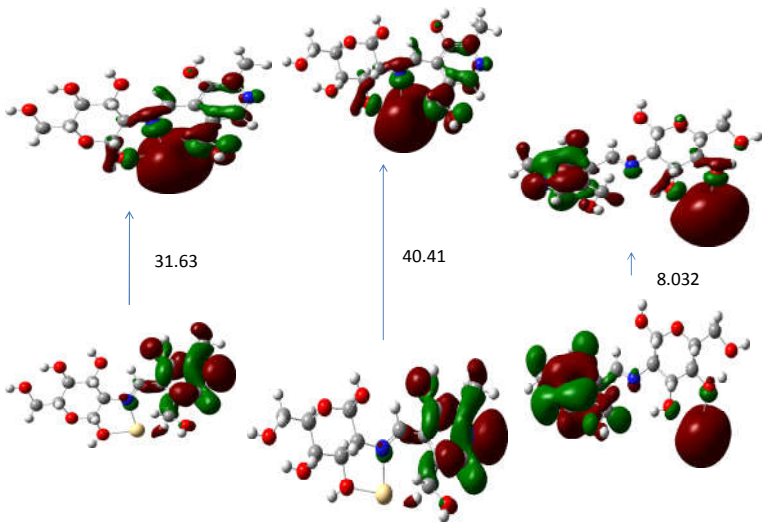

Fig.7.16 Frontier molecular orbitals of Cd (II)-PC complexes

7.5.2 Hg (II)-PC complexes

Hg (II) ion was also studied for the interaction with PC. Like Cd(II), mercury forms complexes with PC. But it can only form two complexes. Hg (II) does not bind on O3 and O4 of PC. In complex (a), Mercury ion also is bonded to PC through N1 and O2 atoms. Bond lengths are 2.355 and 2.345 Å respectively.

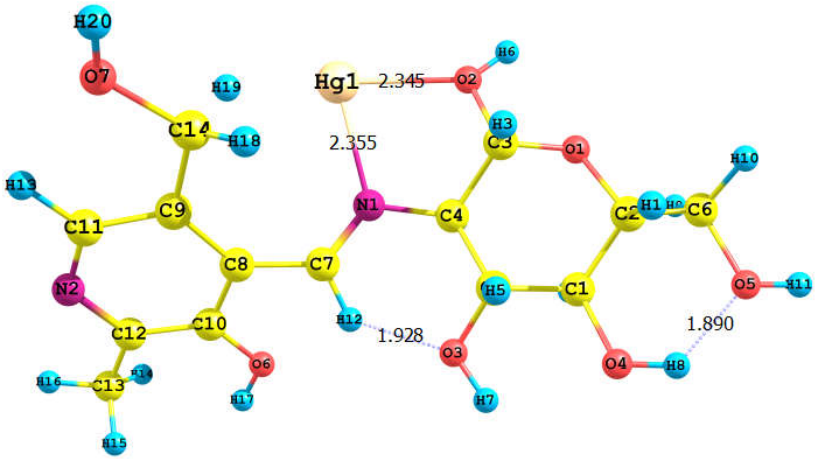

Fig.7.17 Hg (II)-PC complex (a)

Table 7.22 contains the adsorption energies of complexes. Natural electronic configuration shows that delocalization from ligand part is extended to 6p and 7p orbitals. That will stabilize the complex. Donor –acceptor interactions can be clearly understood from the NBO results. Some of the significant delocalizations in Hg (II)-PC complex (a) are discussed below.

Table 7.19 Important donor-acceptor interactions in complex (a)

Donor	Acceptor	$E^{(2)}$ (Kcal/mol)
π C 8 - C 10	LP (1) C 9	55.69
πC 8 - C 10	π^* N 1 - C 7	25.49
πC 8 - C 10	π^* C12 - N 2	19.94
π C 12 - N 2	LP*(1) C 11	53.09
π C 12 - N 2	π^* C 8 - C 10	16.62
LP (1) C 9	LP*(1) C 11	938.23
LP (1) C 9	π^* C 8 - C 10	65.23
LP*(1) C 11	π^* C 12 - N 2	59.97
LP (1) N 2	σ* C 9 - C 11	11.26
LP (1) N 2	σ* C 10 - C 12	12.61
LP (2) O 6	π^* C 8- C 10	33.20
LP (2) O 8	σ* C 14 - H 19	12.03
π^* N 1 - C 7	π^* C 8- C 10	39.40
LP (2) O 2	**LP*(6)Hg**	**11.81**
LP N 1	**LP*(6)Hg**	**25.28**

Delocalization from filled pi orbital of C8-C10 to N1-C7 can enhance the metal chelation capacity of nitrogen atom. The following few transitions are those inside the aromatic ring of PC. These include primary and secondary hyperconjugation effects. The following two delocalizations, LP (2) O2 to LP* of mercury ion and LP N1 to LP* of mercury ion strengthen the metal-PC bonding. They correspond to ligand to metal delocalization.

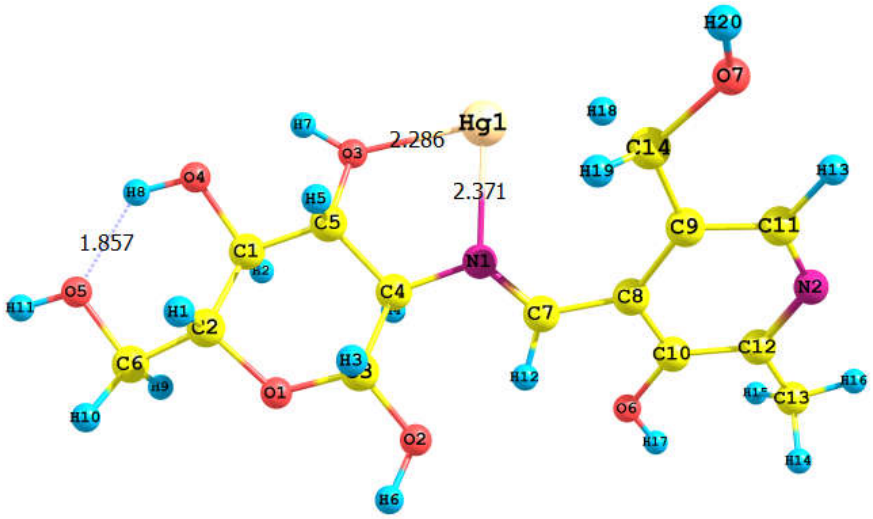

Fig.7.18 Hg (II)-PC complex (b)

Figure 7.18 shows the second complex of mercury and PC. In this N1 and O3 of PC is complexed with mercury ion. Bond lengths of coordination are also shown in figure. Hyper conjugative interactions of complex (b) are given in table 7.20.

Table 7.20 Important donor-acceptor interactions in complex (b)

Donor	**Acceptor**	$E^{(2)}$ **(Kcal/mol)**
πC 8 - C 10	LP (1) C 9	54.69
πC 8 - C 10	π*N 1 - C 7	27.66
πC 8 - C 10	π*C 12 - N 2	20.23
πC 12 - N 2	LP*(1) C 11	52.89
πC 12 - N 2	π*C 8 - C 10	16.99
LP (2) O 2	σ *C 3 - O 1	10.42
LP (2) O 5	σ *O 4 - H 8	11.63
LP (1) C 9	LP*(1) C 11	900.52
LP (1) C 9	π*C 8 - C 10	64.34
LP*(1) C 11	π*C 12 - N 2	60.84
LP (1) N 2	σ *C 9 - C 11	11.28
LP (1) N 2	σ *C 10 - C 12	12.56
LP (2) O 6	π*C 8 - C 10	32.63
LP (2) O 7	σ *C 14 - H 18	12.72
π*N 1 - C 7	π*C 8 - C 10	38.46
π*C 8 - C 10	π*C 12 - N 2	319.01
LP (2) O 3	**LP*(6)Hg**	**15.72**
LP (1) N 1	**LP*(6)Hg**	**23.07**

First few transitions take place inside pyridoxal ring. These include σ - σ *, π- π*, nonbonding to σ *, π* etc. typical transitions from O2 to C3-O1 and O5 to O4-H8 also take place with energies 10.42 and 11.63 Kcal/mol respectively. Two π*- π* transitions from N1-C7 to C8-C10 and C8-C10 to C12-N2 have also occurred. Lone

pair of O3 and N1 to antibonding orbitals of mercury ion is also observed.

Table 7.21 Natural electronic configuration of different Hg (II)-PC complexes

Complexes	NEC of metal ions
a	[core]6S(0.69)5d(9.98)6p(0.01)7p(0.01)
b	[core]6S(0.65)5d(9.98)6p(0.01)7p(0.01)

Electronic configuration of metal ion in two Hg (II)-PC complexes are given in table 7.21. The energy gap or band gap is important in determining the stability of molecules. Here the two complexes have comparable energy gap. Complex (a) has an HLG of 22.59 Kcal/mol and (b) has 26.23 Kcal/mol. Pictorial representation of the frontier molecular orbitals of two complexes are shown in figure 7.19.

Table 7.22 HOMO-LUMO energy gap in Hg (II)-PC complexes

Complexes	*Eads (Kcal/mol)*	E_L	E_H	$\Delta E=E_L-E_H$ *(Hartrees)*	ΔE *Kcal/mol*
PC	-	-0.0569	-0.230	0.174	109.19
a	-214.86	-0.4367	-0.472	0.036	22.59
b	**-220.88**	**-0.4313**	**-0.473**	**0.042**	**26.23**

From the figure follows, the electron density of HOMO and LUMO of complex (a) is located in different sites. But for the complex (b) both are on same side of the complex.

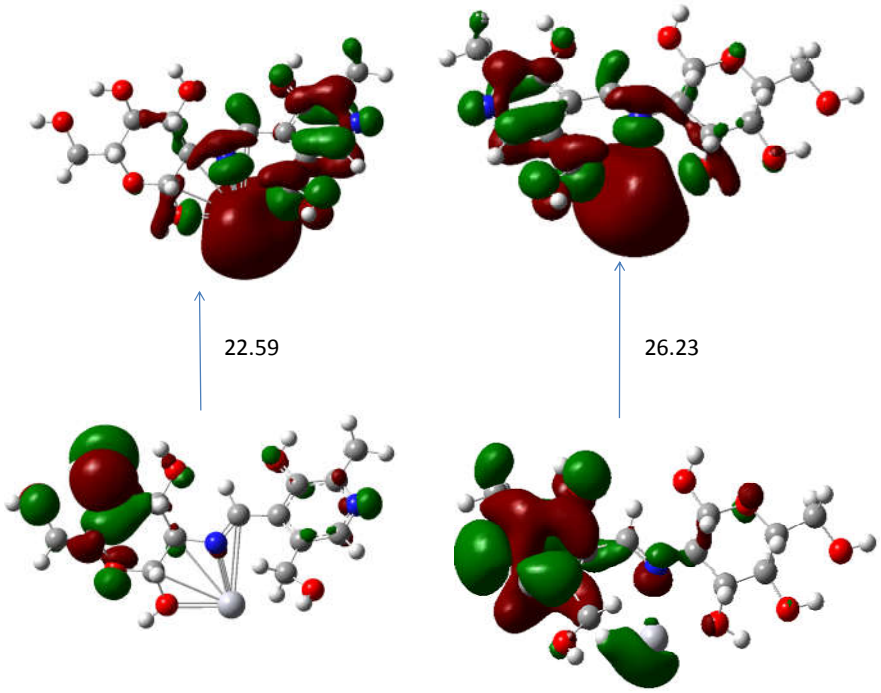

Fig.7.19 Frontier molecular orbitals of Hg (II)-PC complexes

In complex (a) HOMO is located on O1, O4 and O5 region but LUMO is at the pyridoxal part including the bonded metal ion. For (b), HOMO and LUMO is surrounded in the pyridoxal region covering the mercury ion.

7.5.3 Pb (II)-PC complexes

Coordination of Pb (II) ion with PC gives a complex with adsorption energy -224 Kcal/mol. In contrast to cadmium and mercury complexes, lead ion makes a bond with O7 atom. Bond lengths are shown in the fig.7.20. Stability of this complex is higher than that of Cd (II)-PC and Hg (II)-PC complexes. The extra stability is due to the additional bonding with O7 atom. The natural electronic configuration of Pb ion in the complex is given in table 7.23. That shows 6s electrons from ligand are delocalized to 6p orbital of metal ion.

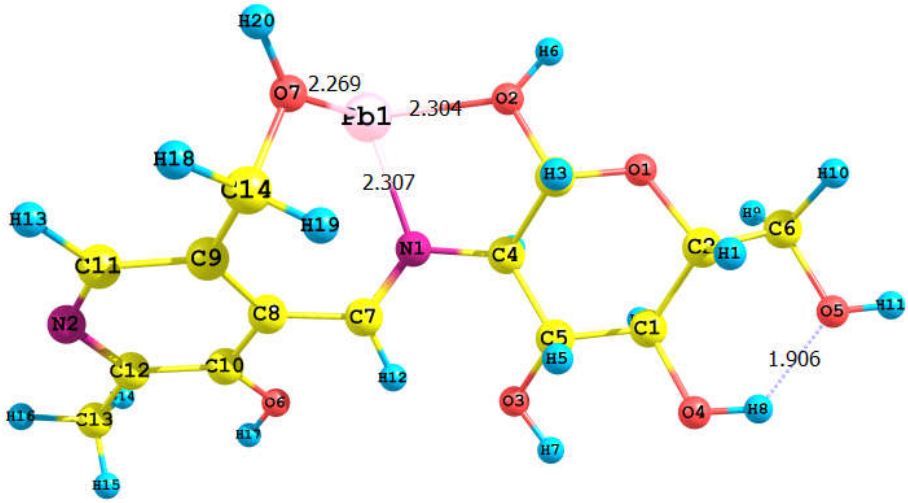

Fig.7.20 Pb (II) - PC complex (a)

The complex (b) in which O3 and O4 of PC is bonded to metal ion and is more stable in energy. Complex (a) has energy close to that of (b). In complex (b) hydrogen bonding exists, this stabilizes the complex.

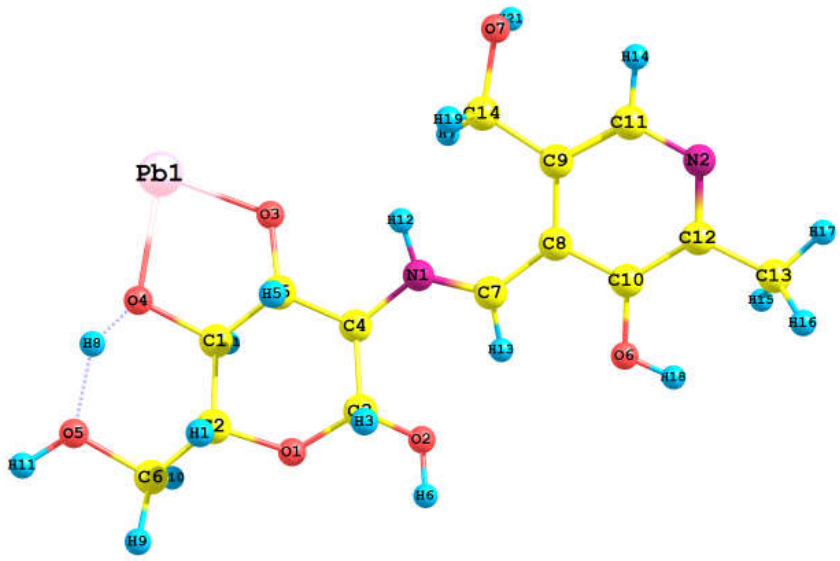

Fig.7.21 Pb (II)-PC complex (b)

The complex (c) is formed between O3 and N1 of PC coordinated. This has slightly low *Eads* value compared to (a) and (b). It has also hydrogen bonding between O5 and H8 which is typical of chitosan and derivatives.

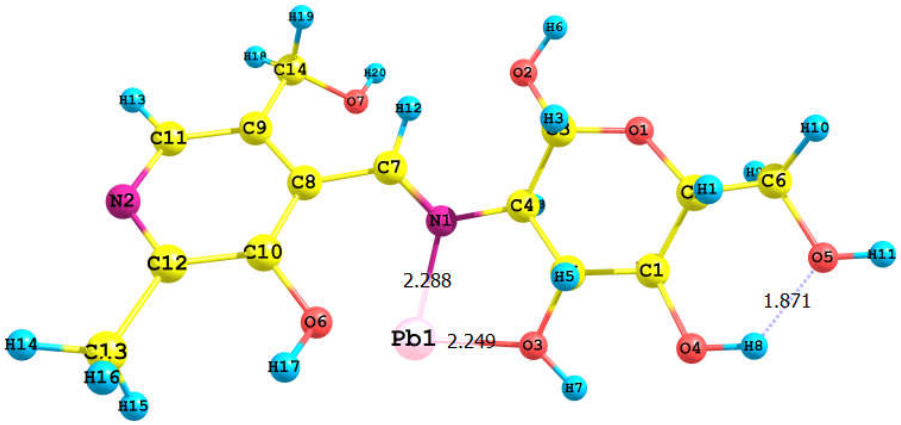

Fig.7.22 Pb (II)-PC complex (c)

Table 7.23 shows the electronic configuration of Pb (II) ion in different Pb (II) - PC complexes. In complex (b) 6p orbital has more electrons than (a) and (c) hence is the extra stability.

Table 7.23 Natural electronic configuration of different Pb (II)-PC complexes

Complexes	NEC of metal ions
a	[core]6S(1.91)6p(0.45)
b	[core]6S(1.92)6p(0.46)
c	[core]6S(1.92)6p(0.43)

Hyperconjugation effects of the lead PC complex (a) are obtained from the natural bond orbital analysis. Charge transfer from pi orbital of C8-C10 to the pi antibonding of N1-C7 with energy 21.27 is observed. This can enhance the metal bonding ability of nitrogen atom. Other delocalizations are take place within the pyridoxal part of PC. Delocalization from pi bonding of C9-C11 to antibonding of C14-O7 has energy 11.64 Kcal/mol. This enables O7 to take part in the coordination of Pb (II) ion.

Table 7.24 Donor –acceptor interactions in Pb (II)-PC complex (a)

Donor	Acceptor	$E^{(2)}$(Kcal/mol)
πC 8 - C 10	π * N 1 - C 7	21.27
π C 8 - C 10	π* C 9 - C 11	18.89
πC 8 - C 10	π* C 12 - N 2	20.78
πC 9 - C 11	π* C 8 - C 10	20.57
π C 9 - C 11	π* C 12 - N 2	16.43
π C 9 - C 11	π* C 14 - O 7	11.64
π C 12- N 2	π* C 8 - C 10	17.68
πC 12 - N 2	π* C 9 - C 11	26.45
LP (1) N 2	σ*C 9 - C 11	11.56
LP (1) N 2	σ*C 10 - C 12	12.61
LP (2) O 6	π* C 8 - C 10	30.97
π* N 1 - C 7	π *C 8 - C 10	29.00
π* C 8 - C10	π* C 9- C 11	158.28
LP (2) O 2	**LP*(4)Pb**	**22.11**
LP (1) N 1	**LP*(2)Pb**	**47.80**
LP (2) O 7	**LP*(3)Pb**	**24.38**
LP*(2)Pb	**RY*(3)Pb**	**11.11**

The highlighted interactions are important in forming the complex. Transitions from filled orbitals of O2, N1 and O7 to unfilled metal ion orbitals are the cause of formation of this system. The following table gives the delocalization energy values of complex (b). Important values are taken into account.

Table 7.25 Donor –acceptor interactions in Pb (II)-PC complex (b)

Donor	Acceptor	$E^{(2)}$ (Kcal/mol)
πC 9 - C 11	LP (1) C 8	52.30
π C 9 - C 11	π*C 12 - N 2	19.87
πC 12 - N 2	LP*(1) C 10	46.06
πC 12 - N 2	π* C 9 - C 11	20.14
LP (1) C 8	π* N 1 - C 7	188.60
LP (1) C 8	π* C 9 - C 11	48.92
LP*(1) C 10	π*C 12 - N 2	60.06
LP (1) N 2	σ* C 9 - C 11	11.08
LP (1) N 2	σ*C 9 – C11	12.77
LP (2) O 6	LP*(1) C 10	59.25
LP (2) O 2	σ*C 3 - O 1	12.99
π* C 12 - N 2	π* C 9 - C 11	102.65
σ C 1- O 4	LP*(1) H 8	12.18
LP (2) O 4	LP*(1) H 8	11.81
LP (3) O 4	LP*(1) H 8	322.07
LP (3) O 4	RY*(1) H 8	11.51
LP (2) O 5	LP*(1) H 8	53.45
LP (3) O 3	**LP*(2)Pb**	**57.85**
LP (2) O 4	**LP*(2)Pb**	**13.43**
LP (2) O 4	**LP*(4)Pb**	**12.34**
LP*(1) H 8	σ*C 1 - O 4	12.27
LP*(1) H 8	RY*(1) H 8	23.41
LP*(2)Pb	LP*(1) H 8	16.67

The first 10 transitions corresponds that in pyridoxal ring. Lone pair of O2 to C3-O1 which is common in all others is seen in this case also. Only one π*- π* transition is observed in PC-Pb complex (b). It

has higher energy value. Another significant delocalization is from LP of O3 to LP* of H8 has energy 322 Kcal/mol. Transitions that result in the formation of complex (b) are shown in highlighted.

Table 7.26 Donor –acceptor interactions in Pb (II)-PC complex (c)

Donor	Acceptor	$E^{(2)}$ (Kcal/mol)
π C8- C 10	LP (1) C 9	38.41
π C8- C 10	π* N 1 - C 7	17.93
π C8- C 10	π *C 12 - N 2	23.88
πC 12 - N 2	LP*(1) C 11	52.88
π C 12 - N 2	π* C8- C 10	18.50
LP (1) C 9	π* C8- C 10	95.78
LP*(1) C 11	π *C 12 - N 2	71.74
LP (1) N 2	σ*C 9 - C 11	11.15
LP (1) N 2	σ*C 10 - C 12	12.27
LP (2) O 5	σ*O 4 - H 8	10.98
π* N 1 - C 7	π* C8- C 10	60.61
π* C8- C 10	π*C 12 - N 2	289.11
LP (2) O 3	LP*(1) H 7	11.01
LP (3) O 3	LP*(1) H 7	382.75
LP (3) O 3	RY*(1) H 7	21.24
LP (1) N 1	**LP*(2)Pb**	**51.44**
LP (2) O 6	**LP*(3)Pb**	**17.65**
LP (2) O 3	**LP*(4)Pb**	**24.16**
LP*(1) H 7	σ*C5 - O 3	27.06
LP*(1) H 7	RY*(1) H 7	43.14
LP*(2)Pb	RY*(2)Pb	11.17
LP*(2)Pb	RY*(3)Pb	10.18

First few transitions are common in pyridoxal ring. Two π*-π* transitions are observed. Highlighted ones show the delocalization that causes the formation of complex (c).

The frontier molecular orbitals of the complexes and PC are examined. The HOMO-LUMO energy gap is calculated from the energy values. Of the three complexes the one with shows greater energy gap of 81.26 Kcal/mol that justifies the *Eads* value of PC-Pb (II) complex.

Table 7.27 HOMO-LUMO energy gap of Pb (II)-PC complexes

Complexes	***Eads (Kcal/mol)***	E_L	E_H	$\Delta E=E_L-E_H$ ***(Hartrees)***	ΔE ***Kcal/mol***
PC	-	-0.0569	-0.2309	0.174	109.19
a	-224.143	-0.3511	-0.4746	0.1235	77.49
b	**-225.335**	**-0.3416**	**-0.4711**	**0.1295**	**81.26**
c	-218.307	-0.3447	-0.4433	0.0986	61.87

The pictorial representation of HOMO-LUMO of PC –metal ion complexes are shown in Fig.7.23.

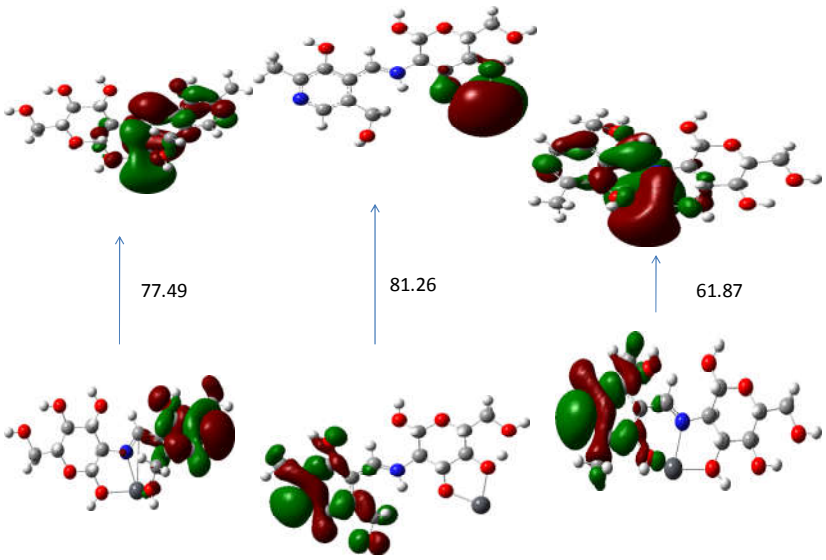

Fig.7.23 Frontier molecular orbitals of Pb (II)-PC complexes

7.5.4 Comparison between metal ions-PC complexes

The following table gives a comparison of PC-metal ion complexes. In case of PC there is two –OH groups present close to the amino group of chitosan part. As a result the complexation tendency of metal ions will be altered.

Adsorption site of PC	E_{ads} **(Kcal/mol) Cd(II)-PC**	E_{ads} **(Kcal/mol) Hg(II)-PC**	E_{ads} **(Kcal/mol) Pb(II)-PC**
N1,O2	-205.82	-214.86	-224.143
N1,O3	-213.23	-220.88	-218.307
O3,O4	-207.08	-	-225.335

Adsorption energy of metal ions with PC is greater than that of chitosan. That shows PC can chelate with metal ion strongly than chitosan do. For Pb (II), all the sites show a remarkable increase in *Eads*. This is due to the presence of two additional –OH groups. Mercury and cadmium ions are less preferable at the O3 and O4 of PC. Mercury cannot even form a complex at this position. N1, O3 is suitable for these two metal ions. The case of N1 and O3 is more needed to explain the polymer of chitosan . The order of stability of complexes at this site is Hg (II) > Pb (II) > Cd (II).

7.6 Conclusion

The three heavy metal ions can interact with chitosan monomer and its derivatives. The stability of the complexes was calculated from adsorption energy values. It is further confirmed with

the HOMO-LUMO of energy gap of the complexes. Mercury and cadmium ions show more reactivity towards nitrogen whereas lead toward oxygen atoms. The order of stability of metal complexes with chitosan is Hg (II) > Cd (II) > Pb (II). Complex formation tendency of metal ions was examined with derivative PC also since it is more reactive than other derivatives.

References

1. J. R. Deans, B. G. Dixon, Water Research.1992, *26*, 469.

2. C. Peniche-Covas, L. W. Alvarez, W. Arguelles-Monal, Journal of Applied Polymer Science.1992, *46*, 1147.

3. P. Udaybhaskar, Journal of Applied Polymer Science.1990, *39*, 739.

4. E. Guibal, Sep. Purif. Technol.2004, *38*, 43.

5. A.A. Radwan, F.K. Alanazi, I.A. Alsarra, Molecules. 2010, *15*, 6257.

6. R. Ghiasi, E. Ebrahimi Mokaram, J. Appl. Chem. Res. 2012,20, 7..

7. S.K. Parida, S. Sahu, S. Sharma, Comput. Theor. Chem. 2014, *1032*, 1.

8. R. S. Vieira, M. M. Beppu, Adsorption .2005, *11*, 731.

9. E.C.N. Lopes, F. S.C. dos Anjos, E.F.S. Vieira, A. R. Cestari , Journal of Colloid and Interface Sci.2003,*263(2),* 542.

10. C. A. Eiden, C. A. Jewell ,J. P. Wightman, Journal of Applied Polymer Sci. 1980,*25(8)*, 1587.

11. G. Gyananath, D. K. Balhal, Cellulose chem. technol. 2012, *46 (1-2)*, 121.

8 Chapter Corrosion Inhibition Activity

Organic molecules are used as inhibitors to protect or prevent metals from corrosion effectively in acidic media [1-18]. Corrosion inhibition activity of chitosan is not much reported previously. Heteroatoms such as oxygen, nitrogen, sulphur, phosphorous etc. containing molecules and those which contain pi bonds are reported for their corrosion inhibition activity [19-22]. The planarity of molecules, their adsorption capacity and metal binding efficiency are important for inhibitory action. The efficiency of delocalization of filled orbitals of (p orbitals) inhibitors to vacant orbitals of metal ion is also important in deciding the inhibitory action of molecules [23, 24].

Since quantum chemical methods are very good tools in determining the molecular structure as well as the electronic structure and reactivity [25] it has become a popular practice to carry out quantum chemical calculations in corrosion inhibition studies. Density functional theory (DFT) [26] overcomes other quantum mechanial methods in developing new criteria for rationalizing, predicting and understanding chemical processes. The chemical concepts which are now widely used as descriptors of chemical reactivity include electronegativity, chemical hardness, softness, Mullikan charges and Fukui functions [27-34]. Recently, quantum chemical calculations have been widely used to study the inhibition mechanism of organic molecules on metal [35-41].

In the present study our aim is to investigate the corrosion inhibition activity of Chitosan and its derivatives by density functional theory calculation methods. B3LYP method of DFT is employed for the entire studies.

8.1 Descriptors used for the study

Chemical hardness (η), softness (S), electrophilicity index (ω) and electronaffinity (χ) of Chitosan and derivatives were calculated from frontier energy gap. The equations used for the calculation are given in chapter 6.

The electrophilicity index measures the tendency of a species to accept electrons. Domingo et al. proposed that nucleophilicity and electropohilicity can be characterized from the values of μ and ω. Lower value of μ and ω shows that the molecule is a good and reactive nucleophile. Obviously a good electrophile can be characterized with a high value of μ and ω [42].

When considering the interaction of metal ion and inhibitor, electrons will flow from lower χ of inhibitor to higher χ of metal until equilibrium is reached (i.e., μ (metal ion) = μ (inhibitor)). The fraction of transferred electrons (ΔN) from inhibitor to metal ion is given as:

$$\Delta N = \frac{\chi_{metal} - \chi_{inhibitor}}{2(\eta_{metal} + \eta_{inhibitor})}$$

The inhibition efficiency of chitosan and derivatives towards iron and copper metals is studied. The theoretical values for electronegativity of iron and copper are χ_{Fe} =7 eV/mol, χ_{Cu} = 4.48

eV/mol. Global chemical hardness ηFe = 0 eV/mol, η_{Cu} = 0 eV/mol according to Pearson's electronegativity scale. This is because metal ions are softer than neutral metallic atoms (for a metallic bulk I = A) [43].

Gomez et al. proposed a simple charge transfer model for donation and back-donation of charges [45]. According to it an electronic back-donation process might be occurs that can govern inhibitor and metal surface interaction. And if charge transfer to the molecule and back-donation from the molecule occurs simultaneously the energy change will be related to hardness of the molecule, as given in the following equation.

$$\Delta E_{back\ donation} = \frac{-\eta}{4}$$

If η > 0 and $\Delta E_{back\ donation} < 0$ then the charge transfer to a molecule, following a back-donation from the molecule will be favored energetically. Using this it is possible to compare the stabilization of inhibiting molecules. That is when there will be an interaction with one metal the stabilization will decrease on increasing the hardness.

For calculating the above parameters the energy values and energy gap of frontier molecular orbitals must be known. The following table gives information about the HOMO and LUMO energy values.

Table 8.1 The HOMO-LUMO energy values of Chitosan and derivatives at B3LYP/6-31G (d) level of DFT

Molecules	**E_H (a.u)**	**E_L (a.u)**	**$\Delta E=E_L-E_H$**	**ΔE (e V)**	**E_L+E_H**	**E_L+E_H (eV)**
Chitosan	-0.2288	0.0412	0.2699	7.34	-0.1876	-5.10
CC	-0.2171	0.0288	0.1883	5.12	-0.2456	-6.68
CCR	-0.2097	0.0268	0.2366	6.44	-0.1829	-4.98
GC	-0.2571	-0.0554	0.2017	5.49	-0.3125	-8.52
GCR	-0.2374	0.0310	0.2684	7.30	-0.2064	-5.61
PyC	-0.2502	-0.0460	0.2042	5.55	-0.2962	-8.05
PyCR	-0.2069	0.0163	0.2232	6.07	-0.1906	-5.19
SC	-0.21372	-0.0298	0.1839	5.01	-0.2435	-6.61
SCR	-0.20658	-0.00848	0.1981	5.40	-0.2151	-5.86
PC	**-0.2177**	**-0.0437**	**0.1740**	**4.73**	**-0.2614**	**-7.11**
PCR	-0.2114	0.0055	0.2029	5.52	-0.2169	-5.90
PMC	-0.2393	-0.0455	0.1938	5.28	-0.2848	-7.75
PMCR	-0.2189	-0.0103	0.2086	5.68	-0.2292	-6.24

The HOMO and LUMO can be used to explain electron donating and accepting ability of molecules. High value of E_{HOMO} indicates better tendency to donate electrons to acceptor molecules with low E_{LUMO}. Thus increase in E_{HOMO} values facilitate adsorption and enhance the inhibition efficiency of molecules. In other words the binding ability of the inhibitor molecules to the metal surface will be increased on increasing HOMO and decreasing LUMO energy values [29, 30].

ΔE ($\Delta E = E_{LUMO} – E_{HOMO}$) is another important parameter to measure reactivity of the inhibitor molecule to the metallic surface adsorption. Shorter the ΔE of the molecule, its inhibition efficiency will be higher. It is because lower energy will be enough to remove an electron from the LUMO. Molecules with low energy gap are usually more polarizable. Hence they have high chemical activity, low kinetic stability and high softness value [46].

The table 8.1 shows that PC has the lowest energy gap (4.73 eV) compared to Chitosan and other derivatives of Chitosan . Thus it will be more reactive towards metal ions. And its *IE* also will be greater. The energy gap decreases in the order PC < SC < CC < PMC < SCR < GC < PCR < PyC < PMCR < PyCR < CCR < GCR < Chitosan . All of the twelve derivatives have lower energy gap than Chitosan . That shows derivatives have *IE* higher than Chitosan . The N-reduced derivatives show higher energy gap than their corresponding Schiff bases. Obviously Schiff bases are expected to have higher *IE* than their corresponding N-reduced form in terms of ΔE.

The global reactivity parameters, chemical hardness (η), softness (S), electronegativity (χ) and electrophilicity index (ω) were calculated as given in Table 8.2. The chemical hardness and softness are important in measuring the molecular stability and reactivity. A hard molecule has a large energy gap whereas a soft molecule is characterized with a small energy gap. The molecule having lowest value of global chemical hardness or the highest value of global softness will show highest ability to donate electrons. And thus will have high inhibition efficiency [29, 30, 47]. The hardness of the

studied molecules increases in the order as shown above in energy gap. Thus PC is more reactive.

The electro negativity denotes electron-accepting ability of a molecule. Chitosan and derivatives can be arranged as; Chitosan < PyCR< GCR < SCR< PCR < CCR < PMCR < SC< CC < PC < PMC < PyC < GC. The trend reveals that N-reduced derivatives have lower electron accepting ability than Schiff bases.

Table 8.2 Descriptors studied for inhibitory action of chitosan and derivatives

Molecules	**η (eV)**	**S**	**χ(eV)**	**ω**
Chitosan	3.67	0.27	2.55	0.8858
CC	2.56	0.39	3.34	2.179
CCR	3.22	0.31	2.99	1.388
GC	2.75	0.36	4.26	3.299
GCR	3.65	0.27	2.81	1.082
PyC	2.78	0.36	4.03	2.921
PyCR	3.04	0.33	2.59	1.103
PC	**2.37**	**0.42**	**3.56**	**2.674**
PCR	2.76	0.36	2.95	1.576
PMC	2.64	0.38	3.85	2.807
PMCR	2.84	0.35	3.12	1.714
SC	2.51	0.398	3.30	2.169
SCR	2.70	0.37	2.93	1.5897

Derivatives have electro negativity higher than Chitosan. This shows their increased reactivity towards metals. The electrophilicity index of the studied molecules was also given in table 8.2.

8.2 Metal ions and back donation

Corrosion inhibition efficiency of Chitosan and derivatives to iron and copper was studied. Fraction of electrons transferred to metal surface (ΔN), ΔN values for Fe and Cu were theoretically calculated as shown in table 8.3. Dipole moment values and $\Delta E_{back\ donation}$ values of Chitosan and derivatives are shown in table 8.3.

Since the reactivity of PC is higher than others, complexation of Fe and Cu with PC was observed. The following figures show the structure of PC-metal complexes. Iron binds with PC at N1, O2 and O7. Their bond lengths are 1.913, 1.924 and 1.893 respectively. The energy of complexation is -339.23 Kcal/mol.

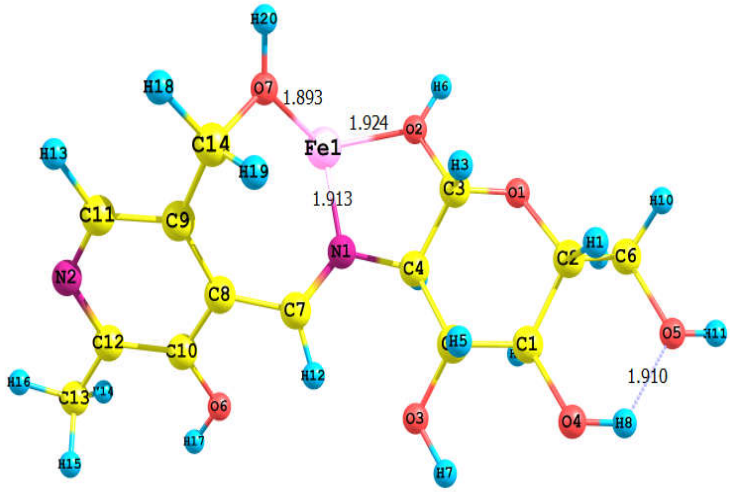

Fig 8.1 Fe-PC complex

Copper forms two complexes with PC. Complex (a) forms with N1 and O2 of PC. The second was formed with O3 and O4 of PC. *Eads* of Cu-PC complex (a) is -319.209 Kcal/mol and that of (b) is -333.52 kcal/mol respectively.

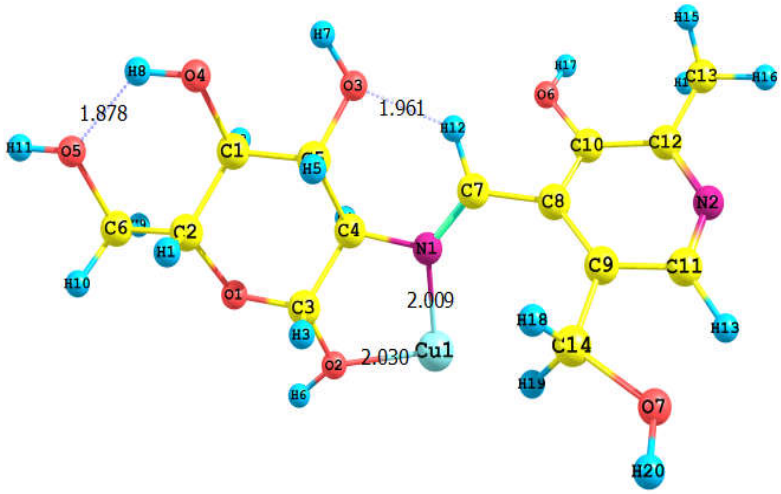

Fig 8.2 Cu-PC complex (a)

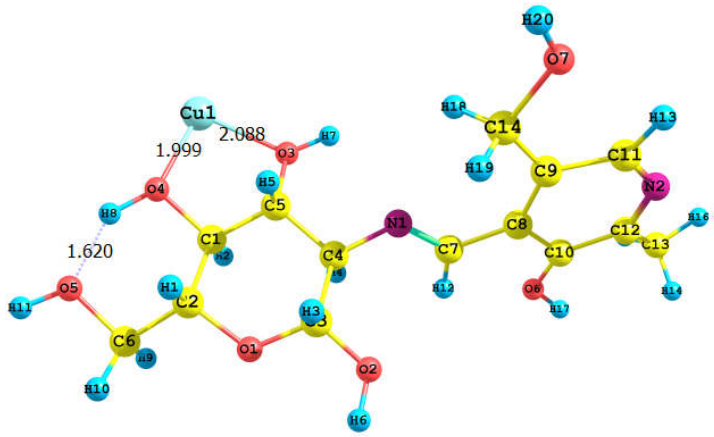

Fig 8.3 Cu-PC complex (b)

According to Lukovits if ΔN < 3.6, the inhibition efficiency increases with increasing electron-donating capacity on metal surface [47]. Chitosan and derivatives are good inhibitors their ΔN values are less than 3.6. All of the derivatives except GC show IE higher than Chitosan monomer.

Table 8.3 ΔN and Back donation of Fe and Cu to chitosan and derivatives

Inhibitors	ΔN **(Fe)**	ΔN **(Cu)**	**Dipole moment (Debye)**	$\Delta E_{back\ donation}$
Chitosan	0.6063	0.2629	3.88	-0.9175
CC	0.6626	0.2226	3.99	-0.6400
CCR	0.7025	0.2314	4.19	-0.8050
GC	0.4982	0.0400	5.12	-0.6875
GCR	0.5739	0.2288	7.44	-0.9125
PyC	0.5359	0.0809	4.72	-0.6950
PyCR	0.7253	0.3109	5.48	-0.7600
PC	**0.7257**	**0.1941**	**7.54**	**-0.5925**
PCR	0.7337	02772	7.72	-0.6900
PMC	0.5966	0.1193	4.16	-0.6600
PMCR	0.6831	0.1761	4.87	-0.7100
SC	0.7371	0.2351	4.13	-0.6275
SCR	0.7537	0.2870	4.24	-0.6750

Fraction of electrons transferred from metal to inhibitor is higher for Fe than that of Cu. The absolute value of ΔN might not correspond to reality only the trend within a set of molecule is significant. It means that ΔN values do not exactly give the number of electrons leaving from donor to the acceptor molecule.

The dipole moment is the most widely used parameter to describe the polarity of the molecule [48]. It is a measure of the polarity of a polar covalent bond and can be defined as the product of charge on the atoms and the distance between the two bonded atoms. As the dipole moment increases the inhibition efficiency increases. The total dipole moment, approximated as the vector sum of individual bond dipole moments that can reflect the global polarity of a molecule. The back donation values are also included in table 8.3. Since it is directly related to the hardness of inhibitor molecule PC has the lower value. This indicates the better interaction between metals and PC.

8.3 *Protonated chitosan monomer*

Most of the adsorption processes took place in acidic conditions. In such conditions Chitosan is protonated i.e., the free amino group will be positively charged. Then the probable mechanism is metal adsorption occurring on the first adsorbed chlorine over layer [49]. Thus *IE* of protonated Chitosan also studied. In the similar line as described above for Chitosan and derivatives, protonated Chitosan also worked theoretically.

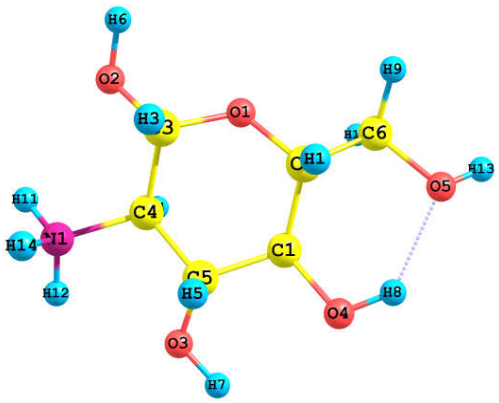

Fig.8.4 Optimized structure of the protonated Chitosan

For calculating the reactivity parameters, E_H (-0.3917) and E_L (-0.1374) is needed. The chemical hardness (η) of protonated Chitosan is 3.46 eV and electronegativity (χ) is 7.21 eV. Thus protonated Chitosan is more reactive than Chitosan evident from the lower value of hardness. Also the band gap is lower for protonated species (6.91 eV) than neutral Chitosan molecule (7.34 eV).

8.4 Conclusion

Corrosion inhibition activity of chitosan and some of its derivatives were examined using computational chemistry tools. The presence of number oxygen and nitrogen atoms in these molecules imparts their inhibition capacity. Inhibition capacity directly depends on the reactivity of molecules. All of the derivatives show better reactivity than chitosan parent, and hence their *IE* is also higher. The pyridoxal hydrochloride derivative was found to more reactive. The chelation ability of Fe and Cu ions with PC was checked. The properties of protonated chitosan monomer were also analyzed.

References

1. F. Bentiss, C. Jama, B. Mernari, H. El Attari, L. El Kadi, M. Lebrini, M. Traisnel, M. Lagrenée, Corrosion Sci. 2009, *51*, 1628.
2. I.B. Obot, N.O. Obi-Egbedi, S.A. Umoren, Corrosion Sci. 2009*, 51*, 1868.
3. S.K. Shukla, M.A. Quraishi, Corrosion Sci. 2009*, 51,* 1007.
4. F. Zhang, Y. Tang, Z. Cao, W. Jing, Z. Wu, Y. Chen, Corrosion Sci. 2012*, 61,* 1.
5. L. Wang, Corrosion Sci. 2001, *43*, 2281.
6. H. Zarrok, R. Saddik, H. Oudda, B. Hammouti, A. El Midaoui, A. Zarrouk, N. Benchat, M. Ebn Touhami, Pharma Chemica.2011*, 3*, 272.
7. A. Zarrouk, I. Warad, B. Hammouti, A. Dafali, S.S. Al-Deyab, N. Benchat, Intern. J. Electrochem. Sci. 2010*, 5*, 1516.
8. A. Popova, M. Christov, T. Deligeorgiev, Corrosion. 2003, *59*, 756.
9. W. Su, J.O. Iroh, Electrochim. Acta. 1999, *44,* 2173.
10. M. Mahdavian, S. Ashhari, Electrochim. Acta. 2010, *55*, 1720.
11. M.S. Morad, A.M.K. El-Dean, Corrosion Sci. 2006*, 48*, 3398.
12. A.Y. Musa, A.A.H. Kadhum, A.B. Mohamad, M.S. Takriff, Corrosion Sci. 2010*, 52*, 3331.
13. K.F. Khaled, Electrochim. Acta. 2003, *48*, 2493.
14. M. Elayyachy, B. Hammouti, A. El Idrissi, A. Aouniti, Portugaliae Electrochim. Acta, 2011, *29,* 57.
15. E.E. Ebenso, I.B. Obot, L.C. Murulana, Intern. J. Electrochem. Sci. 2010*, 5,* 1574.
16. M. Benabdellah, A. Yahyi, A. Dafali, A. Aouniti, B. Hammouti, A. Ettouhami, Arab. J. Chem. 2011*, 4,* 343.

17. M. Bouklah, N. Benchat, B. Hammouti, A. Aouniti, S. Kertit, Mater. Lett. 2006*, 60*, 1901.

18. X. Li, S. Deng, H. Fua, T. Li, Electrochim. Acta. 2009, *54*, 4089.

19. H. Ju, Z.-P. Kai, Y. Li, Corrosion Sci. 2008*, 50,* 865.

20. M.S. Masoud, M.K. Awad, M.A. Shaker, M.M.T. El-Tahawy, Corrosion Sci. 2010*, 52*, 2387.

21. W. Chen, H.Q. Luo, N.B. Li, Corrosion Sci. 2011*, 53,* 3356.

22. A. Döner, R. Solmaz, M. Özcan, G. Kardas, Corrosion Sci. 2011*, 53*, 2902.

23. J. Cruz, L.M.R. Martinez-Aguilera, R. Salcedo, M. Castro, Intern. J. Quantum Chem. 2001*, 85,*546.

24. V.S. Sastry, "Corrosion inhibitors: principles and applications," New York: John Wiley & Sons. (1998).

25. E. Kraka, D. Cremer, J. Amer. Chem. Soc. 2000*,122*, 8245.

26. R.G. Parr, W. Yang, "Density functional theory of atoms and molecules," New York: Oxford University Press. (1989).

27. R.G. Parr, W. Yang, J. Amer. Chem. Soc. 1984*, 106*, 4049.

28. R.G. Pearson, J. Amer. Chem. Soc. 1963*, 85*, 3533.

29. P. Udhayakala, T.V. Rajendiran, S. Gunasekaran, J.Adv.Scient.Res. 2012*,3*,37.

30. P. Udhayakala, T.V. Rajendiran, S. Gunasekaran, J.Comput. Methods Mol. Des. 2012*, 2*, 1.

31. M.R. Arshadi, M. Lashgari, G.A. Parsafar, Mater. Chem. Phys. 2004*, 86*, 311.

32. M.K. Awad, J. Electroanal. Chem. 2004*, 567*, 219.

33. M.H. Cohen, "Strengthening the foundations of chemical reactivity theory," (pp. 143-173). In: Nalewajski, R.F. (Ed**.**)**.** Density functional theory IV **-** theory of chemical reactivity. Heidelberg: Springer. (1996).

34. G. Gece, CorrosionSci. 2008,*50,*2981.

35. G. Gece, S. Bilgic, Corrosion Sci. 2010*, 52*, 3304.

36. M. Lashkari, M.R. Arshadi, Chem. Phys. 2004, *299*, 131.

37. J.H. Henriquez-Roman, L. Padilla-Campos, M.A. Paez, J.H. Zagal, M.A. Rubio, C.M. Rangel, J. Costamagna, G. Cardenas-Jiron, J.Mol.Struct.theochem.2005, *757*,1.

38. E. Jamalizadeh, A.H. Jafari, S.M.A. Hosseini, J. Mol. Struct. Theochem.2008, *870*, 23.

39. E. Jamalizadeh, S.M.A. Hosseini, A.H. Jafari, Corrosion Sci. 2009*, 51,* 1428.

40. L.M. Rodríguez-Valdez, A. Martínez-Villafane, D. Glossman-Mitnik, J. Mol. Struct. theochem .2004*, 681*, 83.

41. O. Blajiev, A. Hubin, Electrochim. Acta.2004, *49*, 2761.

42. L. R. Domingo, M. Aurell, M. Contreras, P. Perez, J. Phys. Chem. A. 2002*, 106,* 6871.

43. R.G. Pearson, Inorg. Chem. 1988, *27*, 734.

44. R.G. Parr, L. Szentpaly, S. Liu, J. Amer. Chem. Soc. 1999*, 121,*1922.

45. B. Gómez , N. V. Likhanova , M. A. Domínguez Aguilar , O. Olivares , J. M. Hallen , J. M. Martínez-Magadán . J. Phys. Chem. A. 2005, *109 (39),* 8950.

46. I. Fleming, "Frontier oritals and organic chemical reactions," New York: John Wiley & Sons. (1976).

47. I. Lukovits, E. Kalman, F. Zucchi, Corrosion.2001, *57,* 3.

48. O. Kikuchi, Quant. Struct.-Act. Relat. 1987, *6*, 179.

49. R. Solmaz, G. Kardas, B. Yazıcı, M. Erbil, Colloids and Surfaces A: Physicochemical and Engineering Aspects .2008,*312*, 7.

9 Chapter Druggability and Toxicity Studies

This chapter includes a virtual screening of chitosan and derivatives for their druggability and toxicity effects. Studies related to druggability were done using molinspiration and OSIRIS property explorer softwares available online [1, 2]. The SMILES notations of molecules under study were generated using Open Babel [3] and were fed into the online molinspiration software to calculate molecular properties like log P, total polar surface area, number of hydrogen bond donors and acceptors, molecular weight, volume, number of rotatable bonds, etc. Bioactivity score of drug targets can be predicted from its GPCR ligands, kinase inhibitors, ion channel modulators, enzymes and nuclear receptors activities.

Log S, druglikeness and drug score were predicted using OSIRIS property explorer. Toxicity studies (mutagenicity, tumorogenicity, irritation and reproduction) were also conducted using the methodology build at OSIRIS. The bioactivity score and drug likeness properties of the derivatives were compared with the parent compound chitosan .

As a first step to examine the druggability of the studied molecules, Lipinski's rule of five was checked. Pharmacokinetic properties of drug like molecules in-silico can be predicted using this rule. The rule five states that a molecule is likely to be orally active if it satisfies the following conditions:

(a) The molecular weight should be below 500.

(b) The calculated octanol/water partition coefficient (log P) should be less than 5.

(c) Number of hydrogen bond donors (OH and NH_2 groups) should not exceed 5.

(d) Number of hydrogen bond acceptors (notably N and O) should not exceed 10.

For calculating log P values, contributions from several small basic and larger fragments, intramolecular hydrogen bonding and charge interactions are to be considered [4]. Log P values should be less than 5, which is the upper limit to penetrate biomembranes according to Lipinski's rule of five.

Exceptions to this rule also take place. For a compound to be orally active it should not violate more than one rule. There are extensions to Lipinski's rule of five which states that polar surface area should likely be less than or equal to 140 $A^{\circ 2}$ and number of rotatable bonds should be less than or equal to 10 [5]. In calculating the transport properties of drugs molecular polar surface area (PSA) is an important property. Usually oxygen, nitrogen and attached hydrogen's are summed up to calculate the polar surface area [6].

9.1 Pharmacokinetic properties

As already stated, pharmacokinetic properties of drug like molecules in-silico were predicted using 'Lipinski's rule of five'. Molecular weight of all the molecules (monosaccharides) studied was less than 500. The number of H-bond donors and acceptors were also analyzed. The number of H-bond acceptors not cross the limits. H-bond donors of some molecules exceed the limit of rule. For example in Chitosan 6 H bond donors present, this is a violation of Lipinski's rule of five. It could be reduced by forming Schiff bases to some

extent. An exception is Schiff base formed with pyridoxal hydrochloride (PC). On reduction of Schiff bases, the number of H-bond donors increased by one. That is again a reason for violation of Lipinski rule as seen in SCR, PCR, PyCR and GCR. Reduced forms CCR and PMCR are fairly good candidates as they do not show any violation.

Log P values of all the molecules studied here fall in the range −4.11–1.16. That is well in agreement with the rule. Low degree of lipophilicity indicates that the molecules are likely to have good water solubility. Chitosan which is not soluble in physiological conditions is made soluble by derivative formation. Table 9.1 gives the results of Lipinski's rule of five. None of the compounds violate more than one condition of this rule.

Table 9.1 Lipinski's parameters of chitosan monomer and derivatives

Compound	Lipinski's Parameters					Extensions	
	milogP	MW	HBA	HBD	Violations	TPSA	nrot
Chitosan	-3.353	179.172	6	6	1	116.17	1
CC	1.158	313.39	6	4	0	102.51	6
CCR	1.078	315.41	6	5	0	102.17	7
SC	-0.828	283.28	7	5	0	122.74	3
SCR	-1.105	285.30	7	6	1	122.40	4
GC	-2.671	235.19	8	5	0	139.81	3
GCR	-4.105	237.21	8	6	1	139.47	4
PC	-1.761	328.32	9	6	1	155.86	4
PCR	-2.868	330.34	9	7	1	155.52	5
PyC	-2.671	249.22	8	5	0	139.81	3
PyCR	-1.761	251.23	8	6	1	139.47	4
PMC	-1.939	268.27	7	4	0	115.40	3
PMCR	-2.216	270.28	7	5	0	115.06	4

The result indicates that, theoretically the studied molecules have any problem for oral consumption. Molecular polar surface area (PSA) values give a good insight to the drug absorption. It includes intestinal absorption, bioavailability, Caco-2 permeability and blood–brain barrier penetration. All the molecules with an exception of two - PC and PCR- have PSA values within the required limit. The conformational flexibility of the molecules can be decided from the number of rotatable bonds. This is important to understand the binding of molecules to receptors or channels. Oral viability criteria suggest that the number of rotatable bonds should be less than or equal to 10. Parent Chitosan monomer has only one rotatable bond. The number is increased from 3 to 7 by preparing derivatives. Thus the molecules exhibit conformational flexibility.

9.2 *Drug activity studies*

Four criteria were studied for the molecules to understand their drug activity. They are GPCR ligand, ion channel modulation, kinase inhibition and nuclear receptor ligand activities. Their activity as protease inhibitors and enzyme inhibitors were also observed. Table 9.2 shows the values. A positive bioactivity score indicates considerable biological activity. Whereas an activity score between −0.5 and 0.00 shows moderate activity and less than −0.5 indicates inactive nature of molecules [7]. Parent Chitosan has bioactivity only against proteases and enzymes. The bioactivity can be increased on derivative formation. All derivatives studied, were found to be potent for enzyme inhibition activity. All compounds studied, are found to be effective in protease inhibition with an exception of SC and GC.

Table 9.2 Bioactivity scores of molecules against drug targets

Compound	GPCR ligand	Ion channel modulator	Kinase inhibitor	Nuclear receptor ligand	Protease inhibitor	Enzyme inhibitor
Chitosan	-0.54	-0.03	-0.68	-0.72	0.07	0.66
CC	0.03	-0.05	-0.16	0.1	0.36	0.71
CCR	0.07	0.04	-0.3	0.02	0.27	0.68
SC	-0.35	-0.18	-0.35	-0.35	-0.05	0.36
SCR	-0.07	-0.05	-0.19	-0.17	0.2	0.52
GC	-0.28	0.12	-0.74	-0.46	-0.23	0.38
GCR	-0.26	-0.04	-0.63	-0.45	0.28	0.62
PC	-0.13	0.15	-0.2	-0.29	0.01	0.55
PCR	0.15	0.19	-0.11	-0.19	0.2	0.68
PyC	-0.32	0.02	-0.74	-0.33	0	0.53
PyCR	-0.22	-0.04	-0.58	-0.46	0.33	0.57
PMC	-0.1	-0.01	-0.3	-0.47	0.03	0.56
PMCR	0.02	0.07	-0.05	-0.37	0.28	0.65

CC and CCR are found to be potent nuclear receptor ligand. Kinase inhibition activity is shown by none of the compounds. PyC, GC, CCR, PMCR and PCR are effective in ion channel modulation whereas CC, CCR, PMCR and PCR show good score towards GPCR ligand activity.

9.3 Toxicology studies

Toxicity risks can be understood from four criteria; mutagenicity, tumorogenicity, irritation and reproduction. Toxicology studies are quite important in the prediction of potential drugs. Their values are given in table 9.3.

Table 9.3 Toxicity parameters of chitosan and derivatives

Compound	Mutagenic	Tumogenic	Irritant	Reproductive effect
Chitosan				
CC				
CCR				
SC				
SCR				
GC				
GCR				
PC				
PCR				
PyC				
PyCR				
PMC				
PMCR				

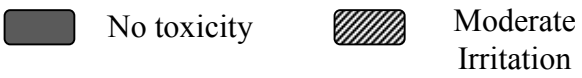

Toxicity predictor examines the fragments in the molecule which are likely to cause toxicity. Preliminary knowledge about the toxicity risks is quite essential in drug designing field. Most of the molecules studied here exhibit no toxicity alerts except CC. Citral derivative of chitosan (CC) has a medium risk of irritation because of the presence of CH_3-C=C-C=N fragment.

9.4 Druglikeness score

OSIRIS property explorer software calculated druglikeness score by summing up the scores of the individual fragments in a molecule under study from a list of 5300 molecular fragments. Based on a collection of 3300 drugs and 15,000 commercially available chemicals (not drugs), the frequency of occurrence of each fragment can be decided. A positive value indicates that the molecule predominantly has fragments that are used in drugs. Drug score takes into account druglikeness, miLog P, log S, molecular weight and toxicity risks and combines them into a global value for a potential new drug candidate. It is calculated using the following equation:

$$DS = \pi\left(\frac{1}{2} + \frac{1}{2}Si\right)\pi ti$$

Where $Si = (1 + S^{ap+b})^{-1}$

DS - the drug score

Si -contributions from milog P, log S, molecular weight and druglikeness (π)

The equation for *Si* gives a spline curve. The parameters'a' and 'b' are for miLog P, log S, molecular weight and drug-likeness and has values (1, −5), (1, 5), (0.012, −6) and (1, 0), respectively. The term 'ti' indicates the contributions from toxicity risk types. The values of 1.0, 0.8 and 0.6 show no risk, medium risk and high risk, respectively. A positive drug score indicates that the molecule predominantly contains pharmachophoric groups and can be a potential drug .The

drugglikeness values for all the compounds studied are in the range −2.51–2.09 (Table 9.4). All the molecules showed a positive drug score indicate that they are potential drug candidates.

Table 9.4 Molecular volume, calculated absorption (% ABS), log S, druglikeness and drug score of all the molecules

Compound	Volume	%ABS	Log S	Druglikeness	Drug score
Chitosan	155.078	68.921695	0.175	0.121	0.755
CC	305.17	73.63405	-1.73	-1.05	0.465
CCR	311.114	73.750315	-1.45	-0.64	0.623
SC	246.476	66.65539	-1.27	0.283	0.748
SCR	252.42	66.771655	-0.77	0.43	0.77
GC	194.025	60.765895	0.368	-0.906	0.629
GCR	199.995	60.88216	0.483	-2.3	0.533
PC	283.7	55.22899	-0.73	0.1	0.713
PCR	289.644	55.345255	0.225	0.245	0.73
PyC	210.612	60.765895	-0.01	0.745	0.816
PyCR	216.582	60.88216	0.105	2.095	0.919
PMC	234.302	69.187	-0.8	0.33	0.76
PMCR	240.246	73.750315	-0.29	0.481	0.781

Log S gives an indication to aqueous solubility. Solubility determines the rate of absorption and distribution characteristics. Most of the commercial drugs generally have log S value higher than −4.00. The compounds studied show Log S values in the range −1.73–0.483, which indicate good solubility. Percentage of absorption (%ABS) is calculated using the equation suggested by Zhao et al. [8] and is given in Table 9.4. The values of %ABS of the molecules under

consideration fall in the range 55.22–73.75 which is an indication of fairly good amount of absorption.

9.5 *Conclusion*

The druggability of chitosan monosaccharide and 12 of its derivatives were analyzed virtually. All the compounds satisfy Lipinski's rule of five and also ADME/Tox studies done using OSIRIS property calculator. The bioactivity of molecules reported on the basis of their interaction with GPCR ligands, nuclear receptor ligands, inhibition of kinases, protease and enzymes and ion channel modulation. The drug score of all the molecules were positive and thus they are found to be potential drug candidates. The chelation of chitosan and chitosan -derived Schiff bases with essential metal ions are likely to be a reason for imparting them with enhanced biological activity. All the molecules studied, are potent lead molecules for further research. Further, derivatization and bioactivity studies on chitosan may yield more interesting molecules with specific activities.

References

1. http://www.molinspiration.com/cgi-bin/properties.

2. http://www.organic-chemistry.org/prog/peo/.

3. N.M. O'Boyle, M. Banck, C.A. James, C. Morley, T. Vandermeersch, G.R. Hutchison, J. Cheminform. (2011)3–33. Epub 2011/10/11. doi: 10.1186/1758-2946-3-PubMed PMID: 21982300; PubMed Central PMCID: PMCPmc3198950.

4. C.A. Lipinski, F. Lombardo, B.W. Dominy, P.J. Feeney, Adv. Drug Deliv. Rev. 2001, *46*, 3.

5. D.F. Veber, S.R. Johnson, H.Y. Cheng, B.R. Smith, K.W. Ward, K.D. Kopple, J. Med.Chem. 2002, *45* ,2615.

6. P. Ertl, B. Rohde, P. Selzer, J. Med. Chem. 2000, *43*, 3714.

7. A. Verma, Asian Pac. J. Trop. Biomed. 2012, *2*, S1735.

8. Y.H. Zhao, M.H. Abraham, J. Le, A. Hersey, C.N. Luscombe, G. Beck, B. Sherborne,I. Cooper, Pharm. Res. 2002, *19,* 1446.

10 Chapter Summary and Conclusion

Chitosan chemistry is widely developed because of its unique properties. Advanced researches are still continuing on chitosan. As already mentioned chitosan find applications in fields, like waste water treatment, metallurgy, food industry etc. Its medicinal applications are also important. Modifications to chitosan biopolymer are another area of active research. The presence of hydroxyl and amino groups of chitosan make it easily amenable for derivatization. Schiff bases of chitosan can be treated as separate class because of its diversity.

Since the synthesis and property studies of Chitosan or its derivatives are conventional, theoretical treatment is the focus of this work. For this chitosan and some of its Schiff bases are modeled. Their N-reduced derivatives are also developed computationally. Choice of derivatives is based on their properties reported. Citral, glyoxylic acid/ oxoacetic acid, pyruvate, pyridine carbaldehyde,pyridoxal hydrochloride and salicylaldehyde are the carbonyl compounds chosen for derivative formation with chitosan .

As a preliminary study, only monosaccharide unit of chitosan and derivatives were considered in this work. B3LYP/6-31G (d) level of DFT was selected for the modeling of molecules. Characteristics of these molecules were analyzed at the same level of theory. Natural bond orbital analysis was carried out for all molecules in order to understand the bond orbitals. The donor-acceptor interactions also can

be obtained from NBO results. Dipole moment, polarizability and hyperpolarizability of these molecules were studied. Local reactivity of molecules interpreted from the natural charge values obtained from NBO results. Global reactivity is calculated from FMOs' of the molecules.

The entire work can be summarized as follows;

Structures of chitosan monomer and its derivatives were developed computationally. Their bond lengths and bond angles were closely observed. The length of -C=N- bond newly formed on Schiff base formation depends on the nature of carbonyl compound attached to chitosan . CC has the longer imine bond, because of the conjugation effect. The double bond character will be lowered. The presence of carboxylic acid group of GC lowers the imine bond length compared to other Schiff bases of chitosan . PyC also has a carboxylic acid group. But the electron donating effect of methyl group dominates the electron withdrawing effect of carboxylic acid group. So its imine bond is longer than GC.

Natural bond orbital analysis gives insight to the different types of donor-acceptor interactions takes place inside the molecule and how it stabilizes them. It also gives the natural charge values of each of all studied molecules. Reactivity parameters of the studied molecules were calculated using corresponding equations. All the derivatives show higher reactivity than parent chitosan molecule. Of these PC is found to be more reactive.

Applications of chitosan are mainly related to its surface activity. Metal chelation, corrosion inhibition and druggabilty of chitosan and derivatives were subjected to study. Heavy metal ions Cd (II), Hg (II) and Pb (II) were chosen for metal chelation studies. Different possibilities of complex formation of chitosan monomer with these metal ions were examined. Their stability was compared on the basis of adsorption energies calculated from the optimized energy values. Results show that mercury and cadmium ions have more binding capacity with amino group of chitosan whereas lead has with hydroxyl groups. This is in accordance with HSAB principle. Metal ions interaction with the derivative PC was also conducted.

Corrosion inhibition activity of chitosan is also studied. Chitosan and derivatives show good inhibition efficiency. Derivatives are more reactive and their inhibition efficiency also higher. Druggabiliy of chitosan and derivatives examined since it has several medicinal uses. Studies were carried out using online softwares, molinspiration and OSIRIS property explorer. Results show that chitosan and the studied derivatives are potential drug candidates. And further studies in this field will be promoted.

Studies at the monomer level of chitosan itself give several properties. This work is only a peripheral touch of chitosan chemistry, but it will be useful to further studies. Extension of the work to dimer, oligomer etc. can perform with more computational facilities and it will give specific properties and applications.